Project Number: <ME-HJ-0501>

Investigation of Variable-Glide Parafoils

A Major Qualifying Project Report:

Submitted to the Faculty

of the

WORCESTER POLYTECHNIC INSTITUTE

In partial fulfillment of the requirements for the

Degree of Bachelor of Science

Submitted by:

____

Michael Forostoski

____

Justin Riley

____

Virgil Vaillancourt

____

Jeffrey Wilfong

Date: May 2, 2006

Keywords
1. Parafoil
2. Deflection
3. Lift

Approved:

____

Professor Hamid Johari

ABSTRACT

The purpose of this project was to investigate the loading changes experienced by a Jalbert parafoil during a flare deflection maneuver, modeled in four stages: baseline, partial, full, and flare deflections. 3-D representations of these stages were generated using CAD software. Wind tunnel testing at various angles of attack resulted in coefficient of lift and efficiency relationships between the stages. Compared to baseline deflection at a constant angle of attack, the partial deflection had a 0.102 lift coefficient increase, the full deflection 0.477, and the flare 0.120, with efficiencies of 99.5%, 133%, and 102%, respectively. With the angle of attack variable, this relationship between the baseline and flare deflection is a lift coefficient increase of 0.675 with 117.4% efficiency.

ACKNOWLEDGEMENTS

The authors of this project would like to thank the following people for their valuable contributions:

Dr. Hamid Johari
Drs. Kenneth Desabrais and Calvin Lee of the Natick Soldier Center
Professor David Olinger
Steve Derosier, Mike O'Donnell, Bill Weir
Barbara Fuhrman
Pat Hickey
XFOIL Yahoo Group

AUTHORSHIP

Michael Forostoski
Abstract, introduction and background, wind tunnel blockage effects

Justin Riley
Generation of solid models, solid model limitations, test results and analysis, conclusion

Virgil Vaillancourt
XFOIL analysis, test regimen, report integration

Jeffrey Wilfong
Model construction, references, appendices, report integration

TABLE OF CONTENTS

LIST OF FIGURES

LIST OF TABLES

NOMENCLATURE

V	Velocity	
ρ	Density	
Re	Reynolds Number	$(\rho_\infty V_\infty d)/\mu_\infty$
Re_{crit}	Critical Reynolds Number	
q_∞	Dynamic pressure	$(1/2)\rho V^2$
C_L	Coefficient of Lift	$L/(q_\infty S)$
C_{Di}	Coefficient of Induced Drag	$C_L^2/\pi AR$
C_{DW}	Coefficient of Wake Drag	$((K_1\tau_1(\text{wing volume}))/C^{3/2})C_{Du}$
α	Angle of Attack	
α_i	Induced Angle of Attack	$-w/V_\infty$
α_{eff}	Effective Angle of Attack	$\alpha - \alpha_i$
ε	Arc-anhedral	
Γ	Bound Circulation	
w	Induced Velocity	$\Gamma/4\pi r$
ε_{sbW}	Solid Blockage Velocity Effect	$(K_1\tau_1(\text{wing volume}))/ C^{3/2}$

Table 1: Nomenclature

1. INTRODUCTION

Since the invention of parachutes and more specifically, parafoils, not many studies have been performed to investigate the aerodynamics of such devices. A parafoil is a rectangular parachute which also provides lift due to its airfoil shape. NASA [1] says, "…rectangular lifting chute: a parafoil lifting body that acts somewhat like a wing." Modeling a parachute or parafoil is quite difficult due to its fabric structure, which changes shape constantly while traveling through air. Modeling these devices is quite difficult and challenging even for the best computational fluid dynamics (CFD) software.

This project was created to investigate the aerodynamics of the Jalbert parafoil for the Natick Soldier Systems Center in Natick, Massachusetts. This task was very daunting due to the lack of data available about the subject. The project group was able to ascertain some data by comparing the airfoil of this parafoil with one from the Selig airfoil collection. By using X-foil code to modify the Selig airfoil, the project group was able to calculate approximate coefficients of drag and lift expected during wind tunnel testing.

Once this data was obtained through analysis, a CAD model of the parafoil in each of its configurations was made and a solid blockage analysis was performed for wind tunnel testing. After scaling of the model was done, the group constructed physical solid models of the parafoil using foam, balsa wood, steel rods, and epoxy. These models were then tested in the wind tunnel to obtain actual lift and drag data.

After obtaining wind tunnel data, the group was able to perform different types of blockage correction analyses and refine even further the data obtained from the wind tunnel. The data were then put into a logical format and submitted in this report.

2. BACKGROUND

Over the past half century, parafoils have been used in many different applications. Parafoils make their presence known in the military, space, and civilian communities, delivering personnel and payloads to their destinations with great accuracy and efficiency. It is necessary, however, to understand the actual dynamics of these craft and explore new ways to make them even more efficient.

In 1964, inventor Domina Jalbert designed the first parafoil. He essentially used knowledge of parachutes and airfoils and combined them. Over the years, research has been conducted to improve the parafoil and obtain accurate data from a parafoil in-flight. Because the shape of the parafoil is determined by the pressure distributions in and around the craft, it is extremely difficult to obtain any type of lift and drag data. Matos et al. [2] referenced Ware and Hassell's research on parafoils to test the longitudinal and lateral stability. They found that the models were in complete stability around the confluence point where the suspension lines meet.

Lingard [3] also conducted research on parafoils and found that by using the Low Aspect Ratio Wing Theory, he was able to determine the glide performance of a ram air parachute, or parafoil. Lingard also found that for low-aspect ratio parafoils, the flow from the leading edge disrupts the flow at the trailing edge which negates the lifting line theory. Hence, the lift must be spread over the entire surface instead of on a single line.

Research for this project has been conducted with parafoils that are solid models. The incredibly scaled down solid models replicate the geometry of parafoils in flight, but lack the dynamic nature of an actual parafoil, which would change shape with different pressure loadings. Although these are not actual parafoils made or a porous fabric, they do provide us with useful data which may be of value to our sponsor and other project groups.

3. DESIGN

3.1. Initial Geometries

3.1.1 Generation of Solid Models Based on Wind Tunnel Blockage and Re Number

In the creation of a solid model of the parafoil, specific goals were to be achieved while staying within the limiting parameters. Specifically, it is desired to have the scale model of the parafoil have the same Reynolds number as the modeled parafoil. In limitations, the physical size of the cross section of the re-circulating wind tunnel along with blockage considerations placed maximum caps on wing span and projection areas. Each of the problems was addressed individually.

The main limiting factor in the size of the parafoil was the compensation for blockage within the wind tunnel. Should the projection area of the parafoil be too large, flow would be choked, and therefore our simulation of “free stream flow” would not be achieved. Previous studies by Filippone [4] showed that a projection area of no more than 5% of the cross sectional area of the wind tunnel would achieve this goal. As the wind tunnel has a cross section of 24” by 24” (576 square inches), the maximum projected area of the parafoil in any state (be it deflected or non-deflected, flared or not) was determined to be 28.8 square inches.

Applying this value to the model with the largest projected area (full deflection), a scale of 7.13% was achieved. Knowing that this would be our maximum possible scale, the next course was to determine how the Reynolds Number produced from this scale model run in the wind tunnel would relate to the Reynolds Number of the full scale parafoil traveling at 10 m/s. As Reynolds Number is a function of chord length and velocity among other variables, the velocity would have to be increased by the same scale by which the chord length was decreased. Namely, the wind tunnel would have to be run at 140.2 m/s (100 / 7.13 = 14.02), a condition unattainable with our wind tunnel. As such, the maximum Reynolds Number we can produce (and thereby closest to actual flight conditions) at any scale is the Reynolds Number produced at maximum allowable blockage, 7.13% scale. Figure 1 below shows the drawings with appropriately scaled dimensions.

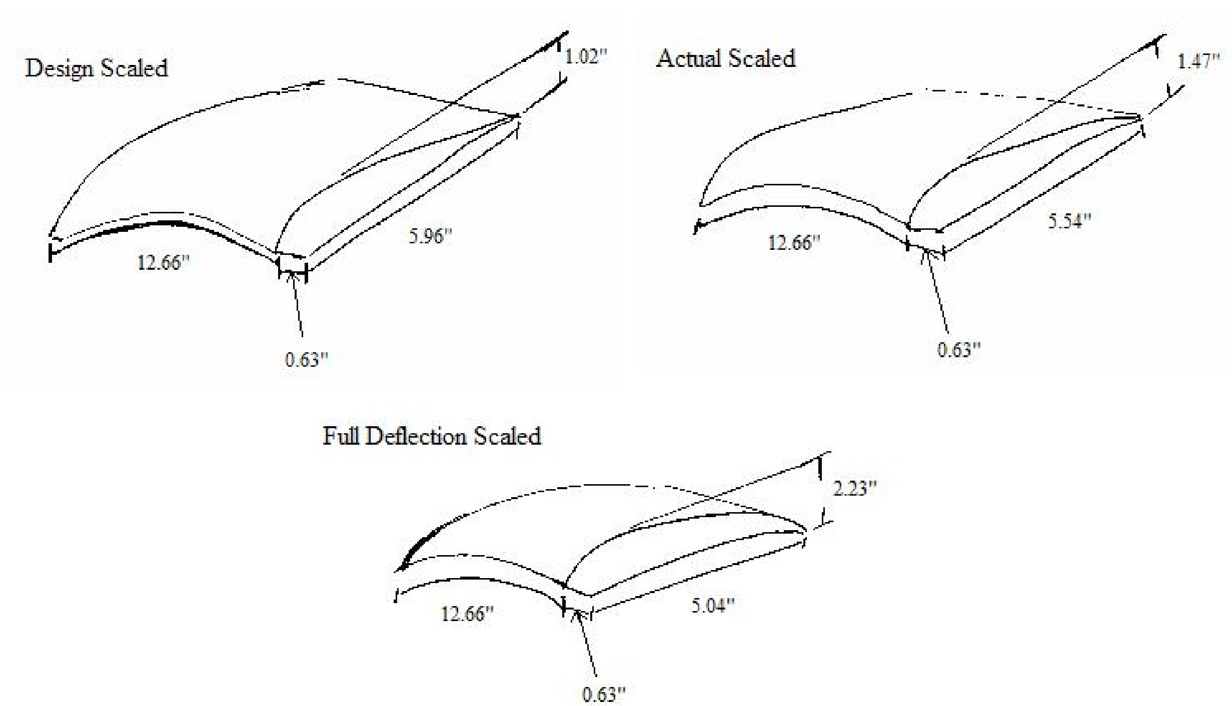

Figure 1: Dimensioned Design Drawings

3.1.2 Generating the Solid Models

The original route to physically construct the parafoil was to have it CNC machined out of aluminum. The first step along that route is to have the part designed in a 3-D CAD package, such as Pro/Engineer Wildfire. A .pdf file had been provided by Dr. Calvin Lee of Natick Soldier Systems Center plotting the comparison of the airfoil design and the inflated cell at the mid-span and at the end of the parafoil, both for the seam and center of the cell. The parafoils studied consisted of 14 individual cells, with two “ribs” forming the sides of a cell and zero-porosity fabric stretched over these ribs. These ribs will be referred to as seams and mid-span between the seams will be the center. It is important to note that the “center” cells are typically larger, as they have more freedom than the semi-rigid “seam” cells. Using the scale calculated from blockage requirements and pixel-based relationships from the provided file (shown in Figure 2), appropriate geometrical relations were made and a defined geometry was created.

The image was transferred into Pro/E through sketching splines and using Pro/E’s *scale* feature to create the appropriately sized figure. This process was completed for the center cells seam and middle splines, along with the seam and middle splines for the outer cells.

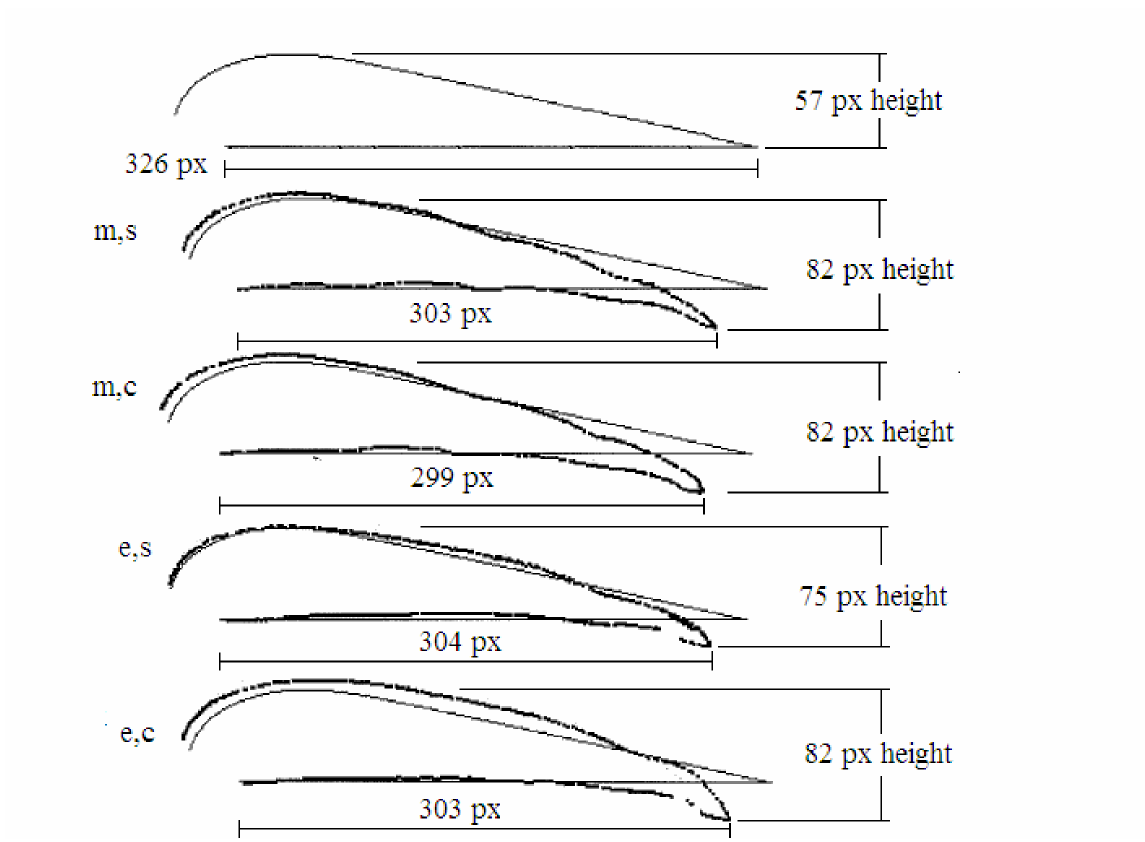

Figure 2: Scans of Seam and Center profiles with pixel measurements

With the splines in Pro/E, the sketched had to be placed in the appropriate location. As the parafoil is of an anhedral shape, the 3-D model cannot be constructed using the standard planes of FRONT, RIGHT, and TOP. Rather, datum planes had to be constructed at appropriate angles from the RIGHT plane, rotated around the FRONT/RIGHT intersecting axis. Through geometrical calculations, the parafoil had a total angle of 81.4°, represented in Figure 3 below by 2*ε.

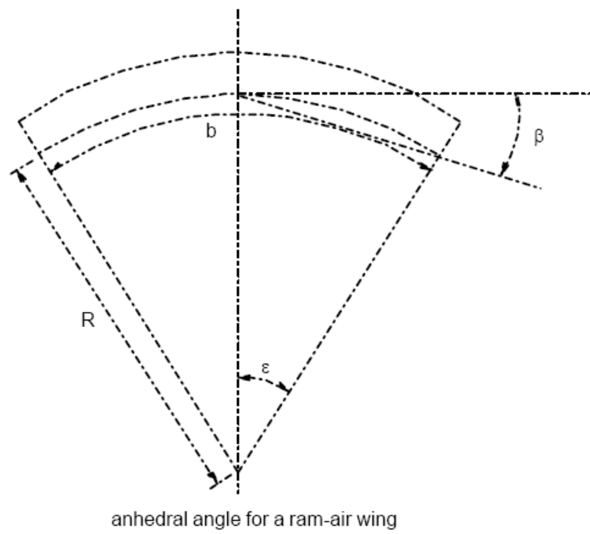

Figure 3: Schematic of the Anhedral Angle for Parafoil Parachute

There are 14 total cells in the parafoil, resulting in a radial span of 5.81° per cell. As the spline sketches must be placed both at the seam and the center of each cell, the created datum planes had to be placed at half of that angle, 2.905°. Figure 4 shows the flare deflection model with datum planes displayed. Note that these datum planes themselves have no impact upon the parafoil model; they only serve as placement locations for the sketches.

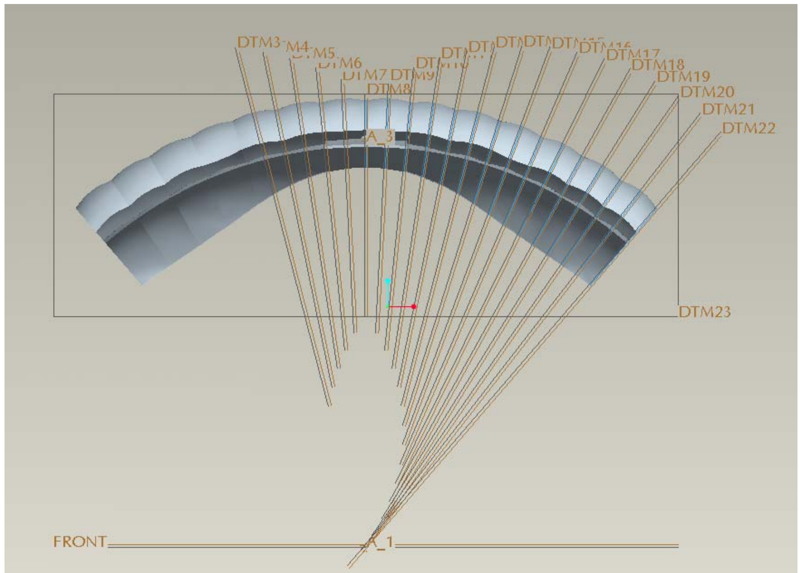

Figure 4: Parafoil Flare Deflection, Pro/E Image with Datum Planes Displayed

With the splines radially placed 8.92" (the line length with 7.13% scale applied) from the FRONT/RIGHT intersecting axis and located on their appropriate datum planes, a *Boundary Blend* was performed on the splines to create a zero-thickness skin over the parafoil's ribs, imitating the actual parafoil which uses a zero-porosity nylon fabric of minimal thickness. To accommodate a mounting device, thickness later was added to the middle two cells only. Figure 5 shows the finished baseline condition parafoil.

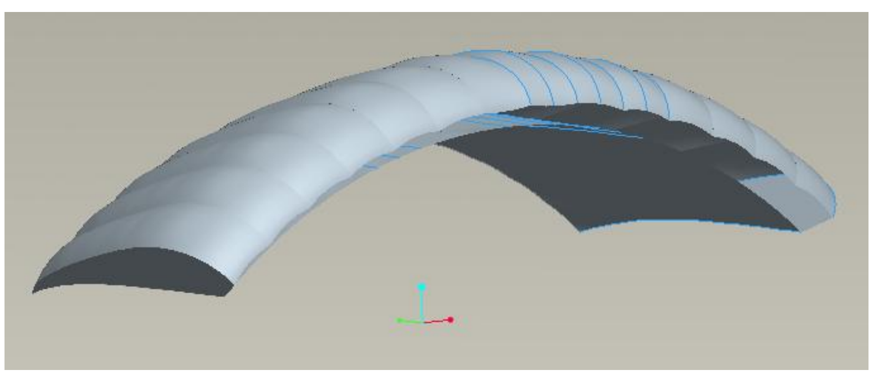

Figure 5: Parafoil in Baseline Deflection, Modeled in Pro/E

The full deflection parafoil's geometry was determined from another .pdf received from Dr. Lee showing the parafoil's shape during a full deflection versus the same parafoil's shape during baseline deflection. Again using software to determine the relations between models and gather the appropriate geometries, the same process as above was followed to create the Pro/E model of the full deflection parafoil. It is displayed below in Figure 6.

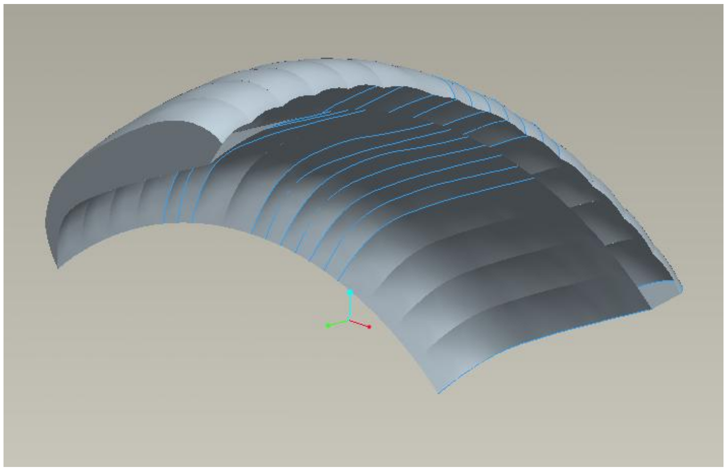

Figure 6: Parafoil in Full Deflection, Modeled in Pro/E

Without a plotted image of a partial deflection, a linear regression on the trailing edge was performed between the baseline and full deflection models. The 4 spines were again plotted on the appropriate datum planes and a *Boundary Blend* again performed. The result is in Figure 7, below.

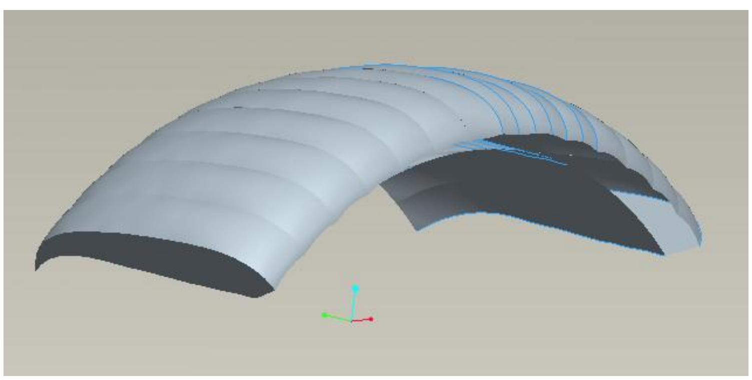

Figure 7: Parafoil in Partial Deflection, Modeled in Pro/E

The final solid model was the flare deflection which, unlike the previous three, required more than the initial four splines. In all, 30 splines were needed to construct the model's surface. The geometry for each spline sketch was created through pixel analysis obtained from an image of a skydiver performing a flare landing, shown in Figure 8. The design of the trailing edge created a linear section from the outer cell toward the center, with the center cells following the circular equation $y = -1.48x^2 + 0.0197x - 0.0063$. The completed image can be seen below in Figure 9, along with a more clear view of the trailing edge in Figure 4, above.

Figure 8: A Skydiver Performing a Flare Landing

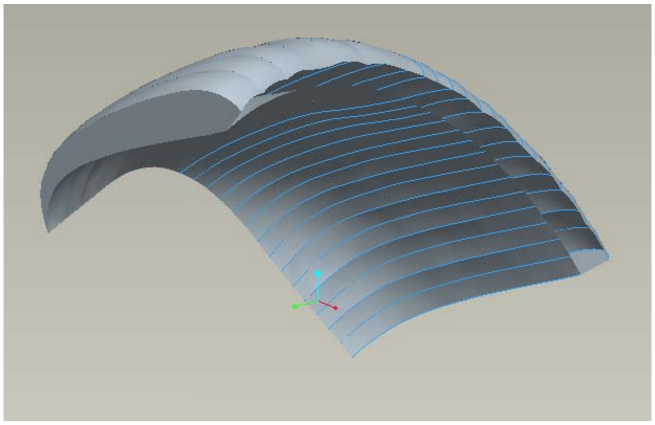

Figure 9: Parafoil in Flare Deflection, Modeled in Pro/E

These models can be imported into GibbsCAM to generate G-code, which is the necessary programming language of CNC machines. As machining is no longer the path being used to physically construct the model, these models are still very useful as they are used to generate the cross sections for Xfoil calculations, as well as serve as guide ribs that can be transferred to balsa wood or another material.

The primary usefulness of these models, however, is their use in computational fluid dynamics programs. Combined with the loading data that will be obtained through testing, a dynamic model can be created within a CFD program that can accurately predict the loading changes experienced during a flare deflection maneuver. This modeling can then be used within simulators for paratrooper training or for further research purposes.

3.2 Numerical Analysis

As a side project to the creation and testing of scaled models for variable glide parafoils, a 2-D profile was created in the Pro Engineer CAD program (Pro/E) in order to model the shape of the parafoil. Once a profile was created, it was imported into the airfoil analysis program X-foil. The goal was to analyze the parafoil shape and get aerodynamic loading data that would compliment the testing results of the wind tunnel experiments. The reason for this is because the dynamometer has force limits which can't be surpassed. If the forces produced are too large for the dynamometer's range then the measurements are not reliable. If the forces are not large enough, then system noise becomes a factor and causes interference in the resulting measurements.

The X-foil program was created by the Massachusetts Institute of Technology (MIT) with the intentions to make testing and analyzing airfoils much quicker and easier. With this program, one can analyze many different airfoils, such as NACA types, just by writing simple lines of code that allows the ability to change airfoils, angle of attacks, flap deflection and model many other procedures that occur in a wind tunnel test. In our case, coordinates were created from profiles that allowed us to import the parafoil shape into X-foil directly. Once the shape was in the program, many different tests were run that would give us some ideas to how the actual scaled models would perform, in the physical sense, inside the wind tunnels.

In order to import the profiles in X-foil, 140 points would have to be created which best described the aerodynamic shape of the airfoil These points were developed from the 2-D profile which was created from the 3-D solid model in a design program called Pro Engineer (Pro/E) as mentioned in ***Generating Solid Models***. From this solid model, certain views were used to help orient the model in a 2-D profile, which was then traced with spline curves. Spline curves are lines that accurately follow the border of the solid model entity and form an identical boundary to that of the solid model. During the tracing of the boundaries, points are plotted along the boundary that eventually were assigned coordinate references.

From these points and spline curves, dimensions were created that allowed us to get the location of the points that would represent the 140 coordinates that can be imported into X-foil. From the dimensioned Pro/E sketch, the coordinates were moved to a Microsoft Excel spreadsheet where they were organized and manipulated in order to successfully import into X-foil. When viewing a saved coordinate file from an airfoil out of the X-foil program, the files show that the coordinates must be in order so the program can accurately load the coordinates into the system. This order is consists of the coordinates starting from the top curve at the tail and continue counter clockwise until the bottom curve tail coordinate. Also the coordinates must be in percent length in reference to the airfoil's chord length. Once the coordinates were organized, they were imported into X-foil. In result, a shape that accurately represented the shape of the parafoil was produced, as shown in Figure 10. The one thing that was noticed after importing the shape was that the coordinates used to represent the shape were flawed because the curves on the profile were not completely smooth when compared to an existing airfoil, which was part of the program. When looking at the spreadsheet, it was realized that the coordinates produced were really the best possible from the Pro/E design program, and that these non smooth curves may affect the data output.

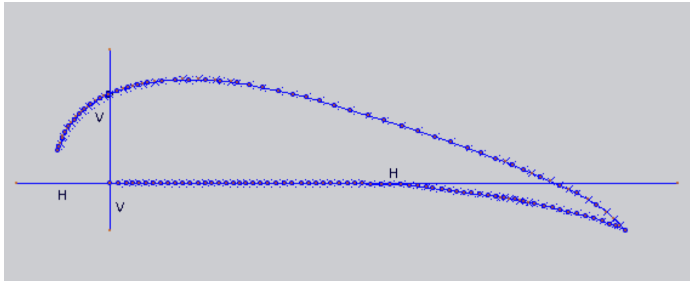

Figure 10: Pro/E Sketch with Traced Points

Once the parafoil was imported into X-foil, a simple test was performed in the inviscid mode of the program with an angle of attack (AoA) equaling zero, which is not the true angle of attack because the leading edge and trailing edge were not on the same level. Even with this small difference between reality angle and computer alignment angle, the lift coefficient before the 3-D corrections was 2.28, as shown in Figure 11. This value is considered pretty large for a 2-D profile no matter what angle of attack.

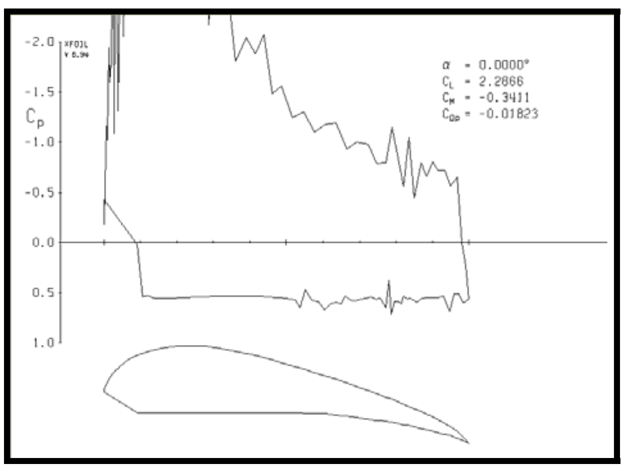

Figure 11: Original Inviscid Test (AoA=0)

After this unfortunate acknowledgement, it was decided that more research about the X-foil program should be performed. After talking with a couple of professors it was found that the parafoil should be in X-foil's viscous mode where a Reynolds number is specified such that it is sufficient for either the testing environment or for the natural environment in which the model will perform. Moreover, X-foil was designed to be most accurate with Reynolds numbers being at least 1-3 million. So from these findings it was decided that the velocities that are being used for testing are not near the 1 million mark for a Reynolds number, so it would be best to test the parafoil with Reynolds numbers of 3, 6, and 9 million, which are in the appropriate Reynolds numbers regime. Even though the X-foil results will no longer predict what may be produced from the wind tunnel data, it will still give us an idea to what the data should look like, and the range it should fall in.

After everything was basically figured out in the program, the team proceeded to test the parafoil profile again in the viscous mode at the previously mentioned Reynolds numbers with different angles of attack. Once these tests were finished, the data was still pretty unreasonable in reference to the lift coefficients and the behavior of the model flow around the parafoil in the viscous mode. As seen below in Figure 12, the modeled flow around the profile shows areas of erratic motion due to the curves being rougher than would be preferred.

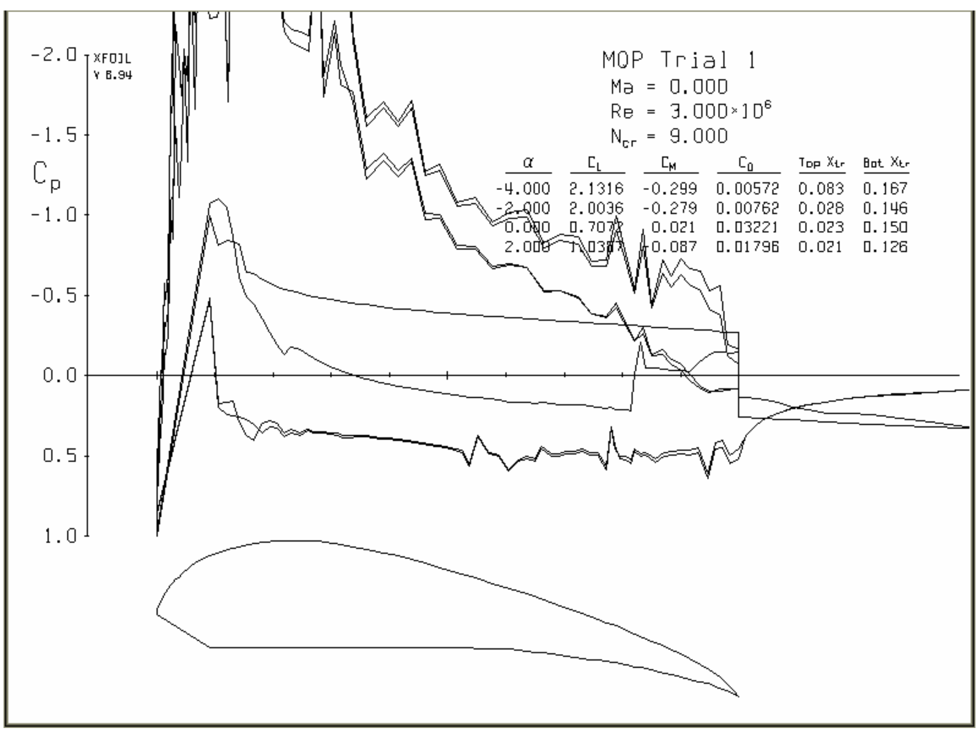

Figure 12: Results of Viscous Run (Re=3*10^6)

After these steps, some corrections or reliability measures took place in order to try and correct the modeled flow for the basic profile of the physical models that were made. The first thing that took place was the reliability test for the X-foil program. In order to check and see how reliable the program is, a simple airfoil such as the NACA 0012, which is a symmetric airfoil, was selected to be studied. This airfoil was tested in X-foil and then compared with the results from a Abbott, I. H. and Von Doenhoff [5] which are accumulated from several experiments and are accurate results for the airfoil. After testing the NACA 0012 airfoil in X-foil at the Reynolds numbers of 3, 6, and 9 million, the program proved to be very accurate in a sense that the lift, drag, and moment coefficients were only off a couple thousandths for the values that were experimentally produced. In result, the program is sufficiently accurate in estimating aerodynamic force coefficients for the parafoils natural performance environment. So the program was sufficient enough to get estimates for the models natural performance conditions. Comparisons are shown below in Figures 13 and 14.

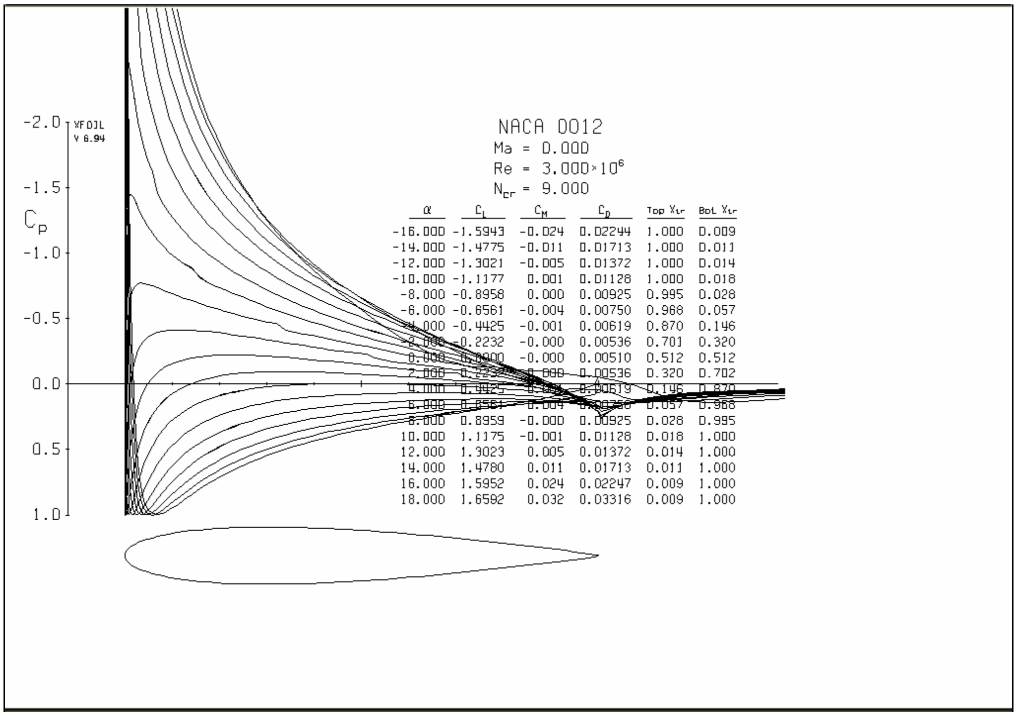

Figure 13: NACA Airfoil 0012 at Re=3*10^6

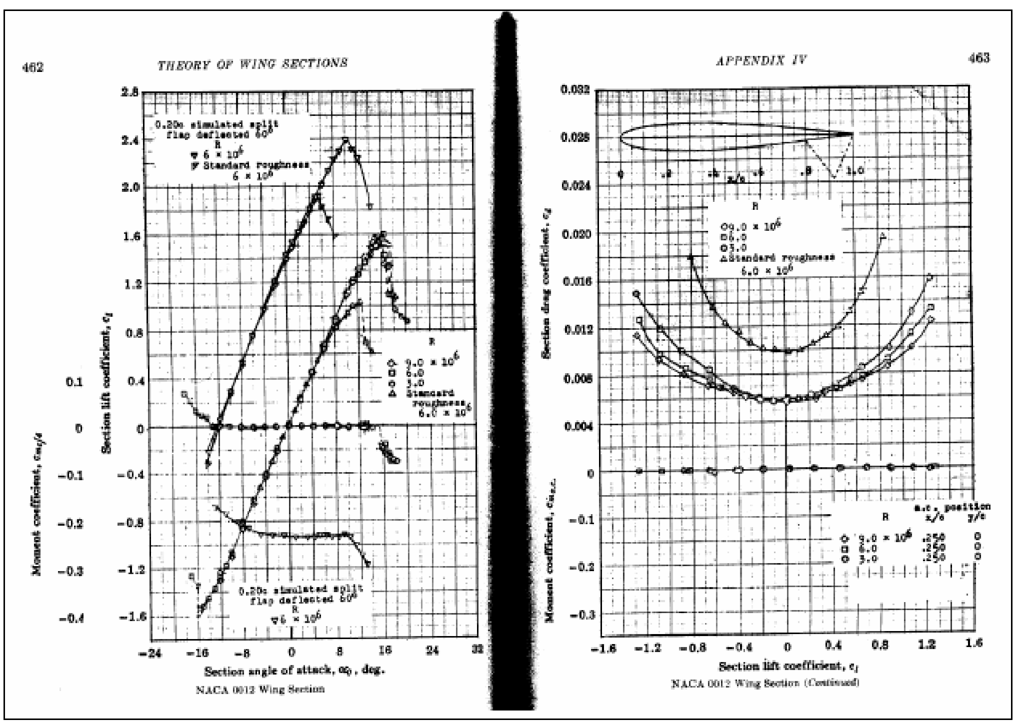

Figure 14: X-foil Reliabilty Verification

Now that it is known that the X-foil program can produce accurate data, attempts were made to smooth out the curves on the 2-D profile. The past procedure used to plot points on the profile was thought to be the cause of the slightly rigid airfoil surface because some points were added to the profile boundary by a different “add point” tool. Due to this uncertainty, new points and coordinates were created just with the spline curve function. These coordinates turned out to be almost similar to the past set and no improvements were observed at the same Reynolds number. The flow around the airfoil remained erratic and the data was unreasonable.

After improving the coordinate plotting procedure, it was noticed that Pro/E only produces dimensions with tolerances as small as a hundredth of an inch. With this observation, it seemed as though the y coordinates for the profile were being considered as equal heights. When this happens the curve will not be accurate to the desired shape and smoothness; the curve then has unnecessary jumps where coordinates get rounded up to 0.19 when they should be 0.185.

In response to this predicament, the team decided to model the shape of an airfoil by using line equations to produce more accurate coordinates (more significant figures). To make this task much easier, a basic profile from our Strong Enterprise [6] drawings was used, which consists of a flat bottom where all y values equal zero. With this profile, several points were taken off the top curve and entered into Microsoft Excel. While in the spreadsheet, a parabolic trend line was applied to the data points in a plot, which produced a parabolic line equation to the sixth power. The new coordinates were created and the imported into X-foil where results showed improvements in smoothness, but the aerodynamic coefficients produced were still inaccurate and inconsistent. See Figure 14 to view the latest result from the program.

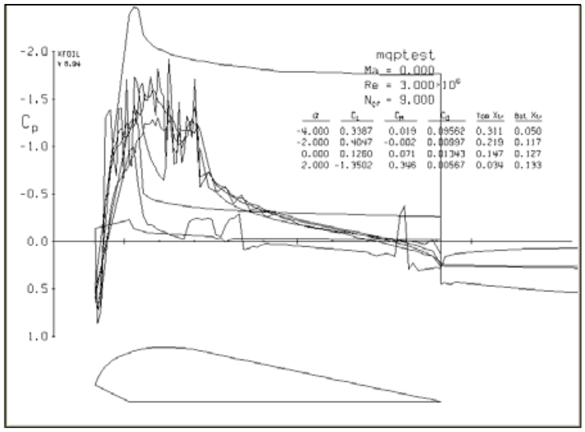

Figure 15: Strong Profile (Re= 3*10^6)

In conclusion to predict how our wind tunnel data will result using the X-foil program, it shows that the importing process into X-foil is really the only failure in doing so. After all, it has been proven that X-foil is reliable when used with large Reynolds numbers, and produces accurate results within that range. If there was a more reliable way to produce smooth and more accurate coordinates for the 2-D profile, there are no doubts that X-foil would produce accurate and useful data.

3.3 Fabrication Methods

3.3.1 Preliminary Analysis: Geometries

In order to obtain reliable and readable results pertinent to this project, it was deduced that there must exist four (4) wind tunnel models, each of varying geometry, which correspond to a parafoil in varied modes of flight, i.e. steady flight, aerial maneuvers, and landing. The four shapes are Baseline, Half Deflection, Full Deflection, and Flare Deflection. The Baseline model represents a parafoil at steady flight conditions, and in which there is no change in geometry – it is virtually flat on the lower surface starting near the leading edge then becomes slightly graduated in the negative Y-direction chordwise; additionally encompasses a constant geometry along the trailing edge spanwise. The Partial Deflection model begins with the same flat bottom near the leading edge (as they all do – it is a common surface on all four models, see Figure 16), however the trailing edge slopes chordwise more so than the Baseline and generally acts as a constant flap along the entire trailing edge. The Full Deflection is relatively similar to the Partial Deflection with a more inclined trailing edge. The Flare model's geometry has a trailing edge deflection of varying-magnitude: small near the center line and growing more towards the wing tips. The four combined geometries should result in a complete analysis of a parafoil flight regimen.

Figure 16: Flat Surface on Each Parafoil

3.3.2 Manufacturing Process Selection

A parafoil is constructed primarily from non-porous nylon which has been stitched together to give its shape. As this would be practically impossible on a small scale model, other construction methods were weighted against each other in an effort to produce the most reliable and repeatable wind tunnel results. In order to reproduce similar results, it was reasoned that the models must be of rigid materials. The following is an account of the various manufacturing techniques considered to fabricate the wind tunnel models for the experiments. It was first believed that machining the parafoils from aluminum would give the best overall shape, reliability, and repeatability, however the downsides were that the tooling may not have been able to give the best result, especially in the areas of the seams or trailing edge, where there exists a small area and tolerances are very tight. Additionally, it was initially suggested that each model would take well over 40 hours of pure machine time, not including preparation or finishing operations. Another possible manufacturing method researched was stereolithography, a process where a laser solidifies a liquid plastic and builds an object from the ground up, in very thin layers. This method would have been relatively fast (hence its general name, rapid prototyping) and render proper tolerances, however, stereolithography is very costly and was thus almost immediately dismissed. Ultimately, it was strongly suggested that the parafoils be hand-constructed from high density foam, which would keep the cost and weight to a minimum. The downside to hand-crafting four models is poor symmetry and a large time commitment, possibly even greater than machining, but as will be subsequently proven, this may have been the best route to pursue.

3.3.3 Preliminary Model Construction

High density foam became the primary material for constructing the parafoil models, and it was believed that smaller pieces of foam could be fashioned into individual sections of the parafoil, as if it had been cut chordwise into 14 pieces; the foam would then be adhered together to give the parafoil its initial shape. To begin the process, a 4' x 8' x 2" sheet of foam was put through a bandsaw in order to create 2" x 2" blocks from which the individual cells could be made. These individual pieces were then fashioned by hand with X-acto knives and sandpaper, which was a delicate and time consuming process. These initial shapes were found through the analysis of 2-D blueprints then transposing them into a 3-D model in ProEngineer.

It was suggested that the ribs on the actual parafoil, which help retain an airfoil-like shape while in flight, be simulated in the wind tunnel models; to be placed between the foam cells, and additionally, the ribs would act as a guide for shaping the foam. Balsa wood was chosen as the material to represent the ribs, as it is thin and light, thus not adding a significant weight or volume to the model. Different shapes of balsa were required, as the geometries of the parafoils are not constant throughout each model. Three pieces of each of the following profiles were required for the Baseline, Half and Full Deflection models: mid seam, mid center, end seam, end center (total of 12, see Figure 17); plus an additional 14 varying-geometry ribs for the flare model, totaling 26 for all four wind tunnel models. In order to be able to cut the balsa wood into the various shapes, it was first necessary to create stencils so that there could exist a precise and repeatable tracing surface. These stencils were first fashioned into the desired shape in ProEngineer then transferred into GibbsCAM in order to be milled from 3/32" thick Lexan (polycarbonate resin thermoplastic). After the stencils had been fabricated, the balsawood could be cut into the individual pieces with an X-acto knife, as shown in Figure 18.

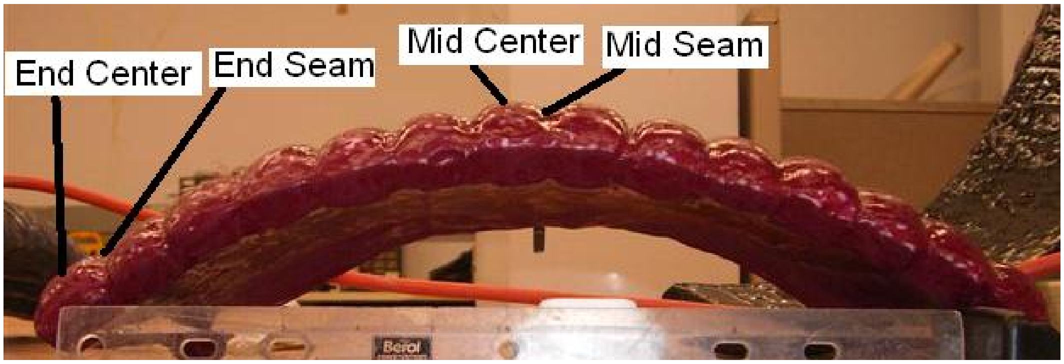

Figure 17: Locations of Rib Geometries

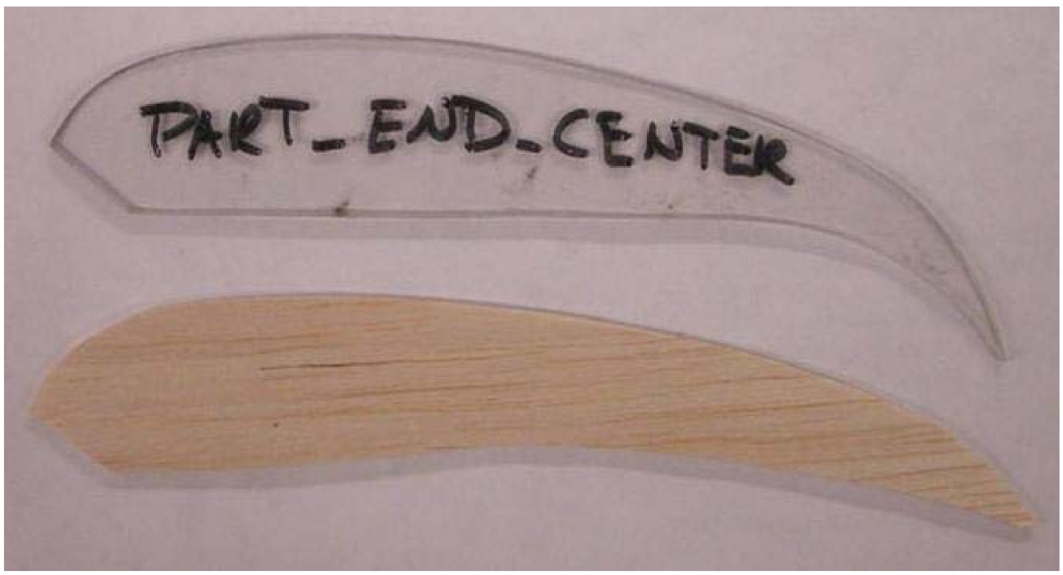

Figure 18: Lexan Rib Template and Resulting Balsa Rib

A major concern that arose was if enough lift was generated at or near the wing tips, the models might bend upward or break completely. This was remedied, however, by two (2) - ¼" steel rods which had been bent and cut to-size to displace the forces evenly throughout the model. The two rods were inserted spanwise through drilled holes in the foam, as shown in Figure 19: one near the quarter chord point, and the other further along the chord, making sure the rear rod was surrounded by enough foam as to not break through a surface if sufficient force arose.

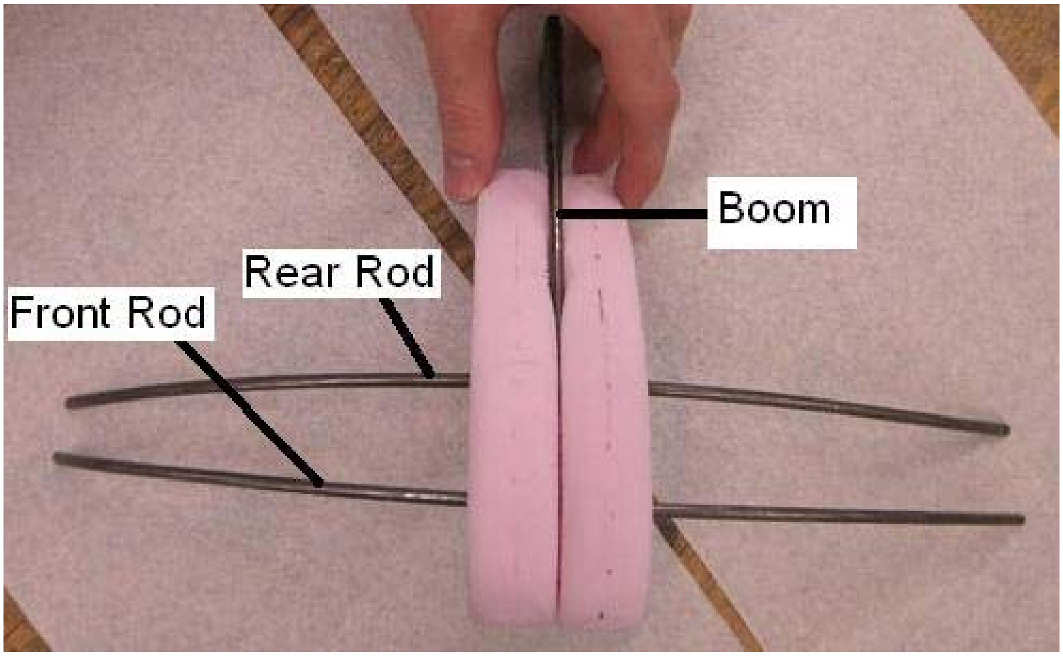

Figure 19: Skeleton Parts

3.3.4 Additional Components

Additionally, a "boom" was welded to the rear rod of each model, in the chordwise direction (perpendicular to the two spanwise rods) so that the models may be connected to the dynamometer; this boom is parallel to the flat section of the bottom surface of each model in order to give a constant geometry throughout the four models. Welded to the rear of the boom is a small steel plate which will then be fastened to the dynamometer connector, through a bolt and flutter-dampening rubber gaskets, among other hardware. The two ¼" spanwise rods, the chordwise boom, and the rear plate all consist of an assembly designated the "skeleton," as seen in Figures 19 and 20. This assembly (built into the core of the models) then inserts into the dynamometer connector - a 1" diameter aluminum rod which has been tapped to match that of the dynamometer threads. On the model-end of the connector rod is a "slit" cut ¼" wide so that each parafoil's steel plate may be inserted and subsequently fastened via the hardware assembly; the plate will be pinched between either side of the connector cradle to ensure a tight fit, as seen in Figures 21 and 22. The bolt allows the models to pivot into different angles of attack, the rubber washers prevent slippage, and the wing nut allows for the models' angle of attack to be easily changed, or the model to be removed from the wind tunnel completely.

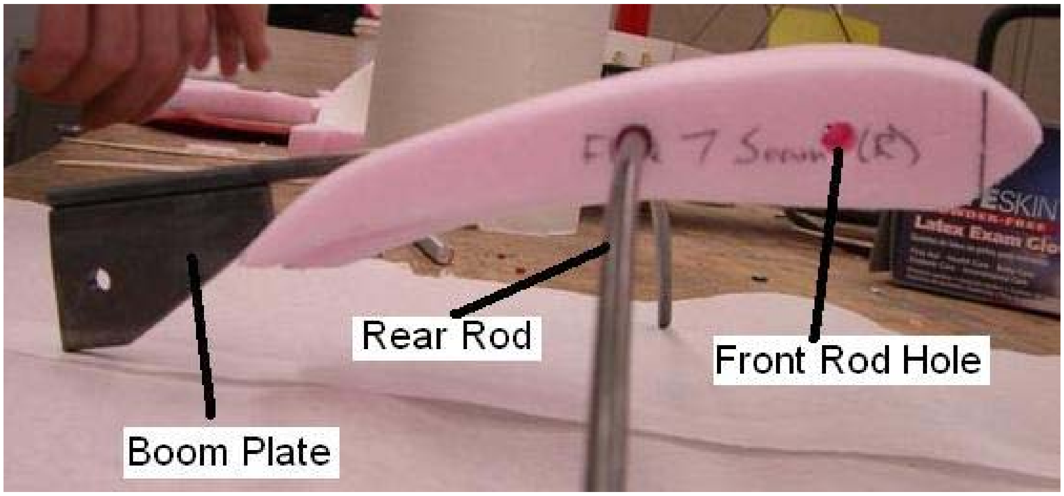

Figure 20: Additional Components

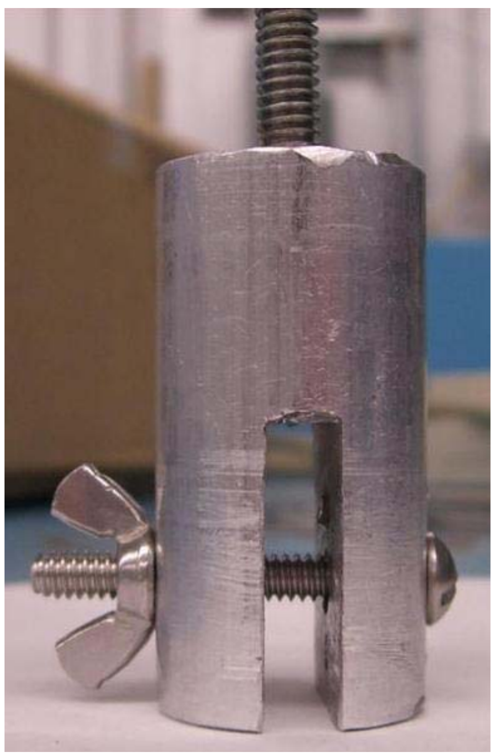

Figure 21: Dynamometer Connector

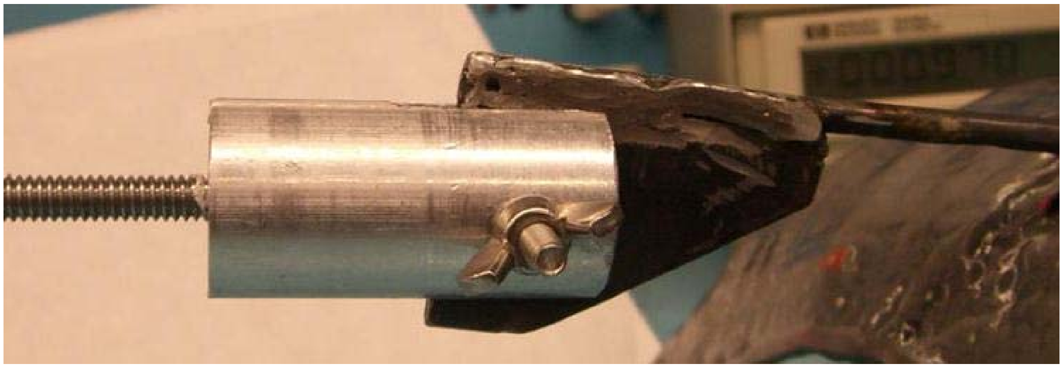

Figure 22: Parafoil Connected to the Dynamometer Connector

Unfortunately, some problems were found after the initial joining of the mounting assembly – the initial design was insufficient and allowed the parafoil to sag. This was remedied by using a flat end mill to countersink a hole equal to approximately half the depth of the rubber washer into the rear plate, as seen in Figure 23. By creating a cavity only half the depth of the rubber washer, the remaining half will be able to contact the opposite side of the dynamometer connector to further prevent slippage. Ultimately it was found that this solution did not fully resolve the problem. As a final measure, it was decided that two holes could be drilled through the aluminum dynamometer connector on the side opposite the rubber washers, and set screws inserted through the holes and coming into contact with the parafoil's end plate to hold the model in place during testing, as seen in Figure 24. This was the decisive provision which ultimately allowed wind tunnel testing to begin, as the entire assembly was impervious to displacement.

Figure 23: Recession for a Rubber Washer

Figure 24: Set Screw Solution

In order to attach the foam, balsa, and skeleton, an adhesive was needed which would not chemically react with the foam. As most adhesives “melt” foam, it was decided to implement epoxy for this task, and when cured, it was found to be extremely hard and would provide a good seal throughout. While integrating the foam sections and balsa ribs onto the spanwise force distribution rods, each piece was adequately bonded to the adjacent piece, resulting in a “rock solid” internal structure after the epoxy cured. To prevent the parts from simply sliding off of the rods or becoming loose while the epoxy cured, a piece of tape was temporarily stretched over the upper and lower surfaces to keep the model in compression. Incidentally, the same epoxy was used as a final coating over the entire outer surface, to be discussed later.

Following the completion of the internal structure, a solid trailing edge was built so as to have a relatively constant edge, as opposed to the previous spacious and jagged edge (Figure 25) in which the ribs and cells resulted. In order to complete this task, strips of balsa approximately 3/8" wide were glued perpendicularly to both the upper and lower surfaces of the trailing edge of the balsa ribs which then created the necessary solid trailing edge structure needed for the models. Additionally, a skin was needed to smooth the area between the rear of the foam and the trailing edge, as it was mostly open air and thus would not be satisfactory if left unfinished. For this, monokote, a model airplane covering was used. Monokote is a heat activated film, which means it shrinks to fit the curvature as it is heated, thus providing excellent coverage especially in crevices and hard-to-reach areas. This was the procedure for the rear of the models only; the leading edges were to be left without a skin.

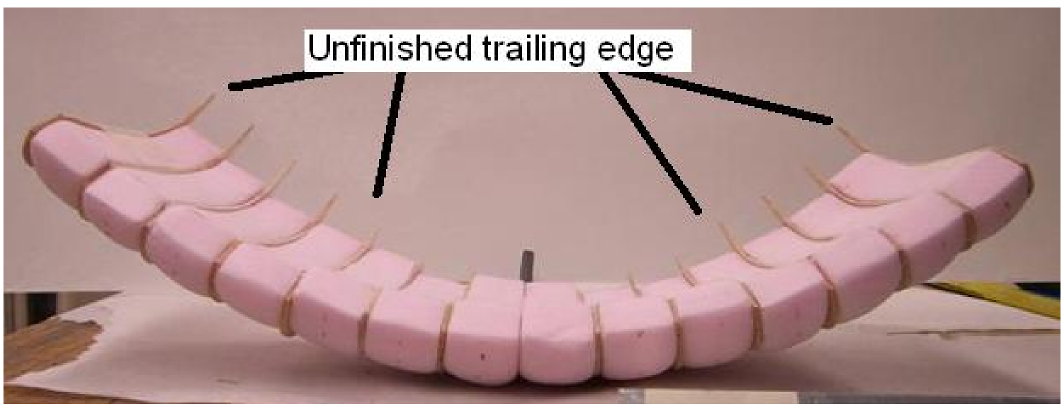

Figure 25: Unfinished Trailing Edge

3.3.5 Coatings and Finishing Operations

In order to strengthen the models throughout and smooth the entire surface, multiple coats of epoxy were brushed onto each model (Figure26); because of the approximate 8 to 10 hour drying time and the multitude of coats applied, this was a time consuming process overall. Each model received approximately five to eight coats of epoxy, depending on the individual model's condition, as some may have been assembled more cautiously than others, thus requiring less coats of epoxy. This process resulted in a smooth hard "shell" over the entire surface which of course reduces the friction drag and adds a higher level of rigidity to the models, making them less susceptible to wear (and accidents).

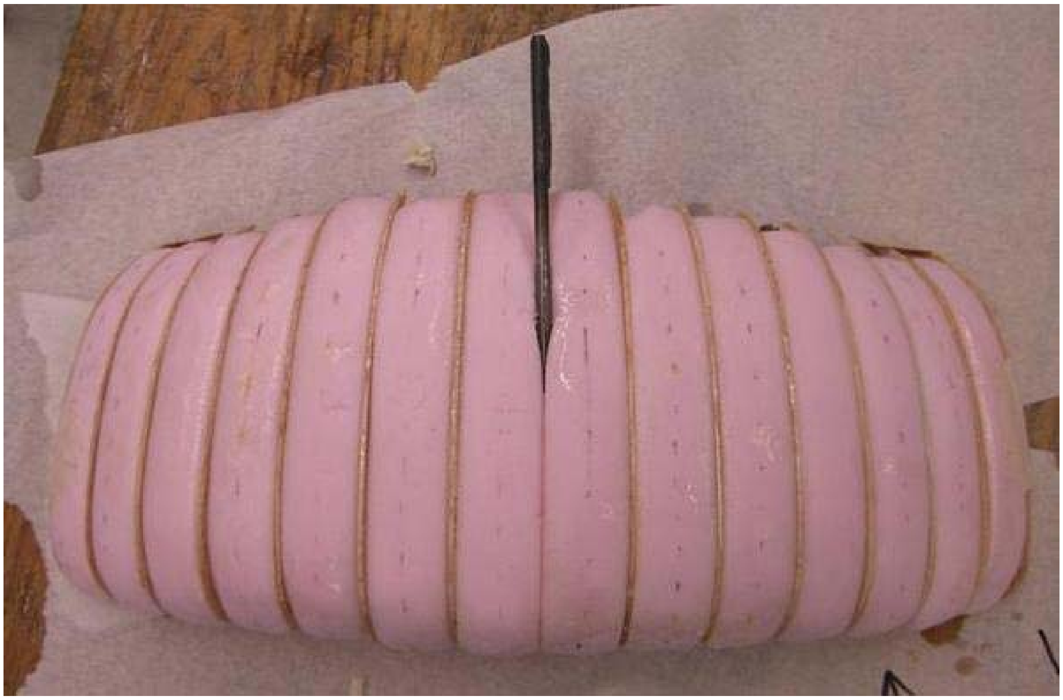

Figure 26: First Coat of Epoxy

After the final coat of epoxy had been applied to each model, it was necessary to sand down the imperfections, i.e. sharp edges of the monokote protruding from the surface, hardened "drips" of epoxy, and general epoxy buildup, especially near the centerline of the lower surface as it bled down the sides while drying. These large imperfections were easily sanded down with a Dremel rotary tool, and the initial sanding took no more than 45 minutes for each model. Following the Dremel sanding stage, secondary manual sanding took place to make the entire surface smooth and to even-out further imperfections. This phase also took approximately 45 minutes per model. After the secondary sanding, it was noticed that every model had other imperfections – mainly: gaps in the epoxy, asymmetry, and holes in the wing tips where the skeleton rods had not completely extended through, just to name a few. With these cases, wood filler was used to patch these holes. Luckily, this compound was quick-drying so that a few hours later, the wood filler could be sanded down to the desired geometry; additionally, multiple applications of wood filler were necessary to be sure most, if not all major imperfections were properly addressed.

Following the smoothing operations, the last step in the construction process was to paint each model a different color for easy identification: Baseline-black, Half Deflection-red, Full Deflection-gray, and Flare Deflection-blue. Two initial base applications were wet sanded to further even out minor imperfections, then two additional layers were applied and sanded to ensure complete smoothness. Additional identifying marks include silver text on each wing tip – the parafoil's geometry (Baseline, Flare, etc) was written on the right wing tip, seen in Figure 27, and on the left wing tip is written a call sign (Figure 28). The identification chapter completed the construction phase of this MQP.

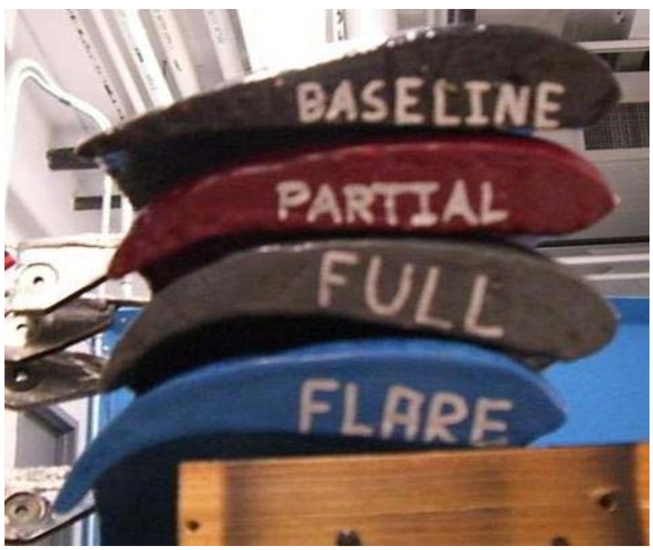

Figure 27: Geometry Descriptions

Figure 28: Call Signs

Completing the multitude of construction phases, the resulting parafoils' dimensions were within 5% of the design specifications. It is important to note that they are each exceptionally sound, structurally, which is beneficial for countering the high forces applied to the parafoils. Additionally, the finishing operations left the parafoils with a magnificently smooth surface finish which is necessary to reduce drag and obtain a surface similar to the actual parafoil modeled. Reflecting on the experience, one advantage to constructing the models independently clearly stands out: in December, the majority of the shop machinists left to pursue other career choices, therefore if the models had needed to be machined this project might be very far behind schedule and may not be able to be completed in the allotted timeframe. Since this project was self-reliant, the work was paced at an appropriate rate, (not delayed by outside assistance) and problems were dealt with immediately by members of the team.

One surprising realization was once a model has finished its construction phase, it was relatively easy to repair if it had become damaged. The initial difficulty in the project was shaping the model and application of the epoxy, however patching a blemish proved to be a simple matter. For example, the boom on the Flare Deflection model became bent (Figure 29), as the model experienced very high lift forces in one experiment. As a result, it was decided to strengthen the boom by re-welding the boom on each model. During the welding of the Flare, the body of the model near where the boom entered the body briefly caught on fire and was left with a small hole and burn marks all around. This mishap was restored by filling the hole with wood filler and covering it with a couple coats of epoxy. Afterwards, the repaired model was indistinguishable from its initial, flaw-free state, before the accident.

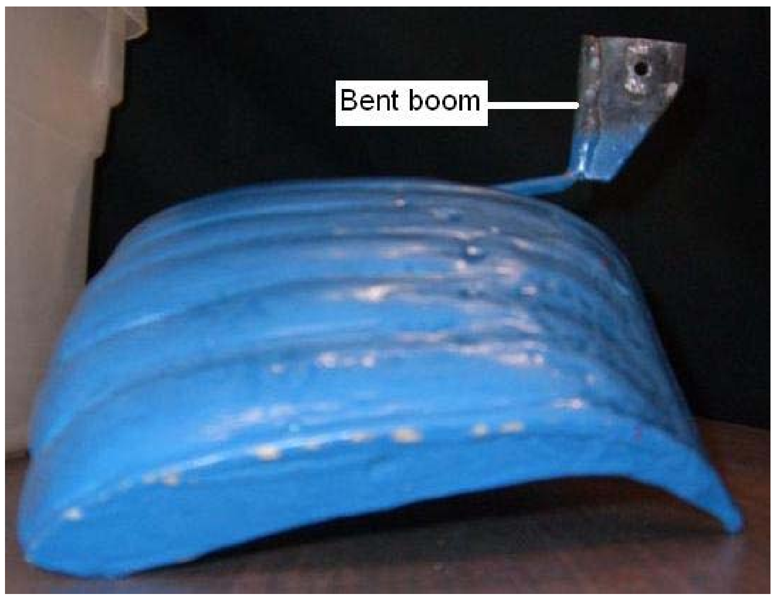

Figure 29: Bent Boom

3.3.6 Project Cost Analysis

This section serves as a justification for following the "handcrafted" route, rather than machining or stereolithography (rapid prototyping). As mentioned before, stereolithography was said to be the most costly, and it was estimated that each wind tunnel model might cost $1,000 or more. This estimate, based on similar-sized objects, is well beyond the budget range of this particular MQP, however, if cost was not a factor, stereolithography would have been the easiest manufacturing process – each model would be complete, to-tolerance, and perfectly symmetrical in a matter of hours and only slight finishing processes would need to be performed.

To machine the parafoil models from aluminum or plastic would be moderately expensive to purchase the raw materials, with "free" machine time via the WPI machine shop in Washburn Shops, utilizing WPI equipment and staff. The decision was weighted more heavily in the direction of the duration of the machining process, which was estimated very early in the project to be 40 hours (probably much more) per model. This time estimate was unacceptable as one MQP project would be selfish to take precedence over more important projects which would be forced to "sit on the back burner."

Ultimately, it was decided that a foam internal structure would provide the best results, for the money. Handcrafting the wind tunnel models mainly via X-acto knives and sandpaper makes the project self-sufficient, and in this way, there are no mechanical malfunctions which could take long periods of time to repair, or absences in staff to lengthen the process – all of the work was performed by the MQP team members. Additionally, as most of the components of the parafoil models were purchased from Home Depot, i.e. not specialty parts, the cost was quite reasonable. A total sum of about $250 was spent on all materials for this project, including foam, steel parts, epoxy, sandpaper, paint, etc. It is certain that stereolithography would result in more precise data, however at a fraction of the price, perhaps 5%, the data obtained from the foam models should be satisfactory.

4. WIND TUNNEL PREPARATION

4.1 Instrumentation

Before testing in the wind tunnel, our group had to become familiar with the equipment that would be used and operated in order to successfully run tests that produce accurate data. The important pieces to this set-up are the following: Meter Cabinet, Dynamometer, Wind Tunnel, an Updated Computer, and finally a Calibration Set. The meter cabinet is basically a display unit for the Pressure, Lift, and Drag readings that are produced from the dynamometer. These values displayed can be adjusted for calibration purposes and other appropriate functions which depend on the experiment. Also, the meter cabinet is equipped with five output channels which correlate with the five readings that it displays. The meter cabinet can be viewed below in Figure 30.

Figure 30: Meter Cabinet

The dynamometer, the most important instrument, is a measuring tool that consists of a couple cantilever beams that are deflected into LVTD sensors which outputs a corresponding voltage. The voltage will have a sign which determines the direction of force upon the cantilever beams. The dynamometer also consists of two adjustment devices for the LVTD sensors, which helps with the calibration process.

4.2 Calibration

Once the group was familiar with the instrumentation, the calibration process was the next step before testing the models in the wind tunnel. This process consists of three main components: dynamometer, meter cabinet, and a calibration set. A calibration set consists of weights that range from 200 gram to 22 kilograms depending on the max weight readings of the dynamometer. The weights gradually ascend from 200 grams to 22 kilograms and can total all together to about 40 kilograms.

The calibration process is used so that the dynamometers readings are consistent with the degree of weight increase on the cantilever beams. This has to be done so that the voltage outputs by the dynamometer can be reliable which makes our data reliable also. The first step is mounting the dynamometer to the table depending on which forces are chosen to be calibrated first. The mounting, as shown below, is for the calibration of the drag forces (Figure 31 Left) and lift forces (Figure 31 Right).

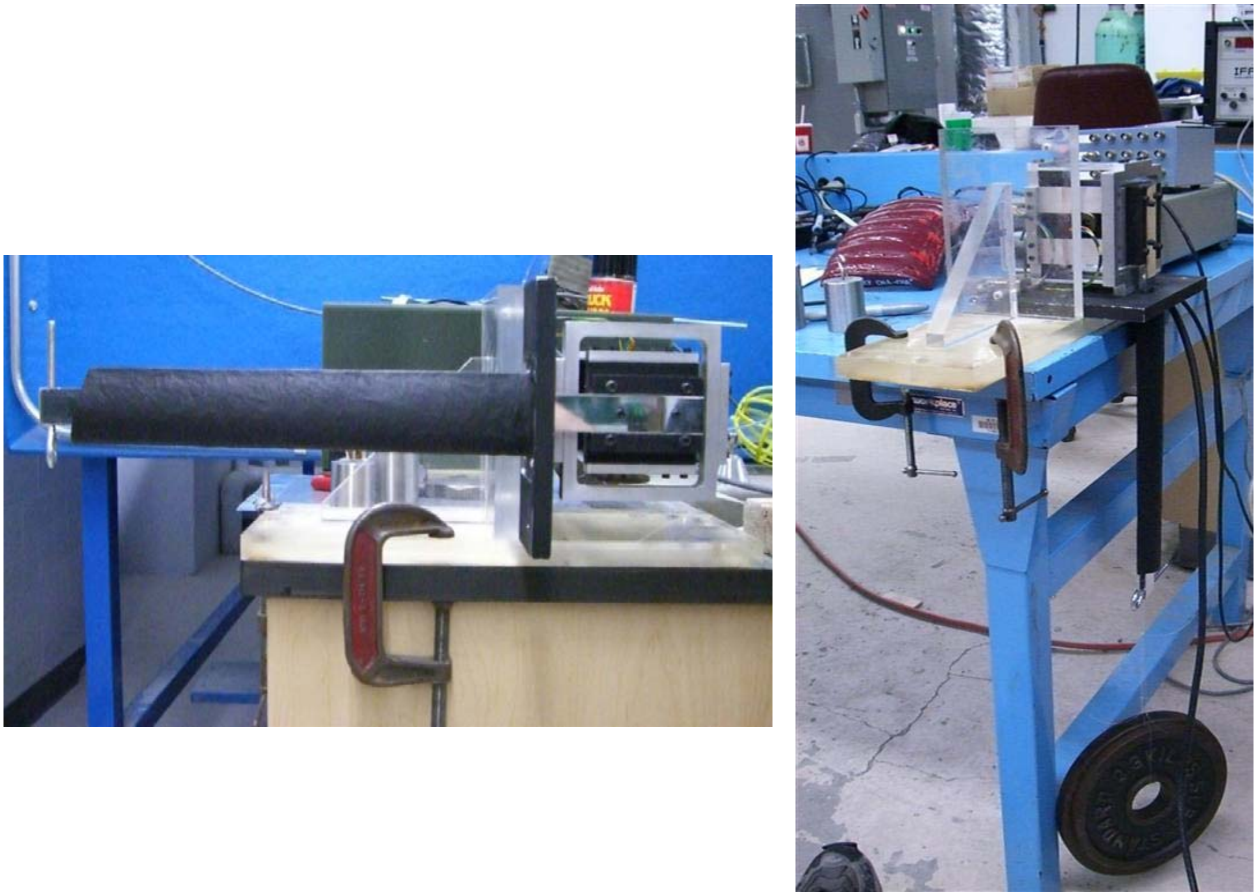

Figure 31: Dynamometer Mounts for Calibration

Once the dynamometer is mounted correctly, the weights can be carefully placed onto the dynamometer stem. After a weight is hung from the stem, the reading from the meter cabinet is recorded in a spreadsheet on the desktop computer nearby. The weights used to calibrate the dynamometer are only appropriate if the expected forces are going to be close to that weight range. For example, if the expected forces for drag are around two pounds of force, then you only want to calibrate the drag up until three pounds of force. Once all of the readings are entered into the spreadsheet with the corresponding weight hanging from the dynamometer, the readings are plotted versus the weights used. From this, a trendline is used to get a line equation for the relationship between the voltage readings and the weight. If the trendline has a reasonable correlation coefficient, at least $R^2 = 0.997$, then calibration for that component is final. If the trendline was not reasonable, then the calibration process was repeated until otherwise. With the appropriate trendline, testing in the wind could begin and the data could be translated into weight forces. Examples of calibration trendlines and resulting equations can be seen in Figures 32 and 33, and an example of the actual meter reading vs. the actual lift force measured can be seen in Figure 34.

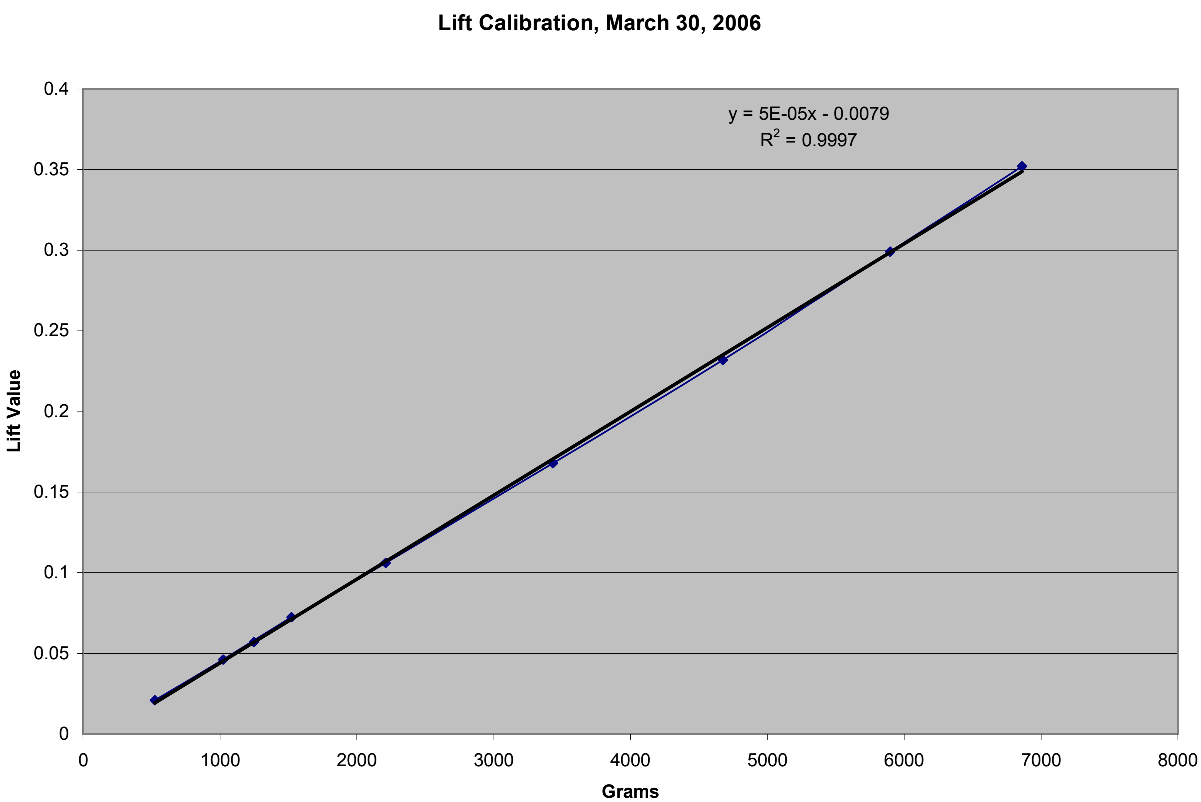

Figure 32: Lift Calibration Example

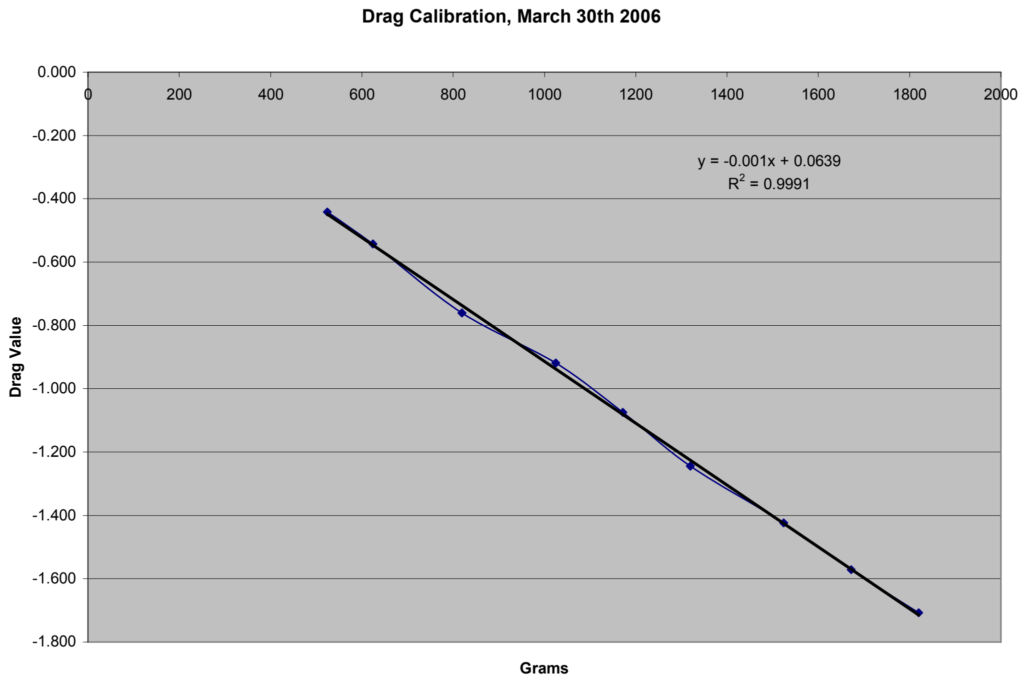

Figure 33: Drag Calibration Example

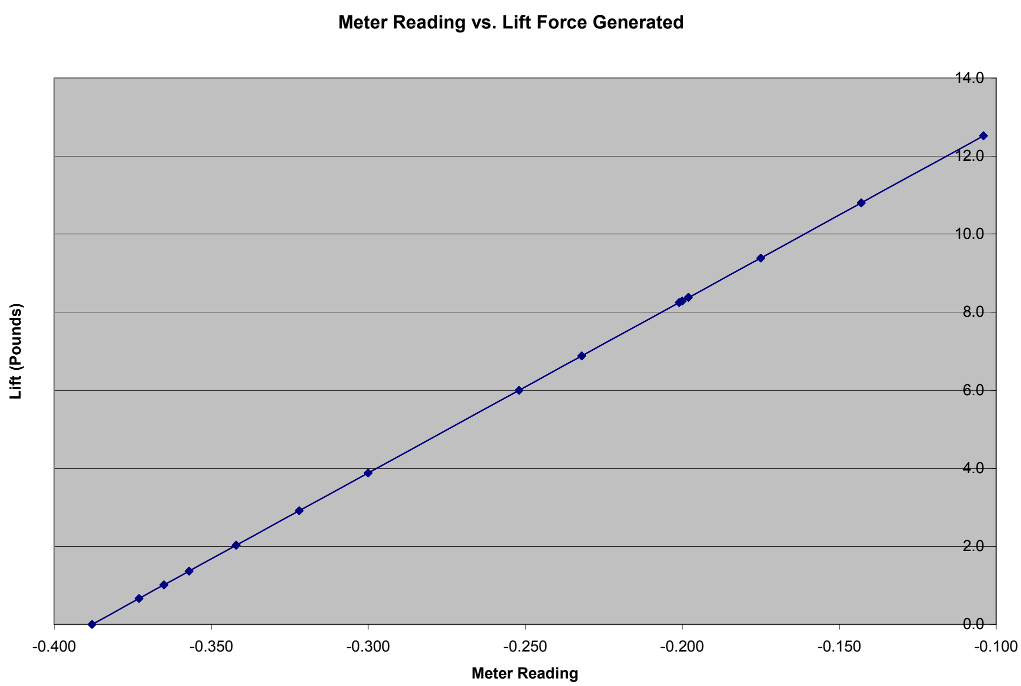

Figure 34: Meter Reading vs. Lift Force Generated

4.3 Mount Setup

When mounting the parafoil in the wind tunnel, the angle of attack was a big part towards accuracy in the wind tunnel. In order to measure the angle of attack, the boom that was designed to connect to the dynamometer was used as shown below in Figure 35. With the digital angle meter resting on the boom the angle of attack could be measured. This wasn't necessary the right angle of attack; in order to get the appropriate angle of attack, the height of the leading and trailing edge was measured to find at what angle on the boom was the actual zero angle of attack for the parafoil. This was done for all models so that the measurements could easily be done with the digital tool and ended up saving a good amount of time.

Figure 35: Measuring the Angle of Attack

4.4 Testing Procedure

The testing procedure after the calibration process is very simple and straight forward. The procedure will be explained by going through one run of a model at one velocity at one angle of attack (side and front views of a mounted model can be seen in Figures 36 and 37).

- Once the dynamometer and meter cabinet are calibrated the model would then be mounted by taking one of the two wind tunnel covers off and setting the model in the tunnel.

- Now that the model is in the tunnel, one of the group members would put their hands through a side hole, and screw on model which is attached to the mounting bracket.

- After the model and bracket are tightened, the angle of attack would be measured by the digital angle meter until it was at the desired angle.

- In order to secure the angle of the model the two set screws on the side of the mounting bracket are tightened and again the angle of attack is examined.

- Now that the model is in the wind tunnel and secure, the wind tunnel cover can be reattached and clamped down.

- After everything is set to be tested, the initial readings of the dynamometer on the meter cabinet are recorded as initial conditions so the difference in voltage reading can be determined, which will give us the component forces when entering into the trend line equation.

- Once the initial readings are taken, the wind tunnel can be started at the first frequency setting.

- After the wind tunnel has reached the desired frequency, another recording will be made off the meter cabinet which will then be done for every velocity after that. Also recorded at every velocity or frequency measurement is the temperature of the air in the wind tunnel. Temperature is also a necessary reading, and can be found on the wind tunnel keypad.

Throughout the testing experience in the wind tunnel, a couple of processes were inconsistent. The calibration procedure was taking a large amount of time and was not resulting in a reliable regression lines at the beginning of testing. After researching the issue and experimenting, it was realized that our meter cabinet is sensitive towards electrical devices and must be moved away from anything carrying current. Another device's electronic waves were interfering with the calibration and consistency of the meter cabinet display. After repositioning our equipment, the calibration process was very consistent and accurate. No more problems occurred after this adjustment.

The second process that gave us trouble was the measuring of the angle of attack for the different parafoils. After adjusting the model to the proper position or angle of attack, the model would then be tightened by set screws. While tightening the set screws it was noticed that the model's angle of attack would change position. This was unfortunate because the movement could not be predicted when tightening the set screws; the movement was inconsistent every time and was a continuous inconvenience. This resulted with inaccuracy in the measure of angle of attack by 0.1 to 0.2 degrees on the digital angle meter.

After completing all the tests for our models, it was noticed that some data points were somewhat off. In result, retests were performed at the desire velocities again and the angle of attack was accurately measured also. This was done by measuring the leading and trailing edge in order to determine the angle of attack and consistently measured while adjusting the set screws. The data was recorded and used appropriately.

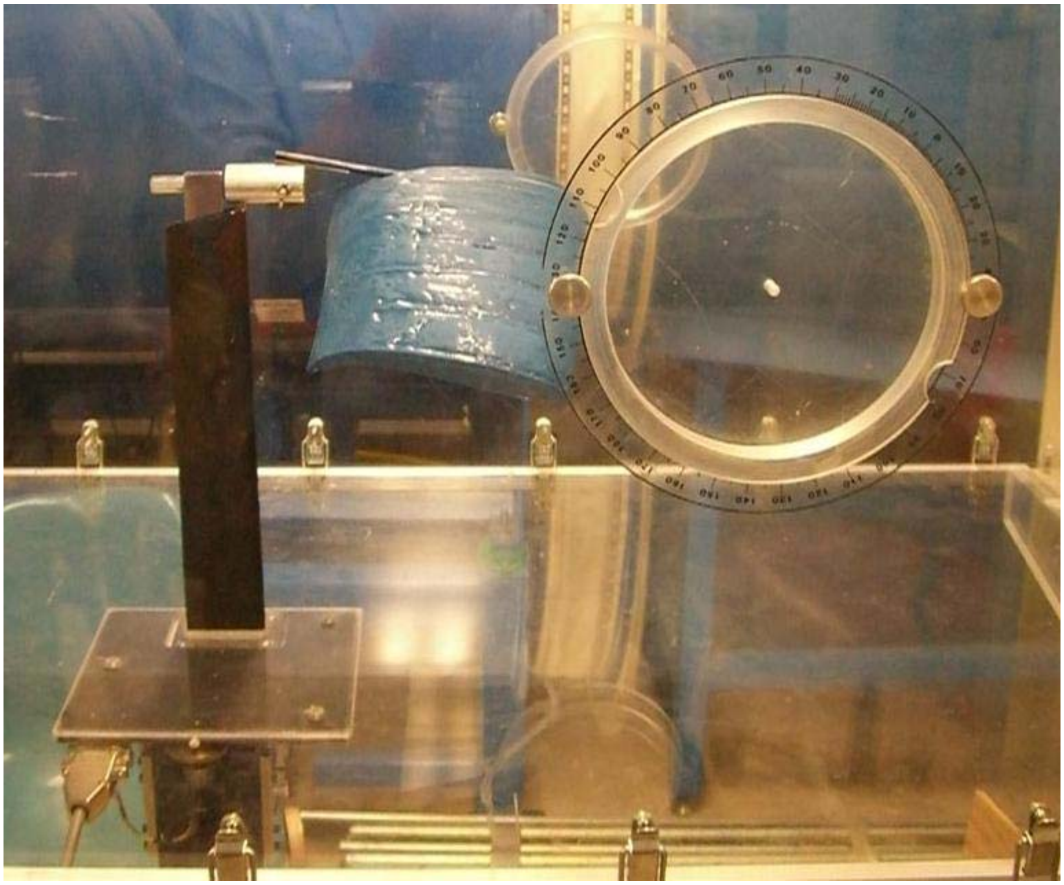

Figure 36: Side View of a Mounted Parafoil

Figure 37: Front View of a Mounted Parafoil

5. RESULTS

5.1 Lift Results

5.1.1 Baseline Deflection Results and Data Analysis

The lift results of the testing of the baseline deflection parafoil plotted against Reynolds number are shown in Figure 38, below. The test data for this parafoil and the other deflections can be found in Appendix A.

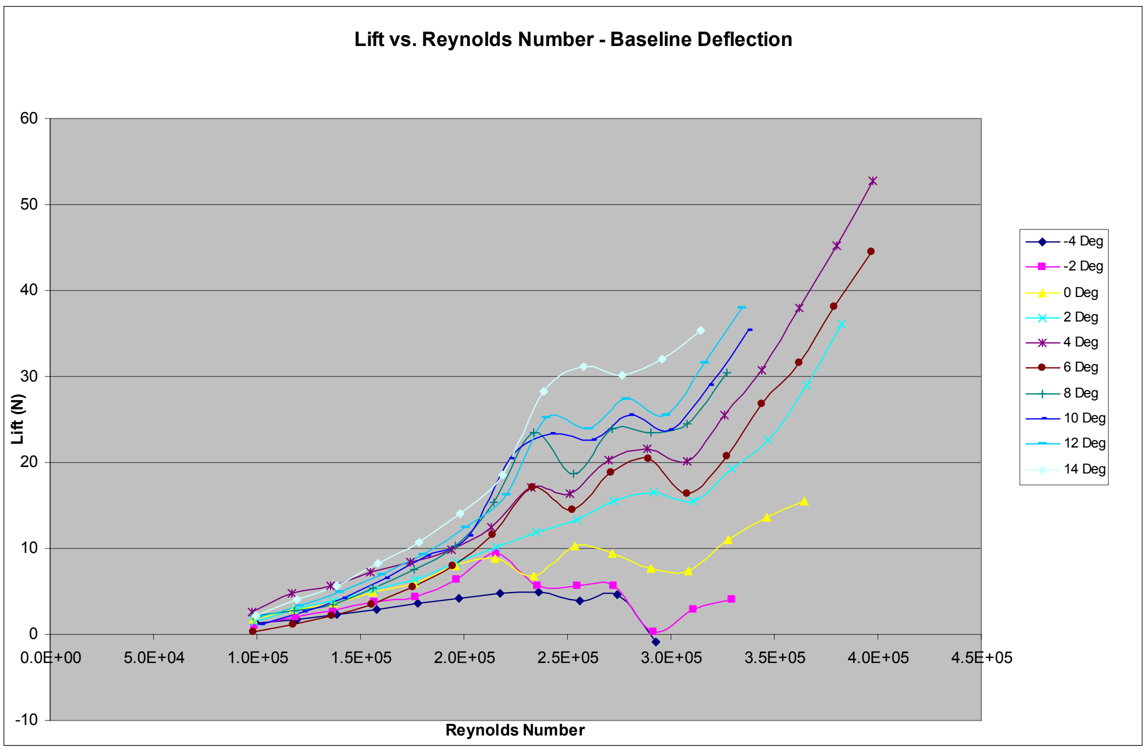

Figure 38: Lift vs. Reynolds Number - Baseline Deflection

What is most apparent in the data is the “dip” which occurs in the 250,000-285,000 Reynolds number range. Flat plate theory, according to Elert [7], has suggested that a critical Reynolds number is reached in the 300,000 to 500,000 range, though it cannot be solved analytically. Historically, the critical Reynolds number is determined for any given object, in this case the parafoils, experimentally. Wikipedia [8] states “The transition between laminar and turbulent flow is often indicated by a critical Reynolds number (Re_{crit}), which depends on the exact flow configuration and must be determined experimentally. Within a certain range around this point there is a region of gradual transition where the flow is neither fully laminar nor fully turbulent, and predictions of fluid behavior can be difficult."

As the data plots show, contrary to the Wikipedia definition, the fluid behavior within this transitional flow region can be predicted somewhat accurately, as the lift-force behavior at varying angles of attack follow a similar pattern. While this is an intriguing behavioral characteristic, it is not useful in determining flow characteristics for full scale parafoils.

Flow fields over a full scale parafoil, such as a Strong Enterprise sport parafoil, are fully turbulent, with Reynolds numbers in the tens of millions. Therefore, much of the data collected within this experiment does not accurately transfer to the full scale case. For the purpose of useful information, data taken with a Reynolds number of 305,000 will be considered in all calculations. This Reynolds number is outside of the Re_{crit} range, with the flow behavior performing similarly to other turbulent regions (Re > 10,000,000).

Unfortunately for the purposes of this project, this deems more than two thirds of all collected data relatively useless, as it lies within the laminar and transitional fluid flow regimes. The majority of the discussion regarding the results of the testing is in reference to those tests in the turbulent regime, particularly at Re = 305,000.

To illustrate the difference in coefficient of lift between the flow regimes, the plots in Figure 39 show coefficient of lift against angle of attack for Reynolds numbers = 305,000.

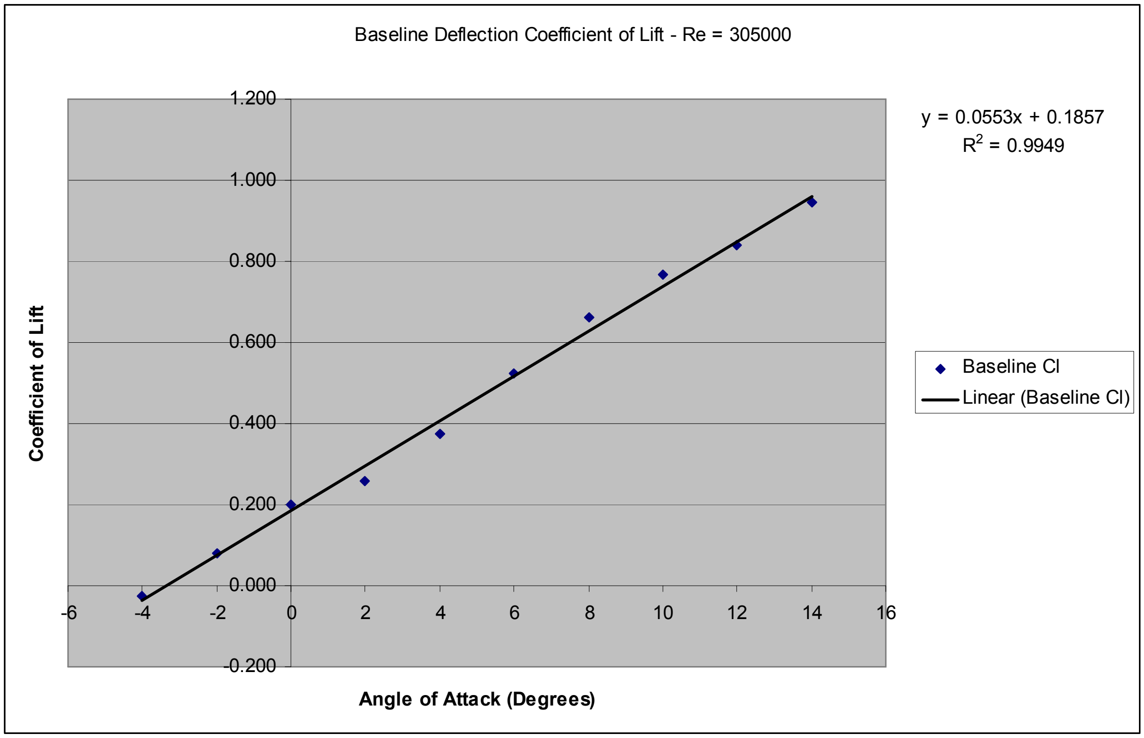

Figure 39: Baseline Deflection Coefficient of Lift at Re=305,000

The maximum coefficient of lift recorded was 0.945 at an angle of attack of 14 degrees. The linear regression equation plotted against the gathered data shows both the efficiency of the wing (5.53%) and the coefficient of lift generated at a zero degree angle of attack (0.1857), indicative of a cambered airfoil. Compared to historical trends, the baseline deflection parafoil's efficiency and coefficient of lift are much lower than the Wortmann FX 63-137's outputs (Figure 40) of approximately 10.25% and 0.73, which were found from the Nihon University Aero Student Group website [9].

The most redeeming attribute of the collected data at Re = 305,000 is the regression coefficient, R^2 of 0.9949. This follows the linear aerodynamic principle that coefficient of lift is a function of angle of attack alone. The validity of this principle allows the baseline deflection parafoil's loading data to reliably be used as a reference when predicting changes in coefficient of lift during deflection maneuvers. As the baseline deflection also is the standard parafoil deflection state during steady-level flight, partial deflection, full deflection, and flare deflection data will be plotted against this standard in order to determine future coefficients of lift.

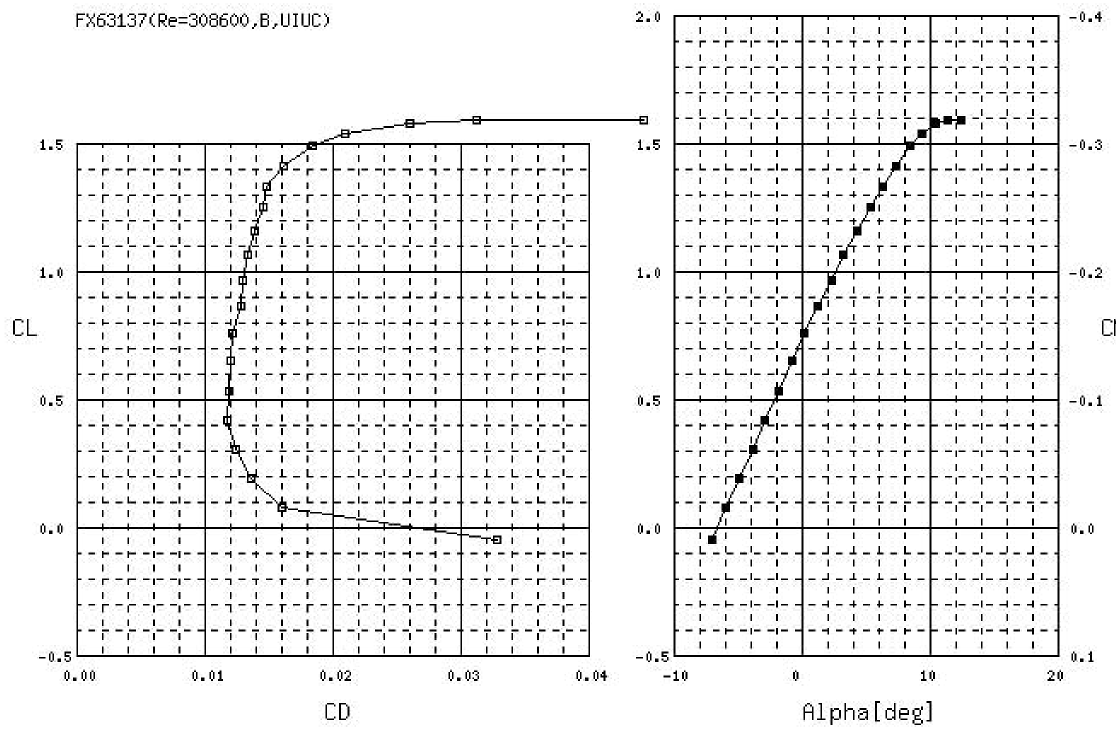

Figure 40: The FX63-137 (Similar Airfoil) Plots at Re = 308,600

5.1.2. Partial Deflection vs. Baseline Deflection

Figure 41 shows the lift generated by the baseline deflection versus Reynolds number. The subsequent plots, Figures 42 and 43, depict the coefficients of lift generated at various angles of attack and Reynolds number = 305,000, as well as comparing this coefficient of lift data to the baseline condition.

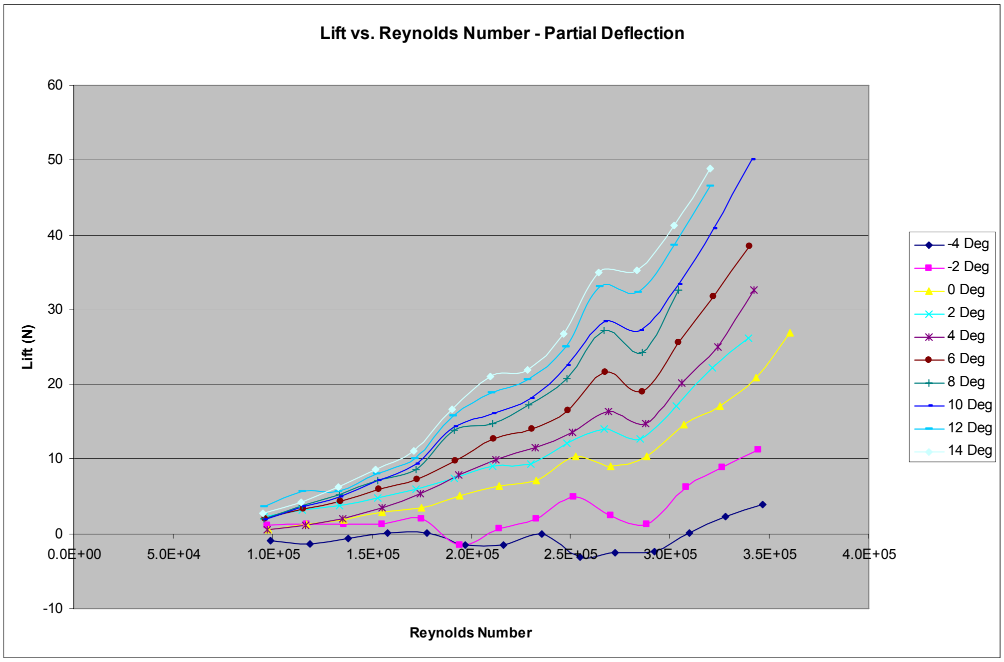

Figure 41: Partial Deflection Lift vs. Reynolds Number

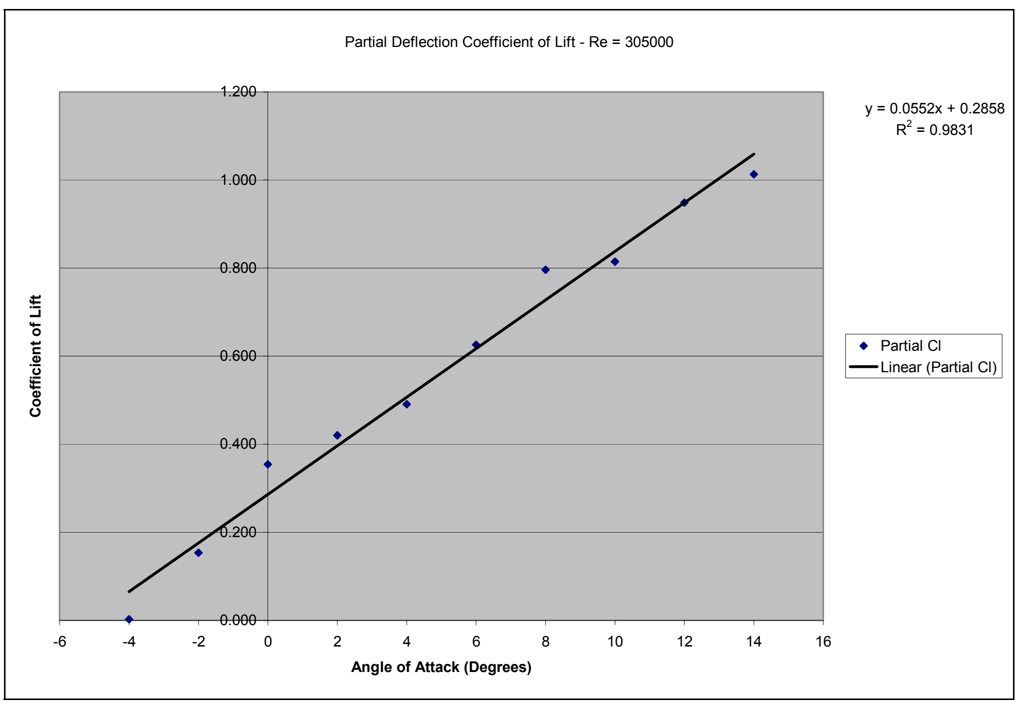

Figure 42: Partial Deflection Coefficient of Lift - Re = 305,000

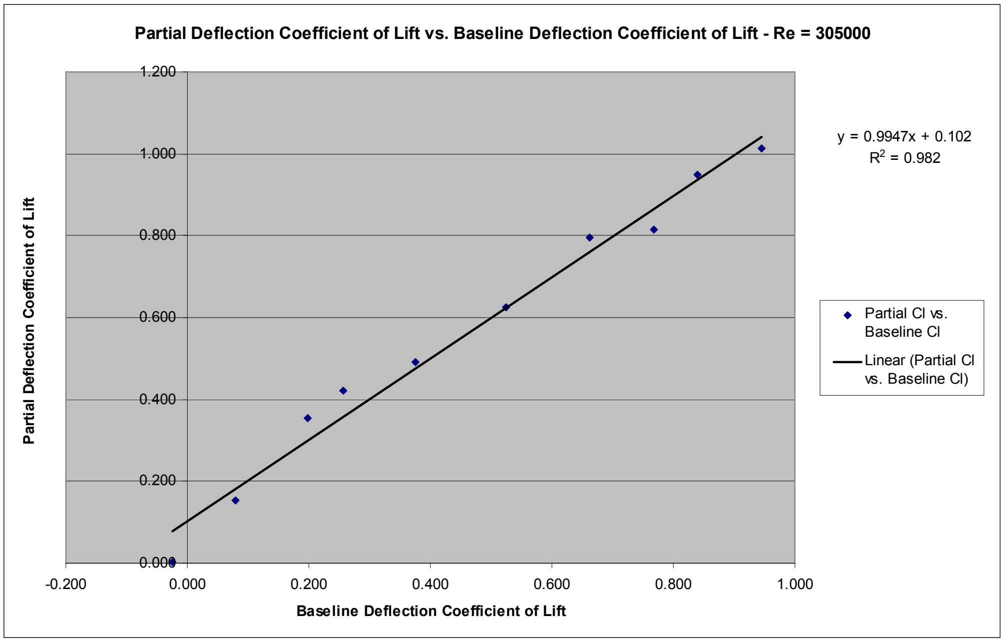

Figure 43: Partial Deflection Coefficient of Lift vs. Baseline Deflection Coefficient of Lift - Re = 305,000

Similar to the baseline deflection condition, the partial deflection parafoil had a lift efficiency of 5.52%. The lift generated at a zero degree angle of attack, however, increased dramatically from 0.1857 to 0.2858. When coefficient of lift plots at Re = 305,000 are plotted against each other in Figure 43, the linear regression depicts both the relative efficiency in lift generation and the increase in coefficient of lift. These numbers are 99.47% and 0.102, respectively. As both coefficient of lift plots are linear by theory, and confirmed with the near 1 values of R^2, the resultant comparison plot of Figure 43 also should be linear, with a R^2 value of 0.982.

The partial deflection parafoil is indicative of the initial stages of performing a flare deflection, along with providing accurate loading data for the "intermediate gores" of the flare deflection parafoil. Both the partial and full deflection states are purely theoretical, 2-D representations of intermediate or end gores of the flare deflection extended across the entirety of the span of each respective deflection state.

This loading data, particularly in comparison to the baseline deflection, can be used in computational fluid dynamics programs to predict the loading responses of certain gores during a flare deflection, with a **coefficient of lift increase of 0.102**. As noted earlier, this applies to the "intermediate" gores when the flare deflection is completed, but will also resemble end gores during the initial stages of the flare deflection maneuver.

5.1.3 Full Deflection vs. Baseline Deflection

Once the theoretical canopy lines have been completely extended and the full deflection state created, significantly greater lift appears. During the testing of the previous deflections (baseline and partial), a large range of velocities could be tested, allowing for accurate comparison at the high end of the available tested Reynolds numbers. However, the increased lift generated by the full deflection limited the velocity range, and therefore the Reynolds numbers, in which testing could be done. This was dramatically brought to realization when excessive lift (> 15 pounds) was generated while testing the flare deflection, creating failure at the boom. The picture below (Figure 44) shows the resulting failure.

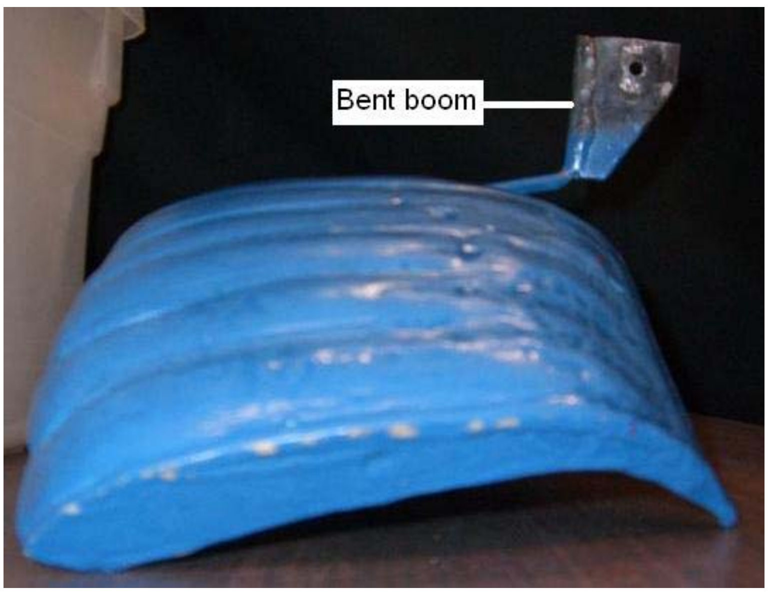

Figure 44: Critical Failure the Boom of the Flare Deflection

Erring on the side of caution, the turbulent flow regime (Re > 300,000) was only entered at angles of attack lower (not including) than 10 degrees. The results of the testing are plotted below in Figure 45.

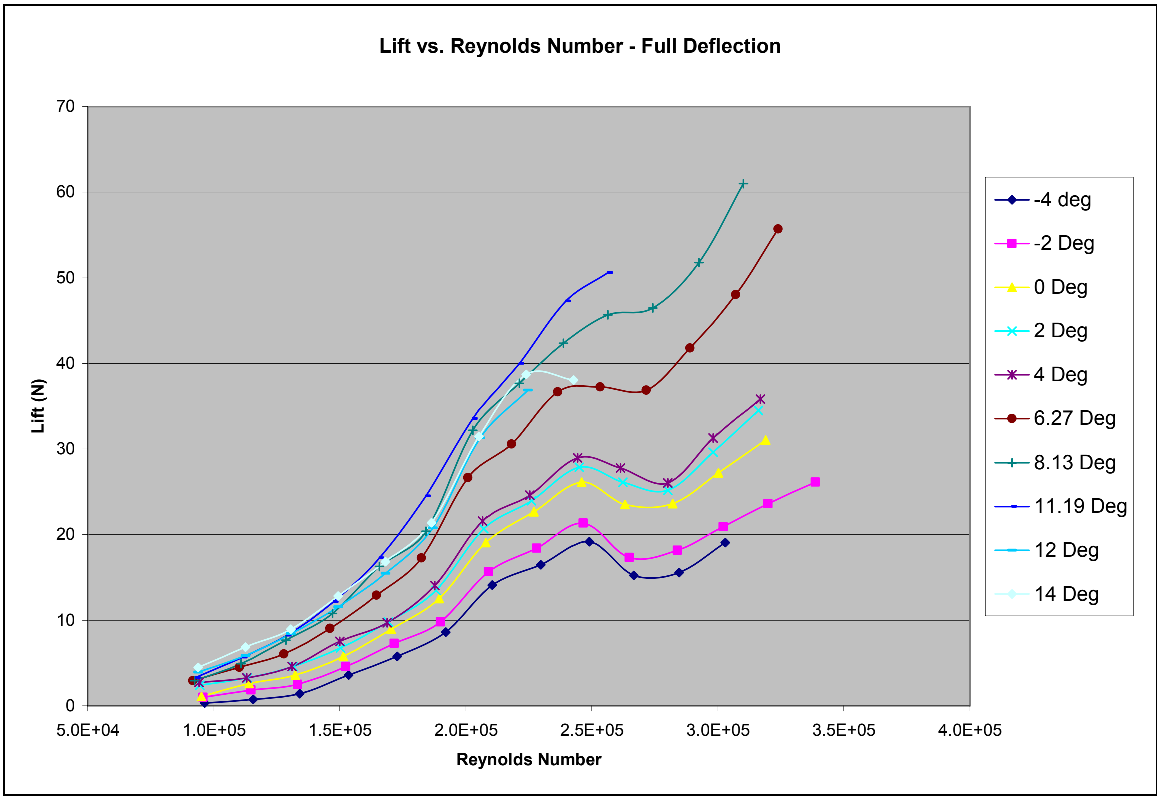

Figure 45: Full Deflection Lift vs. Reynolds Number

While a Reynolds number of 305,000 could not be obtained at angles of attack greater than nine degrees, the coefficient of lift data gathered for the lower angles of attack is plotted in Figure 46. The sample is notably smaller, using only seven data points to form the regression. The linearity of the data may have suffered as a result of this with a R^2 value of only 0.9092, although the full deflection was notably less stable and displayed moderately violent oscillations during testing at higher Reynolds numbers. Nonetheless, the efficiency of lift generated was 7.3%, a notable increase over the 5.5% of the baseline deflection and partial deflection. The coefficient of lift at zero degree angle of attack also was dramatically higher, at 0.6952.

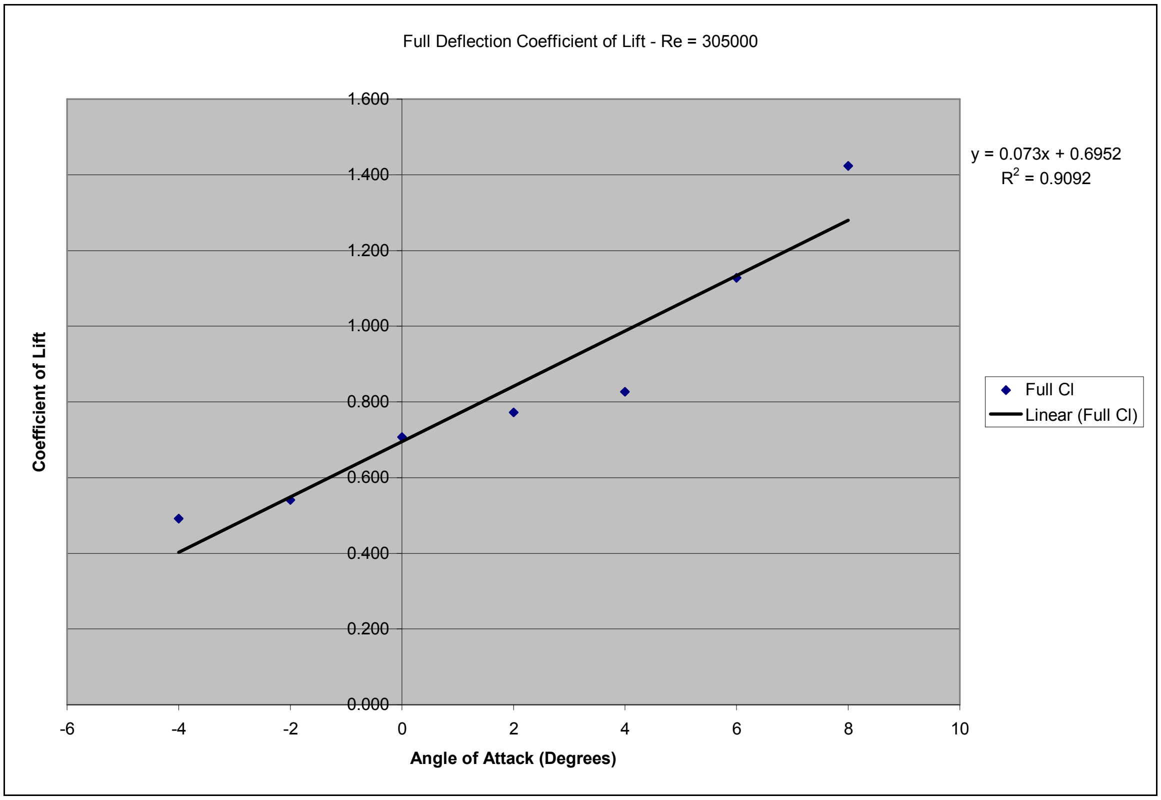

Figure 46: Full Deflection Coefficient of Lift - Re = 305,000

The comparison plot of the full deflection coefficient of lift versus the baseline deflection coefficient of lift is plotted in Figure 47. The regression of this plot shows the notable increase in efficiency of generated lift at slightly above 33% and a dramatic **increase of coefficient of lift of 0.4474**. Again, the full deflection is only a theoretical state, designed to model the end gores of a parafoil in a completed flare deflection and therefore these lift numbers would not occur normally across the entire span of the parafoil.

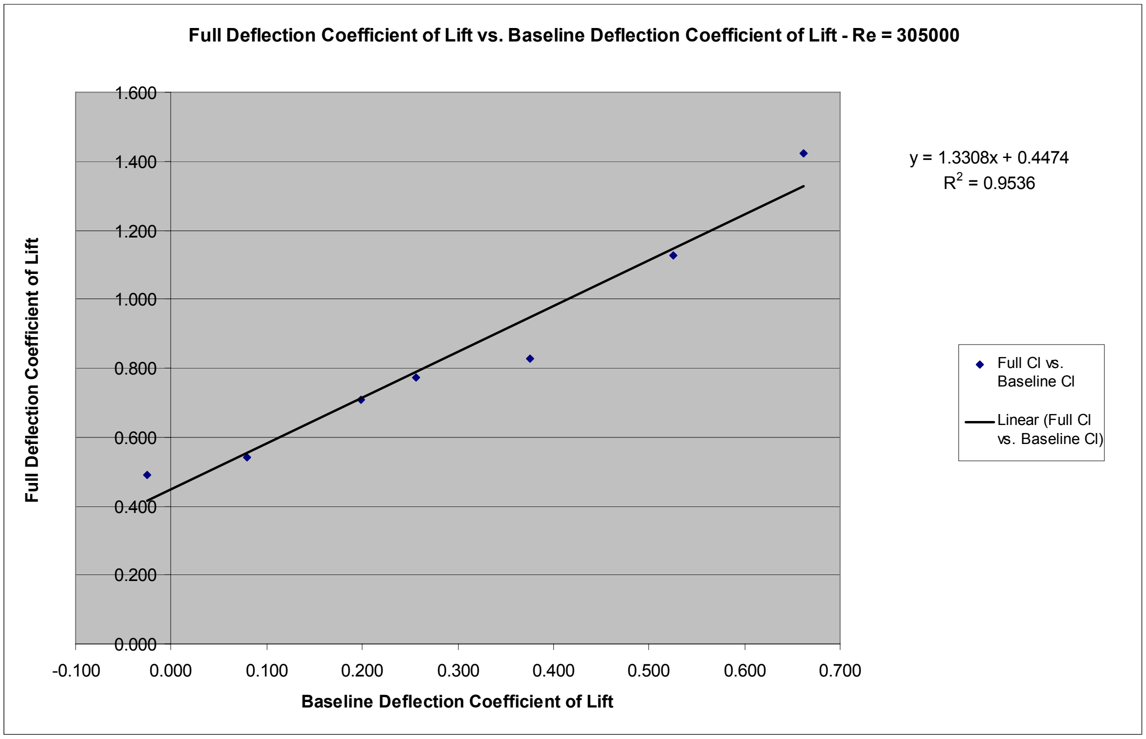

Figure 47: Full Deflection Coefficient of Lift vs. Baseline Deflection Coefficient of Lift - Re = 305,000

5.1.4 Flare Deflection vs. Baseline Deflection

The test results obtained from the partial and full deflection are, when applied to a real-life situation, fictional. This is due to the configuration of the suspension lines attached to the parafoil. When the suspension lines are pulled, only the end cells are deflected, with the center cells still resembling those of the baseline deflection condition. This creates the “flare” appearance. In such a case, varying segments of the parafoil will have aerodynamic properties resembling all three of the prior studied cases.

What must be noted is that there is no one “definitive” angle of attack for such a case, as the definition of angle of attack is measured from the trailing edge to the leading edge in reference to the flow direction. Instead, an “average” angle of attack was taken, using the third seam from each tip as a reference frame. If a different frame of reference were used, a horizontal translation would occur on the coefficient of lift versus angle of attack plots, though the efficiency of lift generated would be the same. The results of the testing are plotted below in Figure 48.

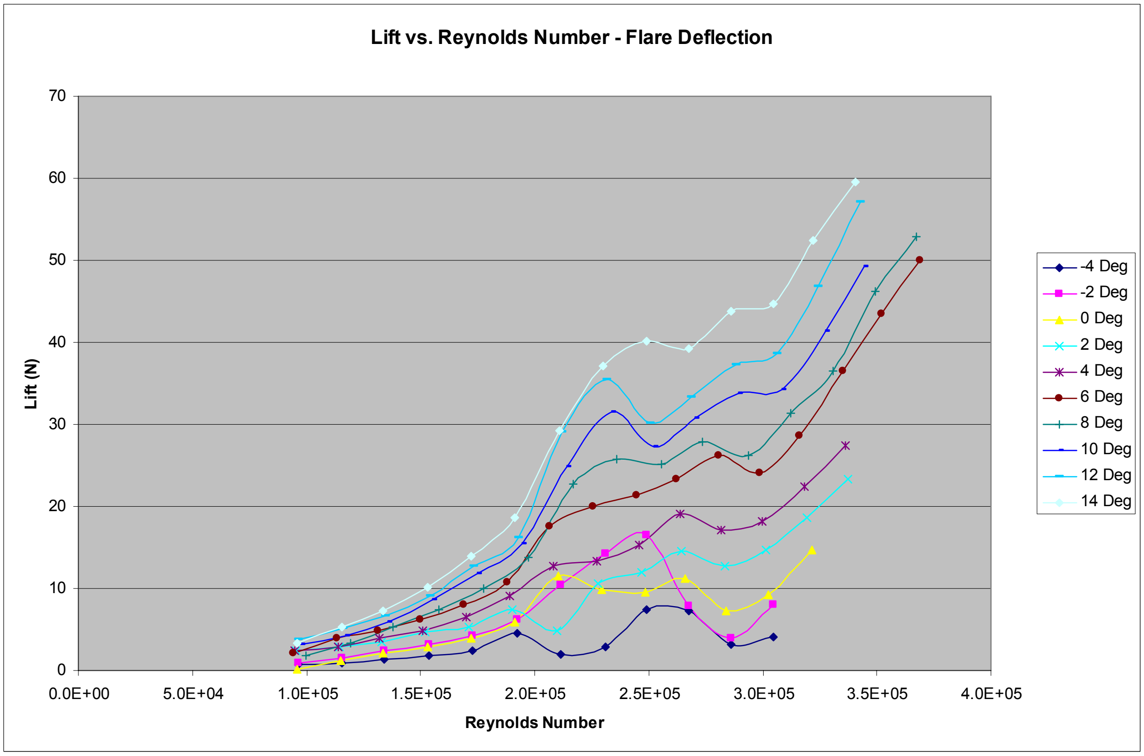

Figure 48: Flare Deflection Lift vs. Reynolds Number

Figure 49 below plots the coefficient of lift for the flare deflection at a Reynolds number of 305,000. The efficiency of lift generated was 5.68%, an increase over both the baseline deflection and partial deflection, but also significantly less than the 7.3% of the full deflection. This is logical, as the flare deflection is composed of the baseline, partial, and full deflections, with the full deflection being the most extreme end. The zero angle of attack coefficient of lift was 0.31 and, while this fits appropriately as a combination of the other deflections, is also debatable for the uncertainty of the angle of attack, described earlier, and may be slightly higher or lower depending upon the interpretation of the angle of attack.

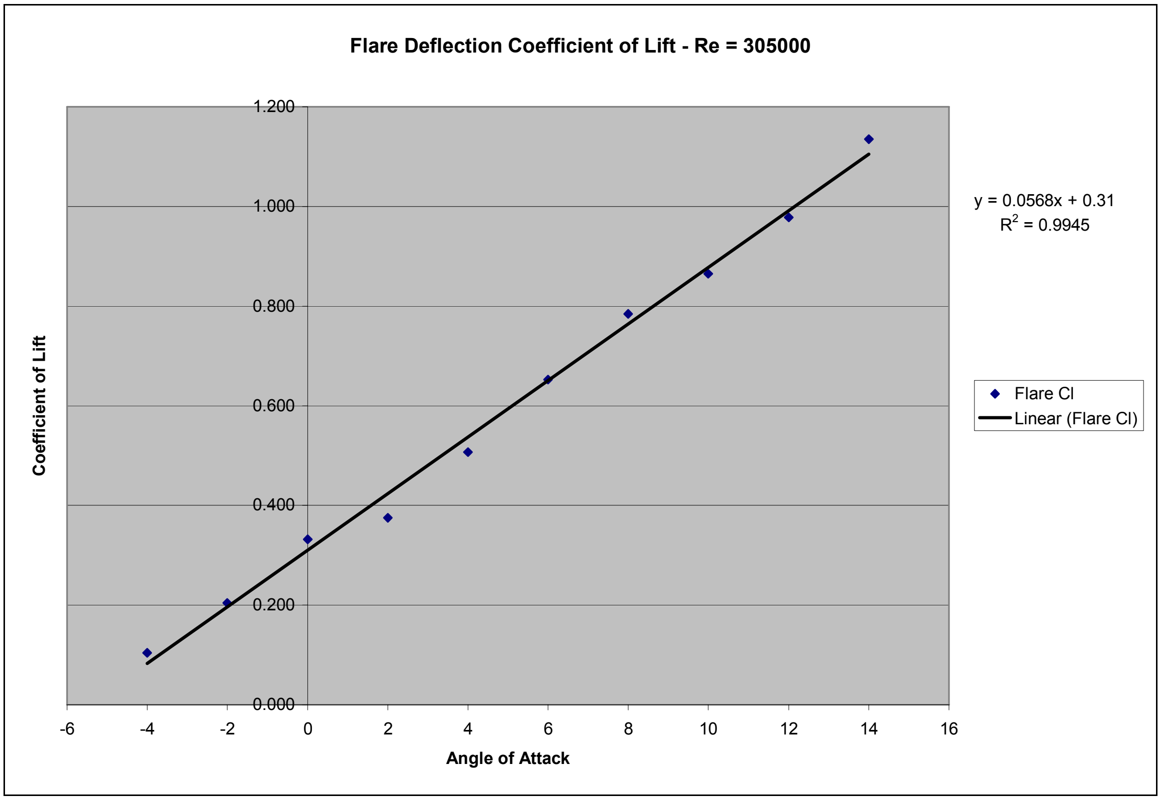

Figure 49: Flare Deflection Coefficient of Lift - Re = 305,000

For a Reynolds number of 305,000, the plot of the flare deflection coefficients of lift against those of the baseline deflection yields Figure 50. The data is extremely linear, with a R^2 value of 0.9958. Compared to the baseline, the efficiency of the flare deflection is 102.3% and **an increase of 0.1205 in coefficient of lift** can be expected during the deflection maneuver.

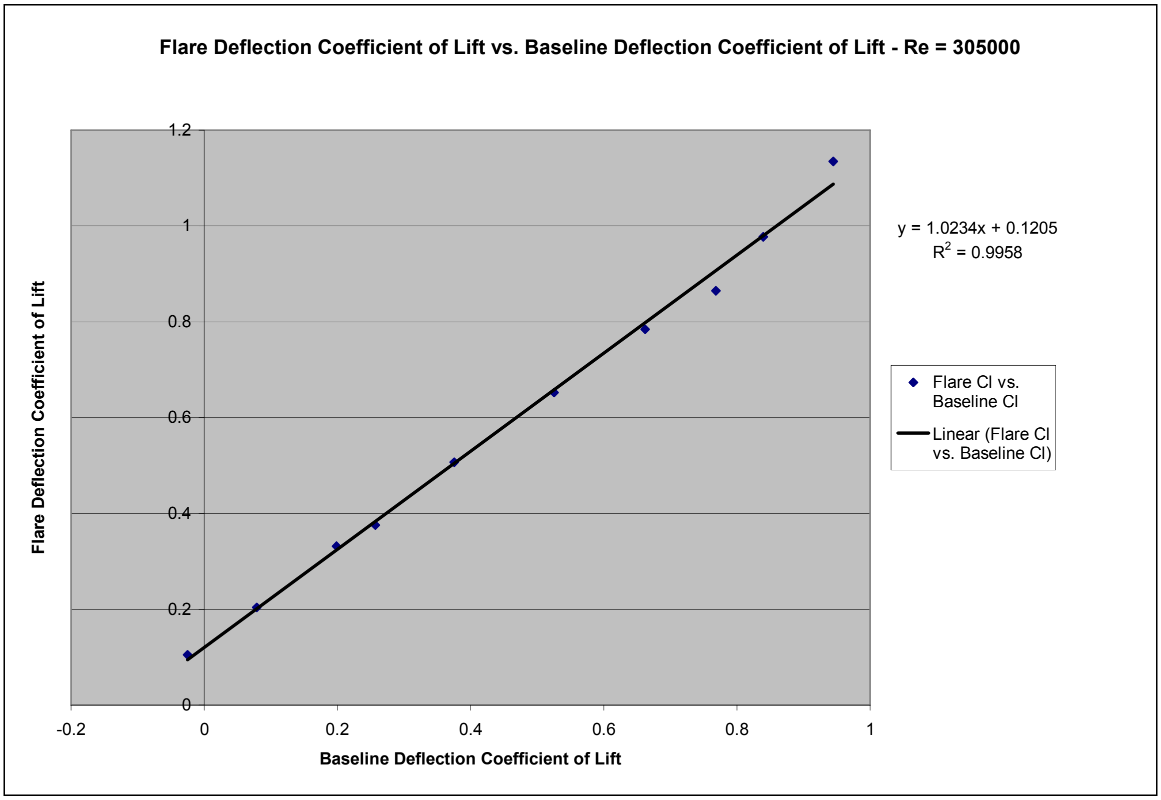

Figure 50: Flare Deflection Coefficient of Lift vs. Baseline Deflection Coefficient of Lift - Re = 305,000

5.2 Lift Results Discussion

While the data collected during the course of this project did not follow the expected values, the expected aerodynamic trends were all present and loading changes can still be accurately predicted during the deflection maneuver.

One of the more interesting segments of the collected data occurs in the transitional regime, in the 230,000 < Re < 300,000 range. The lift graphs are consistent in the behavior of the drop off characteristics, functioning similarly to stall effects. However, applying this to a situation using a full-scale parafoil, the velocity when the parafoil is deployed is great enough to place the lift well into the turbulent regime, and thus these effects will never be experienced.

The useful information gathered within the project pertains mainly to the relation of coefficients of lift at similar angles of attack but different trailing edge deflections. However, this is not the case in the performance of an actual deflection. The action of a flare deflection maneuver is a dynamic situation, with the angle of attack constantly changing. The comparative results discussed in the previous section are for a constant angle of attack, which is a situation which will not occur. As a compromise to theorize what the actual change in coefficient of lift will be during the flare maneuver, another part of the parafoil was held constant instead of the angle of attack. The table below illustrates the angle of attack for each parafoil deflection state when sharing a constant lower leading edge, fixed at zero degrees.

Deflection	Angle of Attack
Baseline	7.960º
Partial	10.635 º
Full	20.695 º
Flare	17.676 º

Table 2: Angle of Attack With a Constant Lower Leading Edge

Translating these relative to a zero degree angle of attack for the baseline condition, to which the rest of the deflections are related in the data.

Deflection	Angle of Attack
Baseline	0 º
Partial	2.675 º
Full	12.735 º
Flare	9.716 º

Table 3: Angle of Attack Relative to the Baseline Deflection

Applying these numbers to the situation of executing a deflection, it shows that the angles of attack will not be held constant during the maneuver. Therefore, the relative lift efficiencies and increases of coefficient of lift, such as 102.3% of the baseline efficiency and a 0.1205 coefficient of lift increase during a flare deflection, is only partially accurate. In order to accurately predict the lift forces generated during a flare type maneuver, an analysis must be done to predict the change angle of attack during the maneuver. This could be accomplished by analyzing video of flare maneuvers from a side angle. Unfortunately, this type of video isn't readily available and attempting to film such a thing is beyond the scope of this project.

Should such data become available, however, it would be simple to create new plots using the data collected during these experiments, all of which can be found in Appendix A.

If one was to assume that the leading edge would be fixed in space during a flare maneuver, then the effective angle of attack would be increased by 9.716 º, as shown in Table 3. Approximating with a 10 º increase, the following table of forces (Table of 4) is generated under turbulent flow conditions, with the plot shown below in Figure 51.

Baseline AoA	C_L	Flare AoA	C_L
-4.00	-0.024879723	6.00	0.6523
-2.00	0.078988375	8.00	0.7844
0.00	0.198299609	10.0	0.8651
2.00	0.256952676	12.0	0.9778
4.00	0.375476484	14.0	1.1348

Table 4: 10 Degree Offset Angle of Attack of Flare Deflection vs. Baseline Deflection

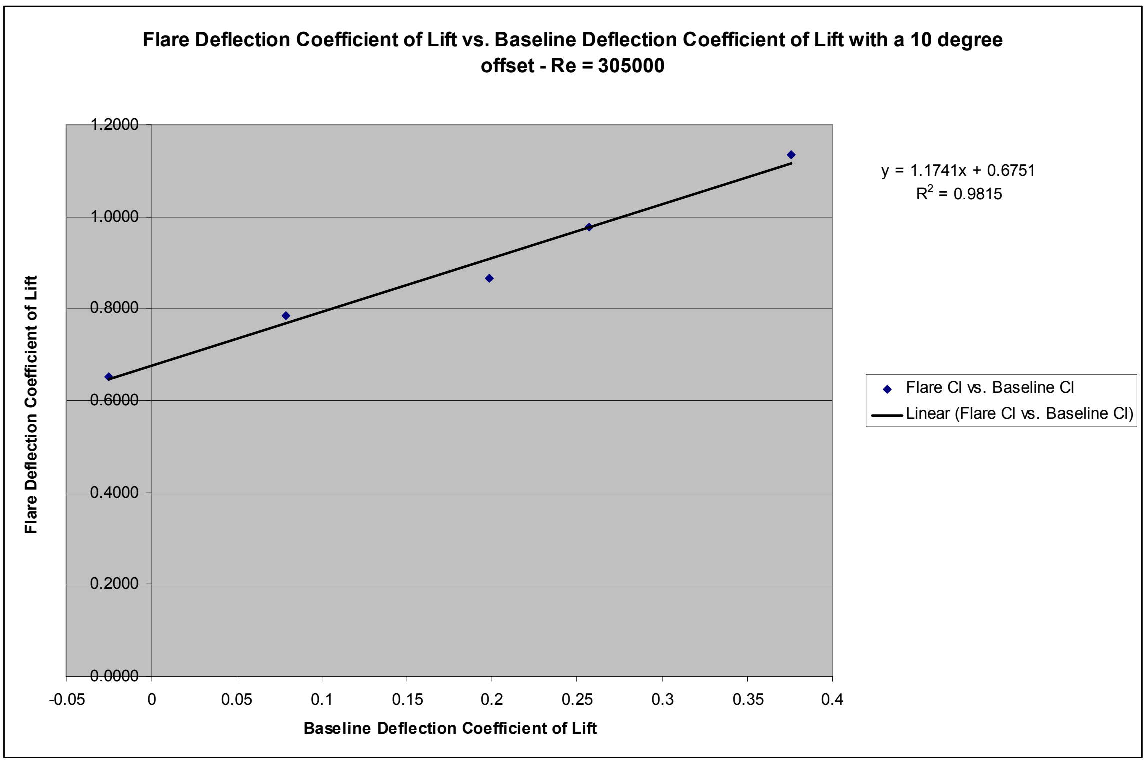

Figure 51: Flare Deflection Coefficient of Lift vs. Baseline Deflection Coefficient of Lift with a 10 Degree Offset - Re = 305,000

The regression of Figure 51 shows that the lift generation efficiency with this 10 degree translation is 117.4%, a reasonable result as it's natural that more lift would be more easily generated at a higher angle of attack. A difference of coefficient of lift of 0.6751 allows the prediction of forces during the flare deflection maneuver.

Plotting the coefficients of lift for all deflections of the scaled parafoil against angle of attack yields Figure 52, below. The only notable trend is how closely the partial deflection coefficient of lift resembles the flare deflection coefficient of lift. This suggests that, on average, each gore resembles the partial deflection, which signifies that the design goals of the scaled parafoils were met, as the partial deflection was designed to be exactly halfway between the baseline and full deflection.

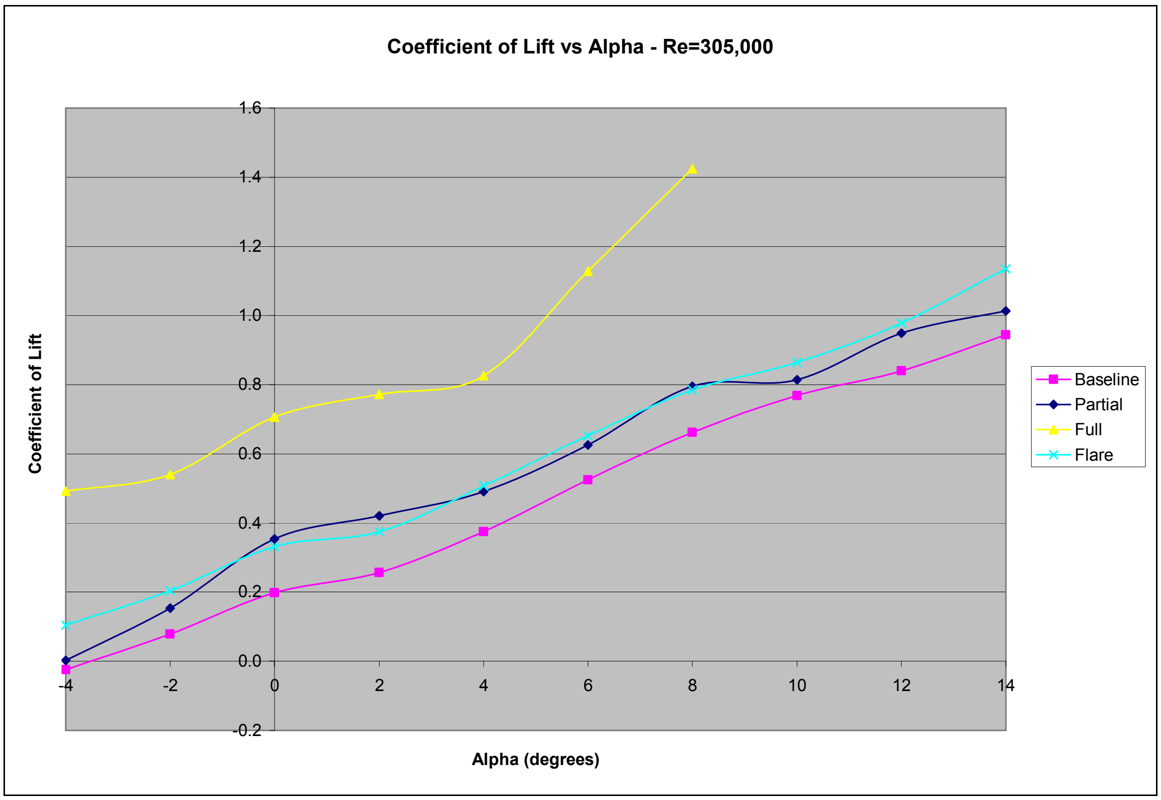

Figure 52: Coefficient of Lift vs. Alpha - Re = 305,000

5.3 Data Correction

Testing any object in a wind tunnel requires that certain measurements be taken and analyzed beforehand to assure that the data collected is not skewed by the wind tunnel itself. It is necessary, when testing airfoils, to compare the size of the airfoil with the size of the wind tunnel test section. The WPI wind tunnel is 24”x24”, thus, the parafoil model cannot have a span of more than 24”.

Dr. Antonio Filippone [4] of the Mechanical, Aerospace, and Civil Engineering departments at the University of Manchester notes, “Blockage ratios of less than 10 % of the wind tunnel’s cross section area] are needed, but sometimes far larger ratios are used. For aeronautical testing the blockage must be less than 5 %”. The overall frontal area of each model was roughly 28.8 square inches, giving a model of 7.13% scale. One reason for doing this is to account for the strength of the semi-infinite trailing vortices from each wing tip. If the wing tip vortices are too large, there would be turbulence induced by the wall on the model which would cause incorrect readings.

To measure these vortices, it was first necessary to understand their origin. Referencing Ludwig Prandtl’s Lifting Line Theory, it can be seen that there is a bound vortex (Γ), or vortex sheet, that covers the entire airfoil. This vortex is “bound” to the airfoil due to skin friction. This bound vortex has an induced velocity *w*, which is defined as:

$$w = \Gamma/(4\pi \mathrm{r})\ \mathrm{m/s}$$

Equation 1: Velocity of Bound Circulation

where r is the distance the circulation is measured from in relation to the origin. The data that was compiled was taken at r = b/2, which corresponds to one wingtip. Please reference Table E.1 for induced vortex velocity data.

Equation 1.1, when written in a different manner, has a relation to the lift of the airfoil, which in turn allows the calculation of the induced drag of the parafoil. Induced drag is drag "induced" by lift and by the bound and trailing vortices. Equation 2 demonstrates the relation between the lift of the parafoil and the velocity of the bound and trailing vortices.

$$w = (\mathrm{SV}/8\pi \mathrm{br})\ \mathrm{C_L}$$

Equation 2: Velocity of Trailing Vortices

In equation 2, S is defined as the planform area of the parafoil, V is the freestream velocity, b is the wingspan, and r is the same as fore mentioned. Note the placement of the coefficient of lift, where it is multiplied into the quantity, thus giving the necessary relation.

By obtaining this relation between lift and circulation, it is now possible to move on to calculate the effective angles of attack and the induced drag. For three-dimensional testing in wind-tunnels, the coefficient of induced drag is defined as:

$$\mathrm{C_{Di}} = \mathrm{C_L}^2/\pi \mathrm{AR}$$

Equation 3: Coefficient of Induced Drag

where AR is the aspect ration of the parafoil. Please reference Table E.2 for induced drag calculations.

By assuming an elliptical list distribution, more efficient effective angles of attack are calculated. An elliptical lift distribution is shown in Figure 1.

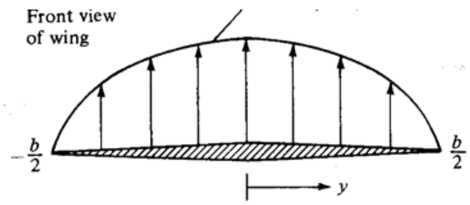

Figure 53: Elliptic Lift Distribution

It is now possible to replace the finite wing, or parafoil, with a horseshoe vortex system consisting of the bound vortex and the two trailing vortices. A horseshoe vortex is depicted in Figure 2.

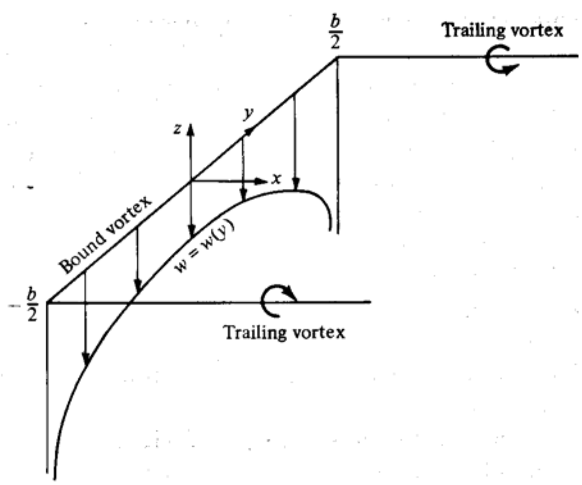

Figure 54: Horseshoe Vortex

Since this distribution for the parafoil is assumed, it is also assumed that the bound vortex moves to infinity at the wingtips where trailing vortices occur. Note the location of the axes of origin on the figure. The left wingtip is denoted by (-b/2) and the right wingtip by (b/2). An equation that represents each trailing vorticy's contribution to this system is:

$$w(\mathrm{y}) = (- \Gamma/4\pi\ (\mathrm{b}/2 + \mathrm{y})) - ((\Gamma/4\pi\ (\mathrm{b}/2 - \mathrm{y}))$$

Equation 4: Vorticy Contribution

This equation allows the calculation of the velocity induced by the bound vortex at *any* point (y) along the span of the parafoil. By finding $w(y_0)$, the data is able to be used to solve for the induced angle of attack. The induced angle of attack is calculated by using Equation 5.

$$\alpha_i = -w/V_\infty$$

Equation 5: Induced Angle of Attack

Thus, the effective angle of attack is determined by equation 6.

$$\alpha_{eff} = \alpha - \alpha_i$$

Equation 6: Effective Angle of Attack

Please reference Table E.3 for induced and effective angles of attack data.

5.3.1 Corrected Coefficient of Drag by Accounting for the Wake Drag

Another phenomenon that occurs when working in a wind tunnel is that of wake drag. The wake drag is found by equation 7.

$$\Delta C_{DW} = ((K_1 \tau_1 \text{ (wing volume)})/C^{3/2})C_{Du}$$

Equation 7: Wake Drag Correction

To find the actual drag of the parafoil, it is necessary to subtract the effects of wake drag from the calculated drag. According to William H. Rae, Jr. and Alan Pope, [10] the effects of wake drag are usually negligible. A look at the data will prove just this, with minor changes in the actual drag calculation. Data reference for this section is in Table E.4. In equation 7, K represents the body-shape factor and the τ value represents the tunnel test section shape. These values were calculated using the charts shown in Table E.4.

5.3.2 Calculation of Solid Blockage in Three Dimensions

The calculation of solid blockage is necessary to compute the velocity of the airflow near the boundaries of the wind tunnel, i.e., at the walls. A source-sink distribution represents the model and is entwined in a series of source-sink distributions that represent the walls of the tunnel. To calculate the effect of the solid-blockage velocity for a wing, use equation 8.

$$\varepsilon_{sbW} = \frac{\Delta V}{V_u} = \frac{K_1 \tau_1 (wing\_volume)}{C^{\frac{3}{2}}}$$

Equation 8: Solid Blockage Velocity Effect for a Wing

This equation is very similar to equation 7. The K and τ values represent the same values. The values for ε can be found in Table E.5.

The data provided by these equations was of negligible impact to the performance of the parafoils. For this reason, the corrections are not included in this report. These equations would most likely give credible results if testing was done on a parafoil of actual size in a larger pressurized wind tunnel.

6. CONCLUSIONS

The lift data gathered can be used to accurately predict forces that the parafoil will experience during a deflection maneuver. Using the baseline deflection as a model, accurate comparisons to the other deflection stages can be made, allowing for the prediction of loading upon any part of a full scale parafoil during a flare deflection. While the flare deflection to baseline deflection comparison yields the only true useful comparison for the entire span of the parafoil, the loading comparisons to the partial and full deflections provide more in-depth knowledge of specific gores of the flare deflection, allowing each gore to be analyzed individually across the entire span. If held at a constant angle of attack, the coefficient of lift increases approximately 0.12 with a very slight increase in the efficiency of lift generation. If the leading edge is held stationary during the flare deflection maneuver allowing the angle of attack to be variable, there is a significant displacement jump in the coefficient of lift of 0.675 and an efficiency increase of 17.4%.

7. REFERENCES

[1] NASA, 2006, “Genesis Sample Return Capsule Floats to Earth on a Parafoil,” http://www.nasa.gov/mission_pages/genesis/multimedia/genesis_2.html.

[2] Matos, C., et al. 1998, “Wind Tunnel Measurements of Parafoil Geometry and Aerodynamics,” AIAA Paper 98-0606, 1998.

[3] Lingard, S., 2004, Heinrich Parachute Systems Short Course: Gliding Parachute Applications.

[4] Filippone, A., 2005, “Wind Tunnel and Experimental Aerodynamics: Blockage,” http://aerodyn.org/WindTunnel/wind_tunnel.html.

[5] Abbott, I. H. and Von Doenhoff, A. E., 1999, Theory of Wing Sections, Dover Publications, New York.

[6] Strong, T., “Ram-air canopy performance criteria and general rules,” Strong Enterprises.

[7] Elert, G., 2005, “Flow Regimes,” http://hypertextbook.com/physics/matter/turbulence.

[8] Wikipedia, 2006, “Reynolds Number,” http://en.wikipedia.org/wiki/Reynolds_number.

[9] Nihon University Aero Student Group, 1994, “NASG Airfoil Database,” http://www.nasg.com/afdb/show-airfoil-e.phtml?id=309.

[10] Pope, A. and Rae, Jr., W., 1984, Low-Speed Wind Tunnel Testing, 2nd ed., John Wiley & Sons, New York.

[11] Anderson, Jr., J. D., 2001, Fundamentals of Aerodynamics. 3rd ed., McGraw-Hill, New York.

[12] Desabrais, K., 2005, “Wind_Tunnel_Speeds.xls.”

[13] Jalbert, D. C., 1966, Multi Cell Wing Type Aerial Device, Patent No. 3285546.

[14] Knacke, T.W., 1992, Parachute Recovery Systems Design Manual, Para Publishing, Santa Barbara, CA.

[15] Scott, J. A., 2004, “Drag Coefficient & Lifting Line Theory,” http://www.aerospaceweb.org/question/aerodynamics/q0184.shtml

[16] Strong Enterprises, Inc., 2004, “Information Central - Ram Air Reserve Canopies,” Stellar Reserve, http://www.strongparachutes.com/Pages/ramairres.html.

8. APPENDICES

Appendix A: Lift Data

A.1 Baseline Deflection

T	$\rho (kg/m^3)$	μ (kg m^{-1} s^{-1})
63	1.188684	0.000017873971
64	1.18548	0.000017897914
65	1.183878	0.000017921844
66	1.180674	0.000017945761
67	1.179072	0.000017969663
68	1.17747	0.000017993552
69	1.174266	0.000018017428
70	1.172664	0.000018041290
71	1.16946	0.000018065138
72	1.16786	0.000018088973
73	1.16626	0.000018112794
74	1.16305	0.000018136602
75	1.16145	0.000018160397
76	1.15985	0.000018184178
77	1.15664	0.000018207946
78	1.15504	0.000018231701
79	1.15344	0.000018255442
80	1.15024	0.000018279170
81	1.14863	0.000018302885
82	1.14703	0.000018326587
83	1.14383	0.000018350276
84	1.14223	0.000018373952
85	1.14062	0.000018397614
86	1.13742	0.000018421264
87	1.13581	0.000018444900
88	1.13422	0.000018468524
89	1.13101	0.000018492134
90	1.12941	0.000018515732
91	1.12781	0.000018539317
92	1.12621	0.000018562888
93	1.123	0.000018586448
94	1.1214	0.000018609994
95	1.11979	0.000018633527

Re = 305000

Alpha	CL
-4	-0.024879723
-2	0.078988375
0	0.198299609
2	0.166960137
4	0.308782944
6	0.438212862
8	0.661924603
10	0.715060484
12	0.769833457
14	0.968658096

Chordlength:	0.155	m
Area:	0.063	m^2
Arc-Anhedral:	22.042	Degrees
Gravity:	9.805	m/s^2

Alpha = -4 deg

Velocity (Hz)	Velocity (m/s)	T (ºF)	ρ(kg/m3)	Q_∞	Re	Lift (g)	Lift (N)	Cl	$Cl_{\beta=0}$
12.8	10.03096	74	1.16305	58.51	99551.96769	133.333	1.307	0.3524	0.4101
15.2	12.04144	75	1.16145	84.20	119184.1496	183.333	1.798	0.3367	0.3919
17.5	13.96815	75	1.16145	113.30	138254.4013	233.333	2.288	0.3185	0.3707
19.9	15.97863	76	1.15985	148.06	157729.3751	300.000	2.942	0.3133	0.3647
22.3	17.98911	76	1.15985	187.67	177575.3665	366.667	3.595	0.3021	0.3517
24.7	19.99959	76	1.15985	231.96	197421.3579	433.333	4.249	0.2889	0.3362
27.1	22.01007	76	1.15985	280.94	217267.3493	483.333	4.739	0.2660	0.3097
29.5	24.02055	77	1.15664	333.68	236148.444	500.000	4.903	0.2317	0.2697
31.9	26.03103	77	1.15664	391.88	255913.6752	400.000	3.922	0.1578	0.1837
34.2	27.95774	78	1.15504	451.41	274117.5206	466.667	4.576	0.1599	0.1861
36.6	29.96822	79	1.15344	517.95	293041.0709	-83.333	-0.817	-0.0249	-0.0290

Alpha = -2 deg

Velocity (Hz)	Velocity (m/s)	T (ºF)	ρ(kg/m3)	Q_∞	Re	Lift (g)	Lift (N)	Cl	$Cl_{\beta=0}$
12.8	10.03096	77	1.15664	58.19	98615.37709	100.000	0.981	0.2657	0.3093
15.2	12.04144	77	1.15664	83.85	118380.6083	200.000	1.961	0.3688	0.4293
17.5	13.96815	78	1.15504	112.68	136953.6538	283.333	2.778	0.3888	0.4526
19.9	15.97863	78	1.15504	147.45	156665.8263	383.333	3.759	0.4020	0.4679
22.3	17.98911	78	1.15504	186.89	176377.9987	450.000	4.412	0.3723	0.4334
24.7	19.99959	78	1.15504	231.00	196090.1712	650.000	6.373	0.4351	0.5065
27.1	22.01007	78	1.15504	279.78	215802.3437	966.667	9.478	0.5343	0.6219
29.5	24.02055	78	1.15504	333.22	235514.5162	583.333	5.720	0.2707	0.3151
31.9	26.03103	79	1.15344	390.79	254541.6747	583.333	5.720	0.2308	0.2687
34.2	27.95774	80	1.15024	449.53	272269.4667	583.333	5.720	0.2007	0.2336
36.6	29.96822	80	1.15024	516.51	291848.7431	33.333	0.327	0.0100	0.0116
39.0	31.9787	81	1.14863	587.32	310589.1597	300.000	2.942	0.0790	0.0919
41.4	33.98918	82	1.14703	662.56	329229.5135	416.667	4.085	0.0972	0.1132

Alpha = 0 deg

Velocity (Hz)	Velocity (m/s)	T (ºF)	ρ(kg/m3)	Q_∞	Re	Lift (g)	Lift (N)	Cl	$Cl_{\beta=0}$
12.8	10.03096	79	1.15344	58.03	98086.68184	183.333	1.798	0.4885	0.5686
15.2	12.04144	79	1.15344	83.62	117745.948	300.000	2.942	0.5548	0.6457
17.5	13.96815	79	1.15344	112.52	136586.078	366.667	3.595	0.5039	0.5865
19.9	15.97863	79	1.15344	147.25	156245.3441	500.000	4.903	0.5251	0.6112
22.3	17.98911	79	1.15344	186.63	175904.6102	600.000	5.883	0.4971	0.5786
24.7	19.99959	79	1.15344	230.68	195563.8764	816.667	8.007	0.5475	0.6372
27.1	22.01007	79	1.15344	279.39	215223.1425	900.000	8.825	0.4981	0.5798
29.5	24.02055	80	1.15024	331.84	233926.7172	700.000	6.864	0.3262	0.3797
31.9	26.03103	80	1.15024	389.71	253505.9935	1050.000	10.295	0.4166	0.4849
34.2	27.95774	81	1.14863	448.90	271536.0841	966.667	9.478	0.3330	0.3876
36.6	29.96822	82	1.14703	515.07	290281.2745	783.333	7.681	0.2352	0.2737
39.0	31.9787	83	1.14383	584.86	308492.481	750.000	7.354	0.1983	0.2308
41.4	33.98918	83	1.14383	660.71	327887.202	1116.667	10.949	0.2614	0.3042
43.8	35.99966	84	1.14223	740.15	346349.2806	1383.333	13.564	0.2890	0.3364
46.2	38.01014	85	1.14062	823.97	364706.7843	1583.333	15.525	0.2972	0.3459

Alpha = 2.07 deg

Velocity (Hz)	Velocity (m/s)	T (ºF)	ρ(kg/m3)	Q_∞	Re	Lift (lbs)	Lift (N)	Lift (g)	Cl	$Cl_{\beta=0}$
12.8	10.03096	77	1.15664	58.19	98615.37709	0.176	0.784	80	0.2126	0.2474
15.2	12.04144	77	1.15664	83.85	118380.6083	0.353	1.569	160	0.2951	0.3434
17.5	13.96815	77	1.15664	112.84	137322.2882	0.485	2.157	220	0.3015	0.3509
19.9	15.97863	77	1.15664	147.65	157087.5193	0.794	3.530	360	0.3770	0.4388
22.3	17.98911	77	1.15664	187.15	176852.7505	1.058	4.706	480	0.3966	0.4616
24.7	19.99959	77	1.15664	231.32	196617.9817	1.411	6.275	640	0.4278	0.4980
27.1	22.01007	77	1.15664	280.16	216383.2129	1.852	8.236	840	0.4636	0.5396
29.5	24.02055	77	1.15664	333.68	236148.444	2.249	10.001	1020	0.4727	0.5502
31.9	26.03103	77	1.15664	391.88	255913.6752	2.028	9.021	920	0.3630	0.4225
34.2	27.95774	77	1.15664	452.04	274855.3551	2.601	11.570	1180	0.4037	0.4698
36.6	29.96822	78	1.15504	518.67	293829.693	1.235	5.491	560	0.1670	0.1943
39.0	31.9787	79	1.15344	589.78	312700.337	2.161	9.609	980	0.2570	0.2991
41.4	33.98918	79	1.15344	666.26	332359.6031	2.601	11.570	1180	0.2739	0.3188
43.8	35.99966	80	1.15024	745.34	350586.5721	3.263	14.511	1480	0.3071	0.3574

Alpha = 4.04 deg

Velocity (Hz)	Velocity (m/s)	T (ºF)	ρ(kg/m3)	Q_∞	Re	Lift (lbs)	Lift (N)	Lift (g)	Cl	$Cl_{\beta=0}$
12.8	10.03096	74	1.16305	58.51	99551.96769	0.220	0.981	100	0.2643	0.3076
15.2	12.04144	74	1.16305	84.32	119504.9174	0.397	1.765	180	0.3301	0.3842
17.5	13.96815	74	1.16305	113.46	138626.4941	0.617	2.745	280	0.3816	0.4442
19.9	15.97863	74	1.16305	148.47	158579.4438	0.926	4.118	420	0.4374	0.5091
22.3	17.98911	74	1.16305	188.19	178532.3935	1.235	5.491	560	0.4602	0.5356
24.7	19.99959	74	1.16305	232.60	198485.3431	1.587	7.060	720	0.4787	0.5571
27.1	22.01007	74	1.16305	281.72	218438.2928	2.205	9.805	1000	0.5489	0.6389
29.5	24.02055	75	1.16145	335.07	237751.3672	2.866	12.747	1300	0.6000	0.6983
31.9	26.03103	75	1.16145	393.51	257650.7604	2.778	12.354	1260	0.4951	0.5763
34.2	27.95774	75	1.16145	453.92	276721.0122	3.439	15.296	1560	0.5315	0.6186
36.6	29.96822	76	1.15985	520.83	295824.3987	2.293	10.197	1040	0.3088	0.3594
39.0	31.9787	76	1.15985	593.05	315670.3901	3.175	14.119	1440	0.3755	0.4370
41.4	33.98918	77	1.15664	668.11	334151.0486	4.145	18.433	1880	0.4351	0.5065
43.8	35.99966	78	1.15504	748.45	352966.2105	5.247	23.336	2380	0.4917	0.5723

Alpha = 6.09 deg

Velocity (Hz)	Velocity (m/s)	T (ºF)	ρ(kg/m3)	Q_∞	Re	Lift (lbs)	Lift (N)	Lift (g)	Cl	$Cl_{\beta=0}$
12.8	10.03096	70	1.172664	59.00	100905.1675	0.176	0.784	80	0.2097	0.2441
15.2	12.04144	70	1.172664	85.02	121129.3356	0.309	1.373	140	0.2546	0.2964
17.5	13.96815	70	1.172664	114.40	140510.83	0.573	2.549	260	0.3515	0.4091
19.9	15.97863	70	1.172664	149.70	160734.9981	0.970	4.314	440	0.4545	0.5290
22.3	17.98911	71	1.16946	189.22	180226.5049	2.549	11.335	1156	0.9447	1.0996
24.7	19.99959	72	1.16786	233.56	199831.0008	2.072	9.217	940	0.6224	0.7244
27.1	22.01007	72	1.16786	282.88	219919.2242	3.660	16.276	1660	0.9074	1.0562
29.5	24.02055	73	1.16626	336.46	239363.4122	2.910	12.943	1320	0.6067	0.7061
31.9	26.03103	73	1.16626	395.14	259397.7309	3.748	16.669	1700	0.6653	0.7744
34.2	27.95774	74	1.16305	454.54	277465.7689	4.365	19.414	1980	0.6736	0.7840
36.6	29.96822	74	1.16305	522.26	297418.7186	3.263	14.511	1480	0.4382	0.5100
39.0	31.9787	74	1.16305	594.69	317371.6682	4.453	19.806	2020	0.5253	0.6114
41.4	33.98918	75	1.16145	670.89	336419.1917	5.644	25.101	2560	0.5901	0.6868
43.8	35.99966	75	1.16145	752.61	356318.5849	7.319	32.553	3320	0.6822	0.7940

Alpha = 8 deg

Velocity (Hz)	Velocity (m/s)	T (ºF)	ρ(kg/m3)	Q_∞	Re	Lift (g)	Lift (N)	Cl	$Cl_{\beta=0}$
12.8	10.03096	78	1.15504	58.11	98350.64938	216.667	2.124	0.5766	0.6711
15.2	12.04144	78	1.15504	83.74	118062.8218	283.333	2.778	0.5232	0.6090
17.5	13.96815	79	1.15344	112.52	136586.078	350.000	3.432	0.4810	0.5598
19.9	15.97863	79	1.15344	147.25	156245.3441	550.000	5.393	0.5776	0.6723
22.3	17.98911	79	1.15344	186.63	175904.6102	766.667	7.517	0.6352	0.7394
24.7	19.99959	79	1.15344	230.68	195563.8764	1050.000	10.295	0.7039	0.8193
27.1	22.01007	80	1.15024	278.61	214347.4409	1566.667	15.361	0.8695	1.0121
29.5	24.02055	80	1.15024	331.84	233926.7172	2400.000	23.532	1.1184	1.3017
31.9	26.03103	81	1.14863	389.16	252823.1521	1900.000	18.630	0.7550	0.8787
34.2	27.95774	81	1.14863	448.90	271536.0841	2433.333	23.859	0.8382	0.9756
36.6	29.96822	82	1.14703	515.07	290281.2745	2400.000	23.532	0.7205	0.8387
39.0	31.9787	84	1.14223	584.04	307664.0096	2500.000	24.513	0.6619	0.7704
41.4	33.98918	84	1.14223	659.79	327006.6451	3100.000	30.396	0.7266	0.8457

Alpha = 10 deg

Velocity (Hz)	Velocity (m/s)	T (ºF)	ρ(kg/m3)	Q_∞	Re	Lift (lbs)	Lift (N)	Lift (g)	Cl	$Cl_{\beta=0}$
12.8	10.03096	67	1.179072	59.32	101860.9636	0.276	1.226	125.0	0.3259	0.3793
15.2	12.04144	67	1.179072	85.48	122276.6995	0.579	2.574	262.5	0.4749	0.5527
17.5	13.96815	67	1.179072	115.02	141841.7798	0.937	4.167	425.0	0.5714	0.6650
19.9	15.97863	68	1.17747	150.31	161821.9296	1.461	6.496	662.5	0.6816	0.7933
22.3	17.98911	68	1.17747	190.52	182182.8588	2.067	9.192	937.5	0.7609	0.8857
24.7	19.99959	68	1.17747	235.48	202543.7879	2.590	11.521	1175.0	0.7716	0.8981
27.1	22.01007	69	1.174266	284.43	222003.5995	4.602	20.468	2087.5	1.1349	1.3210
29.5	24.02055	69	1.174266	338.77	242282.2173	5.236	23.287	2375.0	1.0841	1.2618
31.9	26.03103	70	1.172664	397.31	261855.8386	5.071	22.552	2300.0	0.8952	1.0419
34.2	27.95774	71	1.16946	457.05	280098.6689	5.732	25.493	2600.0	0.8797	1.0239
36.6	29.96822	72	1.16786	524.42	299435.1082	5.346	23.777	2425.0	0.7151	0.8323
39.0	31.9787	73	1.16626	596.33	318665.9236	6.531	29.047	2962.5	0.7682	0.8942
41.4	33.98918	74	1.16305	671.82	337324.6179	7.937	35.298	3600.0	0.8286	0.9645

Alpha = 12 deg

Velocity (Hz)	Velocity (m/s)	T (ºF)	ρ(kg/m3)	Q_∞	Re	Lift (lbs)	Lift (N)	Lift (g)	Cl	$Cl_{\beta=0}$
12.8	10.03096	71	1.16946	58.84	100496.6261	0.468	2.084	212.5	0.5585	0.6501
15.2	12.04144	71	1.16946	84.78	120638.9113	0.744	3.309	337.5	0.6156	0.7165
17.5	13.96815	71	1.16946	114.09	139941.9346	1.102	4.903	500.0	0.6777	0.7888
19.9	15.97863	71	1.16946	149.29	160084.2198	1.571	6.986	712.5	0.7380	0.8590
22.3	17.98911	71	1.16946	189.22	180226.5049	2.094	9.315	950.0	0.7764	0.9036
24.7	19.99959	71	1.16946	233.88	200368.7901	2.811	12.501	1275.0	0.8430	0.9812
27.1	22.01007	71	1.16946	283.27	220511.0753	3.665	16.301	1662.5	0.9076	1.0563
29.5	24.02055	72	1.16786	336.92	240007.4475	5.677	25.248	2575.0	1.1819	1.3756
31.9	26.03103	72	1.16786	395.68	260095.6708	5.374	23.900	2437.5	0.9526	1.1088
34.2	27.95774	73	1.16626	455.79	278597.2862	6.173	27.454	2800.0	0.9500	1.1057
36.6	29.96822	74	1.16305	522.26	297418.7186	5.732	25.493	2600.0	0.7698	0.8960
39.0	31.9787	75	1.16145	593.87	316519.7986	7.110	31.621	3225.0	0.8398	0.9774
41.4	33.98918	77	1.15664	668.11	334151.0486	8.543	37.994	3875.0	0.8969	1.0439

Alpha = 14 deg

Velocity (Hz)	Velocity (m/s)	T (ºF)	ρ(kg/m3)	Q_∞	Re	Lift (lbs)	Lift (N)	Lift (g)	Cl	$Cl_{\beta=0}$
12.8	10.03096	74	1.16305	58.51	99551.96769	0.496	2.206	225.0	0.5946	0.6921
15.2	12.04144	74	1.16305	84.32	119504.9174	0.909	4.045	412.5	0.7565	0.8805
17.5	13.96815	74	1.16305	113.46	138626.4941	1.268	5.638	575.0	0.7837	0.9121
19.9	15.97863	74	1.16305	148.47	158579.4438	1.846	8.212	837.5	0.8723	1.0153
22.3	17.98911	74	1.16305	188.19	178532.3935	2.425	10.786	1100.0	0.9039	1.0521
24.7	19.99959	74	1.16305	232.60	198485.3431	3.169	14.095	1437.5	0.9557	1.1123
27.1	22.01007	74	1.16305	281.72	218438.2928	4.161	18.507	1887.5	1.0361	1.2059
29.5	24.02055	74	1.16305	335.53	238391.2425	6.338	28.189	2875.0	1.3250	1.5422
31.9	26.03103	75	1.16145	393.51	257650.7604	7.000	31.131	3175.0	1.2477	1.4522
34.2	27.95774	75	1.16145	453.92	276721.0122	6.779	30.150	3075.0	1.0476	1.2193
36.6	29.96822	76	1.15985	520.83	295824.3987	7.193	31.989	3262.5	0.9687	1.1274
39.0	31.9787	77	1.15664	591.41	314385.8175	7.964	35.421	3612.5	0.9446	1.0994

A.2 Partial Deflection

T	$\rho (kg/m^3)$	μ (kg m^{-1} s^{-1})
63	1.188684	0.000017873971
64	1.18548	0.000017897914
65	1.183878	0.000017921844
66	1.180674	0.000017945761
67	1.179072	0.000017969663
68	1.17747	0.000017993552
69	1.174266	0.000018017428
70	1.172664	0.000018041290
71	1.16946	0.000018065138
72	1.16786	0.000018088973
73	1.16626	0.000018112794
74	1.16305	0.000018136602
75	1.16145	0.000018160397
76	1.15985	0.000018184178
77	1.15664	0.000018207946
78	1.15504	0.000018231701
79	1.15344	0.000018255442
80	1.15024	0.000018279170
81	1.14863	0.000018302885
82	1.14703	0.000018326587
83	1.14383	0.000018350276
84	1.14223	0.000018373952
85	1.14062	0.000018397614
86	1.13742	0.000018421264
87	1.13581	0.000018444900
88	1.13422	0.000018468524
89	1.13101	0.000018492134
90	1.12941	0.000018515732
91	1.12781	0.000018539317
92	1.12621	0.000018562888
93	1.123	0.000018586448
94	1.1214	0.000018609994
95	1.11979	0.000018633527

Re = 305000

Alpha	Baseline Cl	Partial Cl
-4	-0.025	0.003
-2	0.079	0.153
0	0.198	0.354
2	0.257	0.420
4	0.375	0.491
6	0.525	0.626
8	0.662	0.796
10	0.768	0.815
12	0.840	0.949
14	0.945	1.013

Chordlength:	0.151	m
Area:	0.069	m^2
Arc-Anhedral:	20.563	Degrees
Gravity:	9.805	m/s^2

Alpha = -4 deg

Velocity (Hz)	Velocity (m/s)	T (ºF)	ρ(kg/m3)	Q_∞	Re	Lift (lbs)	Lift (g)	Lift (N)	Cl	$Cl_{\beta=0}$
12.8	10.03096	67	1.179072	59.32	99095.38	-0.220	-100.0	-0.9805	-0.2382	-0.2717
15.2	12.04144	67	1.179072	85.48	118956.8	-0.294	-133.3	-1.3073	-0.2204	-0.2514
17.5	13.96815	67	1.179072	115.02	137990.7	-0.147	-66.7	-0.6537	-0.0819	-0.0934
19.9	15.97863	67	1.179072	150.52	157852.1	0.024	11.1	0.1089	0.0104	0.0119
22.3	17.98911	67	1.179072	190.78	177713.6	0.024	11.1	0.1089	0.0082	0.0094
24.7	19.99959	68	1.17747	235.48	197044.6	-0.343	-155.6	-1.5252	-0.0933	-0.1065
27.1	22.01007	69	1.174266	284.43	215976.1	-0.343	-155.6	-1.5252	-0.0773	-0.0881
29.5	24.02055	69	1.174266	338.77	235704.1	-0.024	-11.1	-0.1089	-0.0046	-0.0053
31.9	26.03103	70	1.172664	397.31	254746.3	-0.710	-322.2	-3.1594	-0.1146	-0.1307
34.2	27.95774	71	1.16946	457.05	272493.8	-0.563	-255.6	-2.5057	-0.0790	-0.0901
36.6	29.96822	71	1.16946	525.14	292089.2	-0.539	-244.4	-2.3968	-0.0658	-0.0750
39.0	31.9787	73	1.16626	596.33	310014	0.024	11.1	0.1089	0.0026	0.0030
41.4	33.98918	74	1.16305	671.82	328166.1	0.514	233.3	2.2878	0.0491	0.0560
43.8	35.99966	75	1.16145	752.61	346644.3	0.882	400.0	3.9220	0.0751	0.0857

Alpha = -2 deg

Velocity (Hz)	Velocity (m/s)	T (ºF)	ρ(kg/m3)	Q_∞	Re	Lift (lbs)	Lift (g)	Lift (N)	Cl	$Cl_{\beta=0}$
12.8	10.03096	72	1.16786	58.76	97505.67	0.245	111.1	1.0894	0.2672	0.3048
15.2	12.04144	72	1.16786	84.67	117048.5	0.294	133.3	1.3073	0.2225	0.2538
17.5	13.96815	72	1.16786	113.93	135777	0.294	133.3	1.3073	0.1654	0.1886
19.9	15.97863	72	1.16786	149.09	155319.8	0.294	133.3	1.3073	0.1264	0.1441
22.3	17.98911	72	1.16786	188.96	174862.7	0.441	200.0	1.9610	0.1495	0.1706
24.7	19.99959	72	1.16786	233.56	194405.5	-0.343	-155.6	-1.5252	-0.0941	-0.1073
27.1	22.01007	72	1.16786	282.88	213948.3	0.171	77.8	0.7626	0.0388	0.0443
29.5	24.02055	73	1.16626	336.46	232864.6	0.441	200.0	1.9610	0.0840	0.0958
31.9	26.03103	74	1.16305	394.05	251330	1.102	500.0	4.9025	0.1793	0.2045
34.2	27.95774	74	1.16305	454.54	269932.4	0.563	255.6	2.5057	0.0794	0.0906
36.6	29.96822	75	1.16145	521.55	288567	0.294	133.3	1.3073	0.0361	0.0412
39.0	31.9787	75	1.16145	593.87	307926.1	1.421	644.4	6.3188	0.1533	0.1749
41.4	33.98918	76	1.15985	669.97	326406.9	2.009	911.1	8.9334	0.1921	0.2192
43.8	35.99966	77	1.15664	749.49	344307.2	2.523	1144.4	11.2213	0.2157	0.2461

Alpha = 0 deg

Velocity (Hz)	Velocity (m/s)	T (ºF)	ρ(kg/m3)	Q_∞	Re	Lift (lbs)	Lift (g)	Lift (N)	Cl	$Cl_{\beta=0}$
12.8	10.03096	71	1.16946	58.84	97768.08	0.138	62.5	0.6128	0.1501	0.1712
15.2	12.04144	72	1.16786	84.67	117048.5	0.303	137.5	1.3482	0.2295	0.2617
17.5	13.96815	72	1.16786	113.93	135777	0.413	187.5	1.8384	0.2325	0.2653
19.9	15.97863	72	1.16786	149.09	155319.8	0.661	300.0	2.9415	0.2843	0.3243
22.3	17.98911	72	1.16786	188.96	174862.7	0.772	350.0	3.4318	0.2617	0.2985
24.7	19.99959	72	1.16786	233.56	194405.5	1.157	525.0	5.1476	0.3176	0.3623
27.1	22.01007	72	1.16786	282.88	213948.3	1.433	650.0	6.3732	0.3247	0.3703
29.5	24.02055	73	1.16626	336.46	232864.6	1.598	725.0	7.1086	0.3045	0.3473
31.9	26.03103	73	1.16626	395.14	252354.9	2.315	1050.0	10.2953	0.3755	0.4283
34.2	27.95774	74	1.16305	454.54	269932.4	2.039	925.0	9.0696	0.2875	0.3280
36.6	29.96822	75	1.16145	521.55	288567	2.342	1062.5	10.4178	0.2878	0.3283
39.0	31.9787	76	1.15985	593.05	307099.8	3.279	1487.5	14.5849	0.3544	0.4043
41.4	33.98918	77	1.15664	668.11	325078.6	3.858	1750.0	17.1588	0.3701	0.4222
43.8	35.99966	78	1.15504	748.45	343383	4.712	2137.5	20.9582	0.4035	0.4603
46.2	38.01014	80	1.15024	830.92	360115.6	6.035	2737.5	26.8412	0.4655	0.5310

Alpha = 2 deg

Velocity (Hz)	Velocity (m/s)	T (ºF)	ρ(kg/m3)	Q_∞	Re	Lift (lbs)	Lift (g)	Lift (N)	Cl	$Cl_{\beta=0}$
12.8	10.03096	77	1.15664	58.19	95937.91	0.524	237.5	2.3287	0.5767	0.6578
15.2	12.04144	77	1.15664	83.85	115166.5	0.717	325.0	3.1866	0.5476	0.6247
17.5	13.96815	77	1.15664	112.84	133593.9	0.854	387.5	3.7994	0.4852	0.5535
19.9	15.97863	77	1.15664	147.65	152822.5	1.075	487.5	4.7799	0.4665	0.5321
22.3	17.98911	77	1.15664	187.15	172051.1	1.350	612.5	6.0056	0.4624	0.5275
24.7	19.99959	77	1.15664	231.32	191279.7	1.653	750.0	7.3537	0.4581	0.5226
27.1	22.01007	77	1.15664	280.16	210508.3	2.039	925.0	9.0696	0.4665	0.5321
29.5	24.02055	77	1.15664	333.68	229736.9	2.094	950.0	9.3147	0.4023	0.4589
31.9	26.03103	78	1.15504	391.34	248297.1	2.728	1237.5	12.1337	0.4468	0.5097
34.2	27.95774	78	1.15504	451.41	266675.1	3.142	1425.0	13.9721	0.4460	0.5088
36.6	29.96822	79	1.15344	517.95	285084.8	2.866	1300.0	12.7465	0.3546	0.4045
39.0	31.9787	80	1.15024	588.14	302972.6	3.858	1750.0	17.1588	0.4204	0.4796
41.4	33.98918	81	1.14863	663.49	321152.9	4.988	2262.5	22.1838	0.4818	0.5496
43.8	35.99966	82	1.14703	743.26	339236.1	5.897	2675.0	26.2284	0.5085	0.5801

Alpha = 4 deg

Velocity (Hz)	Velocity (m/s)	T (ºF)	ρ(kg/m3)	Q_∞	Re	Lift (lbs)	Lift (g)	Lift (N)	Cl	$Cl_{\beta=0}$
12.8	10.03096	73	1.16626	58.67	97244.03	0.122	55.6	0.5447	0.1338	0.1526
15.2	12.04144	73	1.16626	84.55	116734.4	0.269	122.2	1.1984	0.2042	0.2330
17.5	13.96815	73	1.16626	113.77	135412.7	0.441	200.0	1.9610	0.2484	0.2833
19.9	15.97863	73	1.16626	148.88	154903.1	0.784	355.6	3.4862	0.3374	0.3849
22.3	17.98911	73	1.16626	188.71	174393.4	1.225	555.6	5.4472	0.4160	0.4745
24.7	19.99959	73	1.16626	233.24	193883.8	1.764	800.0	7.8440	0.4846	0.5528
27.1	22.01007	74	1.16305	281.72	212507.6	2.229	1011.1	9.9139	0.5071	0.5785
29.5	24.02055	74	1.16305	335.53	231918.8	2.597	1177.8	11.5481	0.4960	0.5658
31.9	26.03103	75	1.16145	393.51	250655.4	3.062	1388.9	13.6181	0.4987	0.5689
34.2	27.95774	75	1.16145	453.92	269207.9	3.674	1666.7	16.3417	0.5188	0.5918
36.6	29.96822	76	1.15985	520.83	287792.6	3.331	1511.1	14.8164	0.4099	0.4676
39.0	31.9787	77	1.15664	591.41	305850.1	4.532	2055.6	20.1547	0.4911	0.5602
41.4	33.98918	78	1.15504	667.19	324206	5.634	2555.6	25.0572	0.5412	0.6174
43.8	35.99966	79	1.15344	747.42	342461.3	7.349	3333.3	32.6833	0.6301	0.7188

Alpha = 6 deg

Velocity (Hz)	Velocity (m/s)	T (ºF)	ρ(kg/m3)	Q_∞	Re	Lift (lbs)	Lift (g)	Lift (N)	Cl	$Cl_{\beta=0}$
12.8	10.03096	76	1.15985	58.35	96329.91	0.441	200.0	1.9610	0.4843	0.5524
15.2	12.04144	76	1.15985	84.09	115637.1	0.759	344.4	3.3773	0.5788	0.6602
17.5	13.96815	76	1.15985	113.15	134139.8	0.980	444.4	4.3578	0.5550	0.6331
19.9	15.97863	76	1.15985	148.06	153446.9	1.347	611.1	5.9919	0.5832	0.6652
22.3	17.98911	76	1.15985	187.67	172754.1	1.641	744.4	7.2993	0.5605	0.6393
24.7	19.99959	76	1.15985	231.96	192061.3	2.205	1000.0	9.8050	0.6091	0.6948
27.1	22.01007	76	1.15985	280.94	211368.4	2.866	1300.0	12.7465	0.6538	0.7458
29.5	24.02055	76	1.15985	334.61	230675.6	3.160	1433.3	14.0538	0.6052	0.6904
31.9	26.03103	77	1.15664	391.88	248965.5	3.723	1688.9	16.5596	0.6089	0.6946
34.2	27.95774	77	1.15664	452.04	267392.9	4.850	2200.0	21.5710	0.6876	0.7844
36.6	29.96822	78	1.15504	518.67	285852	4.287	1944.4	19.0653	0.5297	0.6042
39.0	31.9787	79	1.15344	589.78	304210.3	5.757	2611.1	25.6019	0.6255	0.7136
41.4	33.98918	80	1.15024	664.42	322020.3	7.128	3233.3	31.7028	0.6876	0.7843
43.8	35.99966	81	1.14863	744.30	340149.2	8.647	3922.2	38.4574	0.7446	0.8493

Alpha = 8 deg

Velocity (Hz)	Velocity (m/s)	T (ºF)	ρ(kg/m3)	Q_∞	Re	Lift (lbs)	Lift (g)	Lift (N)	Cl	$Cl_{\beta=0}$
12.8	10.03096	77	1.15664	58.19	95937.91	0.441	200.0	1.9610	0.4856	0.5540
15.2	12.04144	77	1.15664	83.85	115166.5	0.857	388.9	3.8131	0.6553	0.7475
17.5	13.96815	77	1.15664	112.84	133593.9	1.176	533.3	5.2293	0.6678	0.7618
19.9	15.97863	77	1.15664	147.65	152822.5	1.592	722.2	7.0814	0.6911	0.7884
22.3	17.98911	77	1.15664	187.15	172051.1	1.935	877.8	8.6066	0.6627	0.7560
24.7	19.99959	77	1.15664	231.32	191279.7	3.111	1411.1	13.8359	0.8619	0.9832
27.1	22.01007	77	1.15664	280.16	210508.3	3.331	1511.1	14.8164	0.7621	0.8693
29.5	24.02055	78	1.15504	333.22	229120.2	3.870	1755.6	17.2132	0.7444	0.8491
31.9	26.03103	78	1.15504	391.34	248297.1	4.679	2122.2	20.8084	0.7662	0.8741
34.2	27.95774	78	1.15504	451.41	266675.1	6.124	2777.8	27.2361	0.8694	0.9918
36.6	29.96822	78	1.15504	518.67	285852	5.463	2477.8	24.2946	0.6750	0.7700
39.0	31.9787	79	1.15344	589.78	304210.3	7.324	3322.2	32.5744	0.7959	0.9079

Alpha = 10 deg

Velocity (Hz)	Velocity (m/s)	T (ºF)	ρ(kg/m3)	Q_∞	Re	Lift (lbs)	Lift (g)	Lift (N)	Cl	$Cl_{\beta=0}$
12.8	10.03096	77	1.15664	58.19	95937.91	0.416	188.9	1.8521	0.4586	0.5232
15.2	12.04144	77	1.15664	83.85	115166.5	0.808	366.7	3.5952	0.6178	0.7048
17.5	13.96815	77	1.15664	112.84	133593.9	1.102	500.0	4.9025	0.6261	0.7142
19.9	15.97863	77	1.15664	147.65	152822.5	1.592	722.2	7.0814	0.6911	0.7884
22.3	17.98911	77	1.15664	187.15	172051.1	2.107	955.6	9.3692	0.7214	0.8229
24.7	19.99959	77	1.15664	231.32	191279.7	3.209	1455.6	14.2717	0.8891	1.0142
27.1	22.01007	77	1.15664	280.16	210508.3	3.601	1633.3	16.0148	0.8237	0.9396
29.5	24.02055	77	1.15664	333.68	229736.9	4.066	1844.4	18.0848	0.7810	0.8909
31.9	26.03103	78	1.15504	391.34	248297.1	5.046	2288.9	22.4426	0.8264	0.9427
34.2	27.95774	78	1.15504	451.41	266675.1	6.393	2900.0	28.4345	0.9077	1.0354
36.6	29.96822	79	1.15344	517.95	285084.8	6.124	2777.8	27.2361	0.7577	0.8644
39.0	31.9787	79	1.15344	589.78	304210.3	7.496	3400.0	33.3370	0.8145	0.9292
41.4	33.98918	80	1.15024	664.42	322020.3	9.161	4155.6	40.7452	0.8837	1.0081
43.8	35.99966	80	1.15024	745.34	341067.9	11.244	5100.0	50.0055	0.9668	1.1028

Alpha = 12 deg

Velocity (Hz)	Velocity (m/s)	T (ºF)	ρ(kg/m3)	Q_∞	Re	Lift (lbs)	Lift (g)	Lift (N)	Cl	$Cl_{\beta=0}$
12.8	10.03096	78	1.15504	58.11	95680.37	0.808	366.7	3.5952	0.8915	1.0170
15.2	12.04144	78	1.15504	83.74	114857.3	1.274	577.8	5.6651	0.9749	1.1121
17.5	13.96815	78	1.15504	112.68	133235.3	1.274	577.8	5.6651	0.7245	0.8264
19.9	15.97863	78	1.15504	147.45	152412.3	1.813	822.2	8.0619	0.7879	0.8988
22.3	17.98911	78	1.15504	186.89	171589.2	2.278	1033.3	10.1318	0.7812	0.8911
24.7	19.99959	78	1.15504	231.00	190766.2	3.552	1611.1	15.7969	0.9854	1.1241
27.1	22.01007	78	1.15504	279.78	209943.2	4.238	1922.2	18.8474	0.9707	1.1074
29.5	24.02055	79	1.15344	332.76	228505.2	4.630	2100.0	20.5905	0.8917	1.0171
31.9	26.03103	79	1.15344	390.79	247630.7	5.634	2555.6	25.0572	0.9240	1.0540
34.2	27.95774	80	1.15024	449.53	264877.2	7.422	3366.7	33.0102	1.0582	1.2071
36.6	29.96822	80	1.15024	516.51	283924.9	7.275	3300.0	32.3565	0.9027	1.0297
39.0	31.9787	81	1.14863	587.32	302156.5	8.696	3944.4	38.6753	0.9489	1.0825
41.4	33.98918	82	1.14703	662.56	320290.7	10.460	4744.4	46.5193	1.0117	1.1541

Alpha = 14 deg

Velocity (Hz)	Velocity (m/s)	T (ºF)	ρ(kg/m3)	Q_∞	Re	Lift (lbs)	Lift (g)	Lift (N)	Cl	$Cl_{\beta=0}$
12.8	10.03096	79	1.15344	58.03	95423.57	0.612	277.8	2.7236	0.6763	0.7715
15.2	12.04144	79	1.15344	83.62	114549.1	0.955	433.3	4.2488	0.7322	0.8352
17.5	13.96815	79	1.15344	112.52	132877.7	1.421	644.4	6.3188	0.8092	0.9231
19.9	15.97863	79	1.15344	147.25	152003.2	1.935	877.8	8.6066	0.8423	0.9608
22.3	17.98911	79	1.15344	186.63	171128.7	2.499	1133.3	11.1123	0.8580	0.9787
24.7	19.99959	79	1.15344	230.68	190254.2	3.748	1700.0	16.6685	1.0412	1.1878
27.1	22.01007	79	1.15344	279.39	209379.7	4.728	2144.4	21.0263	1.0845	1.2371
29.5	24.02055	79	1.15344	332.76	228505.2	4.924	2233.3	21.8978	0.9483	1.0817
31.9	26.03103	80	1.15024	389.71	246623.2	6.026	2733.3	26.8003	0.9910	1.1304
34.2	27.95774	81	1.14863	448.90	264163.7	7.863	3566.7	34.9712	1.1226	1.2806
36.6	29.96822	81	1.14863	515.79	283160.1	7.912	3588.9	35.1891	0.9831	1.1215
39.0	31.9787	81	1.14863	587.32	302156.5	9.284	4211.1	41.2899	1.0131	1.1556
41.4	33.98918	82	1.14703	662.56	320290.7	10.974	4977.8	48.8071	1.0615	1.2109

A.3 Full Deflection

T	ρ(kg/m³)	μ (kg m^{-1} s^{-1})
63	1.188684	0.000017873971
64	1.18548	0.000017897914
65	1.183878	0.000017921844
66	1.180674	0.000017945761
67	1.179072	0.000017969663
68	1.17747	0.000017993552
69	1.174266	0.000018017428
70	1.172664	0.000018041290
71	1.16946	0.000018065138
72	1.16786	0.000018088973
73	1.16626	0.000018112794
74	1.16305	0.000018136602
75	1.16145	0.000018160397
76	1.15985	0.000018184178
77	1.15664	0.000018207946
78	1.15504	0.000018231701
79	1.15344	0.000018255442
80	1.15024	0.000018279170
81	1.14863	0.000018302885
82	1.14703	0.000018326587
83	1.14383	0.000018350276
84	1.14223	0.000018373952
85	1.14062	0.000018397614
86	1.13742	0.000018421264
87	1.13581	0.000018444900
88	1.13422	0.000018468524
89	1.13101	0.000018492134
90	1.12941	0.000018515732
91	1.12781	0.000018539317
92	1.12621	0.000018562888
93	1.123	0.000018586448
94	1.1214	0.000018609994
95	1.11979	0.000018633527

Re = 305000

Alpha	Baseline Cl	Full Cl
-4	-0.025	0.492
-2	0.079	0.540
0	0.198	0.707
2	0.257	0.772
4	0.375	0.826
6	0.525	1.128
8	0.66	1.424

Chordlength:	0.144	m
Area:	0.064	m^2
Arc-Anhedral:	18.026	Degrees
Gravity:	9.805	m/s^2

Alpha = -4 deg

Velocity (Hz)	Velocity (m/s)	T (ºF)	ρ(kg/m3)	Q_∞	Re	Lift (lbs)	Lift (g)	Lift (N)	Cl	$Cl_{\beta=0}$
12.8	10.03096	63	1.188684	59.80	96321.75425	0.073	33.3	0.3268	0.0850	0.0940
15.2	12.04144	63	1.188684	86.18	115627.2804	0.171	77.8	0.7626	0.1376	0.1522
17.5	13.96815	63	1.188684	115.96	134128.4096	0.318	144.4	1.4163	0.1900	0.2101
19.9	15.97863	63	1.188684	151.75	153433.9357	0.808	366.7	3.5952	0.3685	0.4075
22.3	17.98911	63	1.188684	192.33	172739.4619	1.298	588.9	5.7741	0.4670	0.5164
24.7	19.99959	63	1.188684	237.73	192044.988	1.935	877.8	8.6066	0.5631	0.6228
27.1	22.01007	64	1.18548	287.15	210498.8551	3.175	1440.0	14.1192	0.7648	0.8458
29.5	24.02055	64	1.18548	342.00	229726.5876	3.699	1677.8	16.4506	0.7482	0.8274
31.9	26.03103	64	1.18548	401.65	248954.3201	4.311	1955.6	19.1742	0.7426	0.8212
34.2	27.95774	65	1.183878	462.68	266663.0361	3.429	1555.6	15.2522	0.5128	0.5671
36.6	29.96822	66	1.180674	530.18	284685.656	3.503	1588.9	15.5791	0.4571	0.5055
39.0	31.9787	67	1.179072	602.88	302968.6559	4.287	1944.4	19.0653	0.4919	0.5440

Alpha = -2 deg

Velocity (Hz)	Velocity (m/s)	T (ºF)	ρ(kg/m3)	Q_∞	Re	Lift (lbs)	Lift (g)	Lift (N)	Cl	$Cl_{\beta=0}$
12.8	10.03096	65	1.183878	59.56	95676.05423	0.220	100.0	0.9805	0.2561	0.2832
15.2	12.04144	65	1.183878	85.83	114852.1643	0.416	188.9	1.8521	0.3356	0.3712
17.5	13.96815	65	1.183878	115.49	133229.2699	0.563	255.6	2.5057	0.3375	0.3732
19.9	15.97863	65	1.183878	151.13	152405.38	1.029	466.7	4.5757	0.4709	0.5208
22.3	17.98911	65	1.183878	191.56	171581.4901	1.641	744.4	7.2993	0.5927	0.6555
24.7	19.99959	66	1.180674	236.13	189987.8071	2.205	1000.0	9.8050	0.6459	0.7143
27.1	22.01007	66	1.180674	285.98	209086.5329	3.527	1600.0	15.6880	0.8533	0.9436
29.5	24.02055	66	1.180674	340.62	228185.2587	4.140	1877.8	18.4116	0.8408	0.9298
31.9	26.03103	67	1.179072	399.48	246619.9742	4.801	2177.8	21.3531	0.8314	0.9195
34.2	27.95774	67	1.179072	460.80	264873.7725	3.895	1766.7	17.3222	0.5847	0.6466
36.6	29.96822	67	1.179072	529.46	283921.2142	4.091	1855.6	18.1937	0.5345	0.5911
39.0	31.9787	68	1.17747	602.06	302155.3258	4.703	2133.3	20.9173	0.5404	0.5976
41.4	33.98918	69	1.174266	678.29	319853.3422	5.316	2411.1	23.6409	0.5421	0.5995
43.8	35.99966	69	1.174266	760.91	338772.8556	5.879	2666.7	26.1467	0.5345	0.5911

Alpha = 0 deg

Velocity (Hz)	Velocity (m/s)	T (ºF)	ρ(kg/m3)	Q_∞	Re	Lift (lbs)	Lift (g)	Lift (N)	Cl	$Cl_{\beta=0}$
12.8	10.03096	67	1.179072	59.32	95034.0842	0.245	111.1	1.0894	0.2857	0.3159
15.2	12.04144	67	1.179072	85.48	114081.5259	0.588	266.7	2.6147	0.4758	0.5262
17.5	13.96815	67	1.179072	115.02	132335.3242	0.808	366.7	3.5952	0.4862	0.5377
19.9	15.97863	67	1.179072	150.52	151382.7658	1.298	588.9	5.7741	0.5967	0.6599
22.3	17.98911	67	1.179072	190.78	170430.2075	2.009	911.1	8.9334	0.7284	0.8055
24.7	19.99959	67	1.179072	235.80	189477.6492	2.817	1277.8	12.5286	0.8264	0.9140
27.1	22.01007	68	1.17747	285.21	207965.2979	4.287	1944.4	19.0653	1.0398	1.1499
29.5	24.02055	68	1.17747	339.69	226961.606	5.095	2311.1	22.6604	1.0376	1.1475
31.9	26.03103	68	1.17747	398.94	245957.9142	5.879	2666.7	26.1467	1.0195	1.1274
34.2	27.95774	69	1.174266	458.92	263094.8019	5.291	2400.0	23.5320	0.7976	0.8820
36.6	29.96822	69	1.174266	527.30	282014.3153	5.316	2411.1	23.6409	0.6974	0.7712
39.0	31.9787	70	1.172664	599.60	300125.7977	6.124	2777.8	27.2361	0.7065	0.7814
41.4	33.98918	70	1.172664	677.37	318994.5108	6.981	3166.7	31.0492	0.7130	0.7885

Alpha = 2 deg

Velocity (Hz)	Velocity (m/s)	T (ºF)	ρ(kg/m3)	Q_∞	Re	Lift (lbs)	Lift (g)	Lift (N)	Cl	$Cl_{\beta=0}$
12.8	10.03096	69	1.174266	59.08	94395.80717	0.539	244.4	2.3968	0.6310	0.6979
15.2	12.04144	69	1.174266	85.13	113315.3206	0.735	333.3	3.2683	0.5972	0.6604
17.5	13.96815	69	1.174266	114.56	131446.521	1.029	466.7	4.5757	0.6213	0.6871
19.9	15.97863	69	1.174266	149.90	150366.0344	1.519	688.9	6.7546	0.7009	0.7751
22.3	17.98911	69	1.174266	190.00	169285.5478	2.205	1000.0	9.8050	0.8027	0.8877
24.7	19.99959	69	1.174266	234.84	188205.0612	3.037	1377.8	13.5091	0.8948	0.9895
27.1	22.01007	69	1.174266	284.43	207124.5747	4.654	2111.1	20.6994	1.1320	1.2519
29.5	24.02055	69	1.174266	338.77	226044.0881	5.389	2444.4	23.9678	1.1005	1.2170
31.9	26.03103	69	1.174266	397.85	244963.6015	6.271	2844.4	27.8898	1.0904	1.2059
34.2	27.95774	70	1.172664	458.30	262388.3717	5.879	2666.7	26.1467	0.8874	0.9814
36.6	29.96822	71	1.16946	525.14	280118.3406	5.659	2566.7	25.1662	0.7454	0.8244
39.0	31.9787	72	1.16786	597.15	298108.3833	6.663	3022.2	29.6329	0.7719	0.8536
41.4	33.98918	73	1.16626	673.67	316000.0277	7.758	3518.9	34.5027	0.7966	0.8810

Alpha = 4 deg

Velocity (Hz)	Velocity (m/s)	T (ºF)	ρ(kg/m3)	Q_∞	Re	Lift (lbs)	Lift (g)	Lift (N)	Cl	$Cl_{\beta=0}$
12.8	10.03096	70	1.172664	59.00	94142.347	0.612	277.8	2.7236	0.7181	0.7941
15.2	12.04144	70	1.172664	85.02	113011.06	0.735	333.3	3.2683	0.5980	0.6613
17.5	13.96815	70	1.172664	114.40	131093.5767	1.029	466.7	4.5757	0.6221	0.6880
19.9	15.97863	70	1.172664	149.70	149962.2898	1.690	766.7	7.5172	0.7811	0.8638
22.3	17.98911	70	1.172664	189.74	168831.0028	2.180	988.9	9.6961	0.7949	0.8790
24.7	19.99959	70	1.172664	234.52	187699.7158	3.160	1433.3	14.0538	0.9321	1.0308
27.1	22.01007	70	1.172664	284.04	206568.4289	4.850	2200.0	21.5710	1.1812	1.3063
29.5	24.02055	70	1.172664	338.31	225437.1419	5.536	2511.1	24.6214	1.1320	1.2519
31.9	26.03103	70	1.172664	397.31	244305.855	6.516	2955.6	28.9792	1.1345	1.2547
34.2	27.95774	71	1.16946	457.05	261326.0226	6.246	2833.3	27.7808	0.9455	1.0456
36.6	29.96822	71	1.16946	525.14	280118.3406	5.854	2655.6	26.0377	0.7712	0.8529
39.0	31.9787	72	1.16786	597.15	298108.3833	7.030	3188.9	31.2671	0.8144	0.9007
41.4	33.98918	72	1.16786	674.59	316850.2628	8.059	3655.6	35.8427	0.8264	0.9140

Alpha = 6.27 deg

Velocity (Hz)	Velocity (m/s)	T (ºF)	ρ(kg/m3)	Q_∞	Re	Lift (lbs)	Lift (g)	Lift (N)	Cl	$Cl_{\beta=0}$
12.8	10.03096	78	1.15504	58.11	91759.03663	0.661	300.0	2.9415	0.7874	0.8707
15.2	12.04144	78	1.15504	83.74	110150.0688	1.014	460.0	4.5103	0.8378	0.9265
17.5	13.96815	78	1.15504	112.68	127774.8079	1.367	620.0	6.0791	0.8392	0.9280
19.9	15.97863	78	1.15504	147.45	146165.8401	2.028	920.0	9.0206	0.9516	1.0524
22.3	17.98911	78	1.15504	186.89	164556.8723	2.910	1320.0	12.9426	1.0772	1.1913
24.7	19.99959	79	1.15344	230.68	182456.8827	3.880	1760.0	17.2568	1.1636	1.2868
27.1	22.01007	79	1.15344	279.39	200798.5544	5.997	2720.0	26.6696	1.4848	1.6420
29.5	24.02055	80	1.15024	331.84	218248.5865	6.878	3120.0	30.5916	1.4340	1.5858
31.9	26.03103	80	1.15024	389.71	236515.6295	8.245	3740.0	36.6707	1.4636	1.6186
34.2	27.95774	81	1.14863	448.90	253337.3155	8.378	3800.0	37.2590	1.2910	1.4277
36.6	29.96822	81	1.14863	515.79	271555.1545	8.289	3760.0	36.8668	1.1118	1.2295
39.0	31.9787	82	1.14703	586.50	288995.108	9.392	4260.0	41.7693	1.1078	1.2251
41.4	33.98918	82	1.14703	662.56	307164.0419	10.803	4900.0	48.0445	1.1279	1.2474
43.8	35.99966	83	1.14383	741.19	324006.5509	12.52226	5680.0	55.6924	1.1688	1.2925

Alpha = 8.13 deg

Velocity (Hz)	Velocity (m/s)	T (ºF)	ρ(kg/m3)	Q_∞	Re	Lift (lbs)	Lift (g)	Lift (N)	Cl	$Cl_{\beta=0}$
12.8	10.03096	76	1.15985	58.35	92381.95622	0.661	300.0	2.9415	0.7841	0.8671
15.2	12.04144	76	1.15985	84.09	110897.8386	1.102	500.0	4.9025	0.9069	1.0029
17.5	13.96815	76	1.15985	113.15	128642.2258	1.720	780.0	7.6479	1.0514	1.1627
19.9	15.97863	76	1.15985	148.06	147158.1082	2.425	1100.0	10.7855	1.1330	1.2530
22.3	17.98911	76	1.15985	187.67	165673.9906	3.660	1660.0	16.2763	1.3490	1.4919
24.7	19.99959	76	1.15985	231.96	184189.8729	4.586	2080.0	20.3944	1.3676	1.5124
27.1	22.01007	76	1.15985	280.94	202705.7553	7.231	3280.0	32.1604	1.7806	1.9692
29.5	24.02055	76	1.15985	334.61	221221.6376	8.466	3840.0	37.6512	1.7502	1.9356
31.9	26.03103	77	1.15664	391.88	238761.9446	9.524	4320.0	42.3576	1.6813	1.8593
34.2	27.95774	77	1.15664	452.04	256434.1238	10.274	4660.0	45.6913	1.5722	1.7387
36.6	29.96822	78	1.15504	518.67	274136.7722	10.450	4740.0	46.4757	1.3938	1.5414
39.0	31.9787	78	1.15504	590.59	292527.8044	11.640	5280.0	51.7704	1.3635	1.5079
41.4	33.98918	79	1.15344	666.26	310084.3481	13.713	6220.0	60.9871	1.4238	1.5746

Alpha = 11.19 deg

Velocity (Hz)	Velocity (m/s)	T (ºF)	ρ(kg/m3)	Q_∞	Re	Lift (lbs)	Lift (g)	Lift (N)	Cl	$Cl_{\beta=0}$
12.8	10.03096	74	1.16305	58.51	92879.84072	0.750	340.0	3.3337	0.8862	0.9800
15.2	12.04144	74	1.16305	84.32	111495.5128	1.279	580.0	5.6869	1.0491	1.1602
17.5	13.96815	75	1.16145	113.30	128988.3774	1.852	840.0	8.2362	1.1307	1.2504
19.9	15.97863	75	1.16145	148.27	147554.0824	2.734	1240.0	12.1582	1.2755	1.4106
22.3	17.98911	76	1.15985	187.67	165673.9906	3.880	1760.0	17.2568	1.4303	1.5818
24.7	19.99959	76	1.15985	231.96	184189.8729	5.512	2500.0	24.5125	1.6437	1.8178
27.1	22.01007	76	1.15985	280.94	202705.7553	7.540	3420.0	33.5331	1.8566	2.0532
29.5	24.02055	76	1.15985	334.61	221221.6376	8.995	4080.0	40.0044	1.8596	2.0566
31.9	26.03103	76	1.15985	392.97	239737.52	10.626	4820.0	47.2601	1.8707	2.0688
34.2	27.95774	77	1.15664	452.04	256434.1238	11.376	5160.0	50.5938	1.7409	1.9253

Alpha = 12 deg

Velocity (Hz)	Velocity (m/s)	T (ºF)	ρ(kg/m3)	Q_∞	Re	Lift (lbs)	Lift (g)	Lift (N)	Cl	$Cl_{\beta=0}$
12.8	10.03096	71	1.16946	58.84	93761.18669	0.882	400.0	3.9220	1.0369	1.1467
15.2	12.04144	71	1.16946	84.78	112553.5047	1.323	600.0	5.8830	1.0793	1.1936
17.5	13.96815	71	1.16946	114.09	130562.8095	1.896	860.0	8.4323	1.1497	1.2714
19.9	15.97863	71	1.16946	149.29	149355.1276	2.601	1180.0	11.5699	1.2055	1.3331
22.3	17.98911	71	1.16946	189.22	168147.4456	3.483	1580.0	15.4919	1.2735	1.4083
24.7	19.99959	71	1.16946	233.88	186939.7637	4.674	2120.0	20.7866	1.3824	1.5288
27.1	22.01007	71	1.16946	283.27	205732.0817	7.033	3190.0	31.2780	1.7175	1.8994
29.5	24.02055	71	1.16946	337.38	224524.3998	8.289	3760.0	36.8668	1.6997	1.8797

Alpha = 14 deg

Velocity (Hz)	Velocity (m/s)	T (ºF)	ρ(kg/m3)	Q_∞	Re	Lift (lbs)	Lift (g)	Lift (N)	Cl	$Cl_{\beta=0}$
12.8	10.03096	71	1.16946	58.84	93761.18669	1.014	460.0	4.5103	1.1924	1.3187
15.2	12.04144	71	1.16946	84.78	112553.5047	1.543	700.0	6.8635	1.2592	1.3925
17.5	13.96815	71	1.16946	114.09	130562.8095	2.006	910.0	8.9225	1.2165	1.3453
19.9	15.97863	71	1.16946	149.29	149355.1276	2.888	1310.0	12.8446	1.3383	1.4800
22.3	17.98911	71	1.16946	189.22	168147.4456	3.792	1720.0	16.8646	1.3863	1.5331
24.7	19.99959	72	1.16786	233.56	186438.0178	4.806	2180.0	21.3749	1.4235	1.5743
27.1	22.01007	72	1.16786	282.88	205179.8974	7.077	3210.0	31.4741	1.7306	1.9139
29.5	24.02055	72	1.16786	336.92	223921.7769	8.708	3950.0	38.7298	1.7880	1.9774
31.9	26.03103	72	1.16786	395.68	242663.6564	8.554	3880.0	38.0434	1.4955	1.6539

A.4 Flare Deflection

T	ρ(kg/m³)	μ (kg m⁻¹ s⁻¹)
63	1.188684	0.000017873971
64	1.18548	0.000017897914
65	1.183878	0.000017921844
66	1.180674	0.000017945761
67	1.179072	0.000017969663
68	1.17747	0.000017993552
69	1.174266	0.000018017428
70	1.172664	0.000018041290
71	1.16946	0.000018065138
72	1.16786	0.000018088973
73	1.16626	0.000018112794
74	1.16305	0.000018136602
75	1.16145	0.000018160397
76	1.15985	0.000018184178
77	1.15664	0.000018207946
78	1.15504	0.000018231701
79	1.15344	0.000018255442
80	1.15024	0.000018279170
81	1.14863	0.000018302885
82	1.14703	0.000018326587
83	1.14383	0.000018350276
84	1.14223	0.000018373952
85	1.14062	0.000018397614
86	1.13742	0.000018421264
87	1.13581	0.000018444900
88	1.13422	0.000018468524
89	1.13101	0.000018492134
90	1.12941	0.000018515732
91	1.12781	0.000018539317
92	1.12621	0.000018562888
93	1.123	0.000018586448
94	1.1214	0.000018609994
95	1.11979	0.000018633527

Re = 305000

Alpha	Baseline Cl	Flare Cl
-4	-0.025	0.105
-2	0.079	0.204
0	0.198	0.332
2	0.257	0.375
4	0.375	0.507
6	0.525	0.652
8	0.66	0.784
10	0.77	0.865
12	0.84	0.978
14	0.945	1.135

Baseline AoA	Cl	Flare AoA	Cl
-4.0000	-0.02487972	6.0000	0.6523
-2.0000	0.078988375	8.0000	0.7844
0.0000	0.198299609	10.0000	0.8651
2.0000	0.256952676	12.0000	0.9778
4.0000	0.375476484	14.0000	1.1348

Chordlength:	0.1492758	m
Area:	0.066434083	m^2
Arc-Anhedral:	18.5322	Degrees
Gravity:	9.805	m/s^2

Alpha = -4 deg

Velocity (Hz)	Velocity (m/s)	T (ºF)	ρ(kg/m3)	Q_∞	Re	Lift (lbs)	Lift (g)	Lift (N)	Cl	$Cl_{\beta=0}$
12.8	10.03096	73	1.16626	58.67	96414.38	0.176	80.0	0.7844	0.2012	0.2238
15.2	12.04144	73	1.16626	84.55	115738.48	0.220	100.0	0.9805	0.1746	0.1942
17.5	13.96815	73	1.16626	113.77	134257.40	0.309	140.0	1.3727	0.1816	0.2020
19.9	15.97863	73	1.16626	148.88	153581.49	0.397	180.0	1.7649	0.1784	0.1985
22.3	17.98911	73	1.16626	188.71	172905.58	0.529	240.0	2.3532	0.1877	0.2088
24.7	19.99959	73	1.16626	233.24	192229.67	1.014	460.0	4.5103	0.2911	0.3238
27.1	22.01007	73	1.16626	282.49	211553.76	0.441	200.0	1.9610	0.1045	0.1162
29.5	24.02055	73	1.16626	336.46	230877.86	0.661	300.0	2.9415	0.1316	0.1464
31.9	26.03103	74	1.16305	394.05	249185.76	1.676	760.0	7.4518	0.2847	0.3166
34.2	27.95774	74	1.16305	454.54	267629.46	1.631	740.0	7.2557	0.2403	0.2673
36.6	29.96822	75	1.16145	521.55	286105.06	0.705	320.0	3.1376	0.0906	0.1007
39.0	31.9787	76	1.15985	593.05	304479.71	0.926	420.0	4.1181	0.1045	0.1163

Alpha = -2 deg

Velocity (Hz)	Velocity (m/s)	T (ºF)	ρ(kg/m3)	Q_∞	Re	Lift (lbs)	Lift (g)	Lift (N)	Cl	$Cl_{\beta=0}$
12.8	10.03096	72	1.16786	58.76	96673.80	0.220	100.0	0.9805	0.2512	0.2794
15.2	12.04144	73	1.16626	84.55	115738.48	0.353	160.0	1.5688	0.2793	0.3107
17.5	13.96815	73	1.16626	113.77	134257.40	0.529	240.0	2.3532	0.3113	0.3463
19.9	15.97863	73	1.16626	148.88	153581.49	0.705	320.0	3.1376	0.3172	0.3529
22.3	17.98911	73	1.16626	188.71	172905.58	0.970	440.0	4.3142	0.3441	0.3828
24.7	19.99959	73	1.16626	233.24	192229.67	1.411	640.0	6.2752	0.4050	0.4505
27.1	22.01007	73	1.16626	282.49	211553.76	2.337	1060.0	10.3933	0.5538	0.6160
29.5	24.02055	73	1.16626	336.46	230877.86	3.219	1460.0	14.3153	0.6404	0.7124
31.9	26.03103	74	1.16305	394.05	249185.76	3.704	1680.0	16.4724	0.6292	0.6999
34.2	27.95774	74	1.16305	454.54	267629.46	1.764	800.0	7.8440	0.2598	0.2890
36.6	29.96822	75	1.16145	521.55	286105.06	0.882	400.0	3.9220	0.1132	0.1259
39.0	31.9787	76	1.15985	593.05	304479.71	1.808	820.0	8.0401	0.2041	0.2270

Alpha = 0 deg

Velocity (Hz)	Velocity (m/s)	T (ºF)	ρ(kg/m3)	Q_∞	Re	Lift (lbs)	Lift (g)	Lift (N)	Cl	$Cl_{\beta=0}$
12.8	10.03096	75	1.16145	58.43	95765.06	0.044	20.0	0.1961	0.0505	0.0562
15.2	12.04144	75	1.16145	84.20	114959.01	0.265	120.0	1.1766	0.2103	0.2340
17.5	13.96815	75	1.16145	113.30	133353.21	0.485	220.0	2.1571	0.2866	0.3188
19.9	15.97863	74	1.16305	148.47	152957.72	0.661	300.0	2.9415	0.2982	0.3317
22.3	17.98911	74	1.16305	188.19	172203.33	0.882	400.0	3.9220	0.3137	0.3490
24.7	19.99959	74	1.16305	232.60	191448.94	1.323	600.0	5.8830	0.3807	0.4235
27.1	22.01007	75	1.16145	281.33	210129.01	2.601	1180.0	11.5699	0.6190	0.6886
29.5	24.02055	75	1.16145	335.07	229322.96	2.205	1000.0	9.8050	0.4405	0.4900
31.9	26.03103	75	1.16145	393.51	248516.91	2.161	980.0	9.6089	0.3676	0.4089
34.2	27.95774	76	1.15985	453.29	266194.83	2.513	1140.0	11.1777	0.3712	0.4129
36.6	29.96822	77	1.15664	519.39	284176.13	1.631	740.0	7.2557	0.2103	0.2339
39.0	31.9787	78	1.15504	590.59	302426.64	2.072	940.0	9.2167	0.2349	0.2613
41.4	33.98918	78	1.15504	667.19	321440.01	3.307	1500.0	14.7075	0.3318	0.3691

Alpha = 2 deg

Velocity (Hz)	Velocity (m/s)	T (ºF)	ρ(kg/m3)	Q_∞	Re	Lift (lbs)	Lift (g)	Lift (N)	Cl	$Cl_{\beta=0}$
12.8	10.03096	77	1.15664	58.19	95119.41	0.529	240.0	2.3532	0.6087	0.6771
15.2	12.04144	77	1.15664	83.85	114183.95	0.661	300.0	2.9415	0.5280	0.5874
17.5	13.96815	76	1.15985	113.15	132995.35	0.794	360.0	3.5298	0.4696	0.5223
19.9	15.97863	76	1.15985	148.06	152137.79	1.058	480.0	4.7064	0.4785	0.5322
22.3	17.98911	76	1.15985	187.67	171280.23	1.190	540.0	5.2947	0.4247	0.4724
24.7	19.99959	76	1.15985	231.96	190422.67	1.676	760.0	7.4518	0.4836	0.5379
27.1	22.01007	76	1.15985	280.94	209565.11	1.102	500.0	4.9025	0.2627	0.2922
29.5	24.02055	77	1.15664	333.68	227776.86	2.381	1080.0	10.5894	0.4777	0.5314
31.9	26.03103	77	1.15664	391.88	246841.40	2.690	1220.0	11.9621	0.4595	0.5111
34.2	27.95774	78	1.15504	451.41	264399.91	3.263	1480.0	14.5114	0.4839	0.5383
36.6	29.96822	78	1.15504	518.67	283413.28	2.866	1300.0	12.7465	0.3699	0.4115
39.0	31.9787	79	1.15344	589.78	301614.95	3.307	1500.0	14.7075	0.3754	0.4176
41.4	33.98918	80	1.15024	664.42	319272.92	4.189	1900.0	18.6295	0.4221	0.4695
43.8	35.99966	81	1.14863	744.30	337247.24	5.247	2380.0	23.3359	0.4719	0.5250

Alpha = 4 deg

Velocity (Hz)	Velocity (m/s)	T (ºF)	ρ(kg/m3)	Q_∞	Re	Lift (lbs)	Lift (g)	Lift (N)	Cl	$Cl_{\beta=0}$
12.8	10.03096	79	1.15344	58.03	94609.46	0.529	240.0	2.3532	0.6104	0.6790
15.2	12.04144	78	1.15504	83.74	113877.43	0.661	300.0	2.9415	0.5288	0.5882
17.5	13.96815	78	1.15504	112.68	132098.58	0.882	400.0	3.9220	0.5239	0.5828
19.9	15.97863	78	1.15504	147.45	151111.94	1.102	500.0	4.9025	0.5005	0.5567
22.3	17.98911	78	1.15504	186.89	170125.31	1.455	660.0	6.4713	0.5212	0.5798
24.7	19.99959	78	1.15504	231.00	189138.67	2.028	920.0	9.0206	0.5878	0.6539
27.1	22.01007	78	1.15504	279.78	208152.04	2.866	1300.0	12.7465	0.6858	0.7629
29.5	24.02055	78	1.15504	333.22	227165.40	2.998	1360.0	13.3348	0.6024	0.6701
31.9	26.03103	79	1.15344	390.79	245518.04	3.439	1560.0	15.2958	0.5892	0.6554
34.2	27.95774	79	1.15344	450.78	263690.28	4.277	1940.0	19.0217	0.6352	0.7065
36.6	29.96822	80	1.15024	516.51	281502.55	3.836	1740.0	17.0607	0.4972	0.5531
39.0	31.9787	81	1.14863	587.32	299578.61	4.101	1860.0	18.2373	0.4674	0.5199
41.4	33.98918	81	1.14863	663.49	318412.93	5.027	2280.0	22.3554	0.5072	0.5642
43.8	35.99966	82	1.14703	743.26	336341.91	6.173	2800.0	27.4540	0.5560	0.6185

Alpha = 6 deg

Velocity (Hz)	Velocity (m/s)	T (ºF)	ρ(kg/m3)	Q_∞	Re	Lift (lbs)	Lift (g)	Lift (N)	Cl	$Cl_{\beta=0}$
12.8	10.03096	80	1.15024	57.87	94224.51	0.485	220.0	2.1571	0.5611	0.6241
15.2	12.04144	80	1.15024	83.39	113109.69	0.882	400.0	3.9220	0.7079	0.7875
17.5	13.96815	80	1.15024	112.21	131207.99	1.102	500.0	4.9025	0.6576	0.7315
19.9	15.97863	80	1.15024	146.84	150093.17	1.411	640.0	6.2752	0.6433	0.7156
22.3	17.98911	80	1.15024	186.11	168978.35	1.808	820.0	8.0401	0.6503	0.7233
24.7	19.99959	80	1.15024	230.04	187863.53	2.425	1100.0	10.7855	0.7057	0.7851
27.1	22.01007	80	1.15024	278.61	206748.71	3.968	1800.0	17.6490	0.9535	1.0607
29.5	24.02055	80	1.15024	331.84	225633.89	4.497	2040.0	20.0022	0.9073	1.0093
31.9	26.03103	80	1.15024	389.71	244519.08	4.806	2180.0	21.3749	0.8256	0.9184
34.2	27.95774	81	1.14863	448.90	261909.99	5.247	2380.0	23.3359	0.7825	0.8704
36.6	29.96822	81	1.14863	515.79	280744.30	5.908	2680.0	26.2774	0.7669	0.8530
39.0	31.9787	82	1.14703	586.50	298774.41	5.423	2460.0	24.1203	0.6190	0.6886
41.4	33.98918	83	1.14383	660.71	316263.43	6.437	2920.0	28.6306	0.6523	0.7256
43.8	35.99966	83	1.14383	741.19	334970.60	8.201	3720.0	36.4746	0.7407	0.8240
46.2	38.01014	85	1.14062	823.97	351777.74	9.789	4440.0	43.5342	0.7953	0.8847
48.6	40.02062	86	1.13742	910.87	368871.13	11.244	5100.0	50.0055	0.8264	0.9192

Alpha = 8 deg

Velocity (Hz)	Velocity (m/s)	T (ºF)	ρ(kg/m3)	Q_∞	Re	Lift (lbs)	Lift (g)	Lift (N)	Cl	$Cl_{\beta=0}$
12.8	10.03096	63	1.188684	59.80	99581.18	0.397	180.0	1.7649	0.4442	0.4941
15.2	12.04144	63	1.188684	86.18	119539.99	0.750	340.0	3.3337	0.5823	0.6477
17.5	13.96815	64	1.18548	115.65	138108.40	1.190	540.0	5.2947	0.6891	0.7666
19.9	15.97863	64	1.18548	151.34	157986.78	1.676	760.0	7.4518	0.7412	0.8245
22.3	17.98911	65	1.183878	191.56	177387.63	2.249	1020.0	10.0011	0.7859	0.8742
24.7	19.99959	65	1.183878	236.77	197212.64	3.086	1400.0	13.7270	0.8727	0.9708
27.1	22.01007	65	1.183878	286.76	217037.65	5.115	2320.0	22.7476	1.1941	1.3282
29.5	24.02055	66	1.180674	340.62	235906.81	5.776	2620.0	25.6891	1.1353	1.2628
31.9	26.03103	66	1.180674	400.02	255651.82	5.644	2560.0	25.1008	0.9445	1.0507
34.2	27.95774	67	1.179072	460.80	273836.83	6.261	2840.0	27.8462	0.9096	1.0118
36.6	29.96822	67	1.179072	529.46	293528.82	5.908	2680.0	26.2774	0.7471	0.8310
39.0	31.9787	68	1.17747	602.06	312379.95	7.055	3200.0	31.3760	0.7844	0.8726
41.4	33.98918	69	1.174266	678.29	330676.85	8.201	3720.0	36.4746	0.8094	0.9004
43.8	35.99966	70	1.172664	759.87	349296.17	10.406	4720.0	46.2796	0.9168	1.0198
46.2	38.01014	71	1.16946	844.80	367310.18	11.905	5400.0	52.9470	0.9434	1.0494

Alpha = 10 deg

Velocity (Hz)	Velocity (m/s)	T (ºF)	ρ(kg/m3)	Q_∞	Re	Lift (lbs)	Lift (g)	Lift (N)	Cl	$Cl_{\beta=0}$
12.8	10.03096	69	1.174266	59.08	97590.06	0.705	320.0	3.1376	0.7994	0.8893
15.2	12.04144	69	1.174266	85.13	117149.79	0.970	440.0	4.3142	0.7628	0.8485
17.5	13.96815	69	1.174266	114.56	135894.54	1.323	600.0	5.8830	0.7730	0.8599
19.9	15.97863	69	1.174266	149.90	155454.27	1.940	880.0	8.6284	0.8664	0.9638
22.3	17.98911	69	1.174266	190.00	175014.00	2.646	1200.0	11.7660	0.9321	1.0369
24.7	19.99959	69	1.174266	234.84	194573.73	3.483	1580.0	15.4919	0.9930	1.1046
27.1	22.01007	69	1.174266	284.43	214133.46	5.600	2540.0	24.9047	1.3180	1.4661
29.5	24.02055	69	1.174266	338.77	233693.19	7.099	3220.0	31.5721	1.4028	1.5605
31.9	26.03103	70	1.172664	397.31	252572.91	6.129	2780.0	27.2579	1.0327	1.1487
34.2	27.95774	71	1.16946	457.05	270169.03	6.923	3140.0	30.7877	1.0140	1.1279
36.6	29.96822	71	1.16946	525.14	289597.26	7.584	3440.0	33.7292	0.9668	1.0754
39.0	31.9787	72	1.16786	597.15	308196.06	7.716	3500.0	34.3175	0.8651	0.9623
41.4	33.98918	72	1.16786	674.59	327572.15	9.304	4220.0	41.3771	0.9233	1.0270
43.8	35.99966	74	1.16305	753.64	344611.89	11.067	5020.0	49.2211	0.9831	1.0936

Alpha = 12 deg

Velocity (Hz)	Velocity (m/s)	T (ºF)	ρ(kg/m3)	Q_∞	Re	Lift (lbs)	Lift (g)	Lift (N)	Cl	$Cl_{\beta=0}$
12.8	10.03096	72	1.16786	58.76	96673.80	0.838	380.0	3.7259	0.9545	1.0618
15.2	12.04144	72	1.16786	84.67	116049.88	1.146	520.0	5.0986	0.9064	1.0083
17.5	13.96815	72	1.16786	113.93	134618.63	1.499	680.0	6.6674	0.8809	0.9799
19.9	15.97863	72	1.16786	149.09	153994.72	2.028	920.0	9.0206	0.9108	1.0131
22.3	17.98911	72	1.16786	188.96	173370.80	2.866	1300.0	12.7465	1.0154	1.1295
24.7	19.99959	72	1.16786	233.56	192746.89	3.660	1660.0	16.2763	1.0490	1.1668
27.1	22.01007	72	1.16786	282.88	212122.97	6.526	2960.0	29.0228	1.5443	1.7179
29.5	24.02055	72	1.16786	336.92	231499.06	7.981	3620.0	35.4941	1.5858	1.7640
31.9	26.03103	72	1.16786	395.68	250875.14	6.790	3080.0	30.1994	1.1489	1.2780
34.2	27.95774	73	1.16626	455.79	268720.87	7.496	3400.0	33.3370	1.1009	1.2247
36.6	29.96822	73	1.16626	523.71	288044.96	8.378	3800.0	37.2590	1.0709	1.1913
39.0	31.9787	74	1.16305	594.69	306120.68	8.686	3940.0	38.6317	0.9778	1.0877
41.4	33.98918	75	1.16145	670.89	324492.96	10.538	4780.0	46.8679	1.0516	1.1697
43.8	35.99966	76	1.15985	751.57	342764.59	12.831	5820.0	57.0651	1.1429	1.2713

Alpha = 14 deg

Velocity (Hz)	Velocity (m/s)	T (ºF)	ρ(kg/m3)	Q_∞	Re	Lift (lbs)	Lift (g)	Lift (N)	Cl	$Cl_{\beta=0}$
12.8	10.03096	74	1.16305	58.51	96022.80	0.750	340.0	3.3337	0.8576	0.9540
15.2	12.04144	74	1.16305	84.32	115268.41	1.190	540.0	5.2947	0.9452	1.0514
17.5	13.96815	74	1.16305	113.46	133712.11	1.631	740.0	7.2557	0.9626	1.0708
19.9	15.97863	74	1.16305	148.47	152957.72	2.293	1040.0	10.1972	1.0338	1.1500
22.3	17.98911	74	1.16305	188.19	172203.33	3.131	1420.0	13.9231	1.1137	1.2388
24.7	19.99959	74	1.16305	232.60	191448.94	4.189	1900.0	18.6295	1.2056	1.3411
27.1	22.01007	74	1.16305	281.72	210694.54	6.570	2980.0	29.2189	1.5612	1.7366
29.5	24.02055	74	1.16305	335.53	229940.15	8.333	3780.0	37.0629	1.6627	1.8495
31.9	26.03103	74	1.16305	394.05	249185.76	9.039	4100.0	40.2005	1.5356	1.7082
34.2	27.95774	74	1.16305	454.54	267629.46	8.818	4000.0	39.2200	1.2988	1.4448
36.6	29.96822	75	1.16145	521.55	286105.06	9.833	4460.0	43.7303	1.2621	1.4039
39.0	31.9787	76	1.15985	593.05	304479.71	10.053	4560.0	44.7108	1.1348	1.2623
41.4	33.98918	77	1.15664	668.11	322305.22	11.773	5340.0	52.3587	1.1796	1.3122
43.8	35.99966	78	1.15504	748.45	340453.38	13.404	6080.0	59.6144	1.1989	1.3337

A.5 Plots

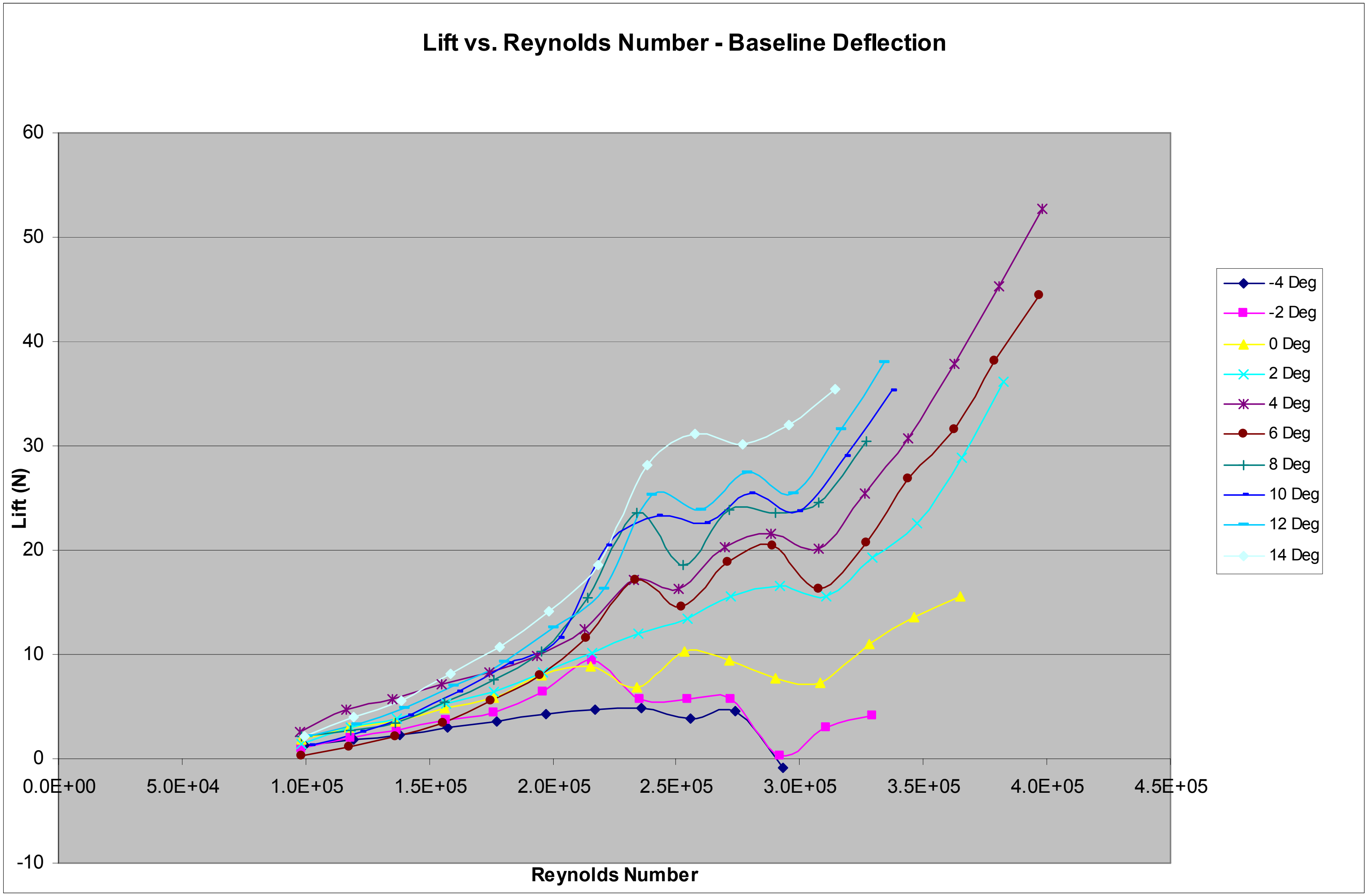
Lift vs. Reynolds Number - Baseline Deflection
Lift (N)
Reynolds Number
60
50
40
30
20
10
0
-10
0.0E+00
5.0E+04
1.0E+05
1.5E+05
2.0E+05
2.5E+05
3.0E+05
3.5E+05
4.0E+05
4.5E+05
-4 Deg
-2 Deg
0 Deg
2 Deg
4 Deg
6 Deg
8 Deg
10 Deg
12 Deg
14 Deg

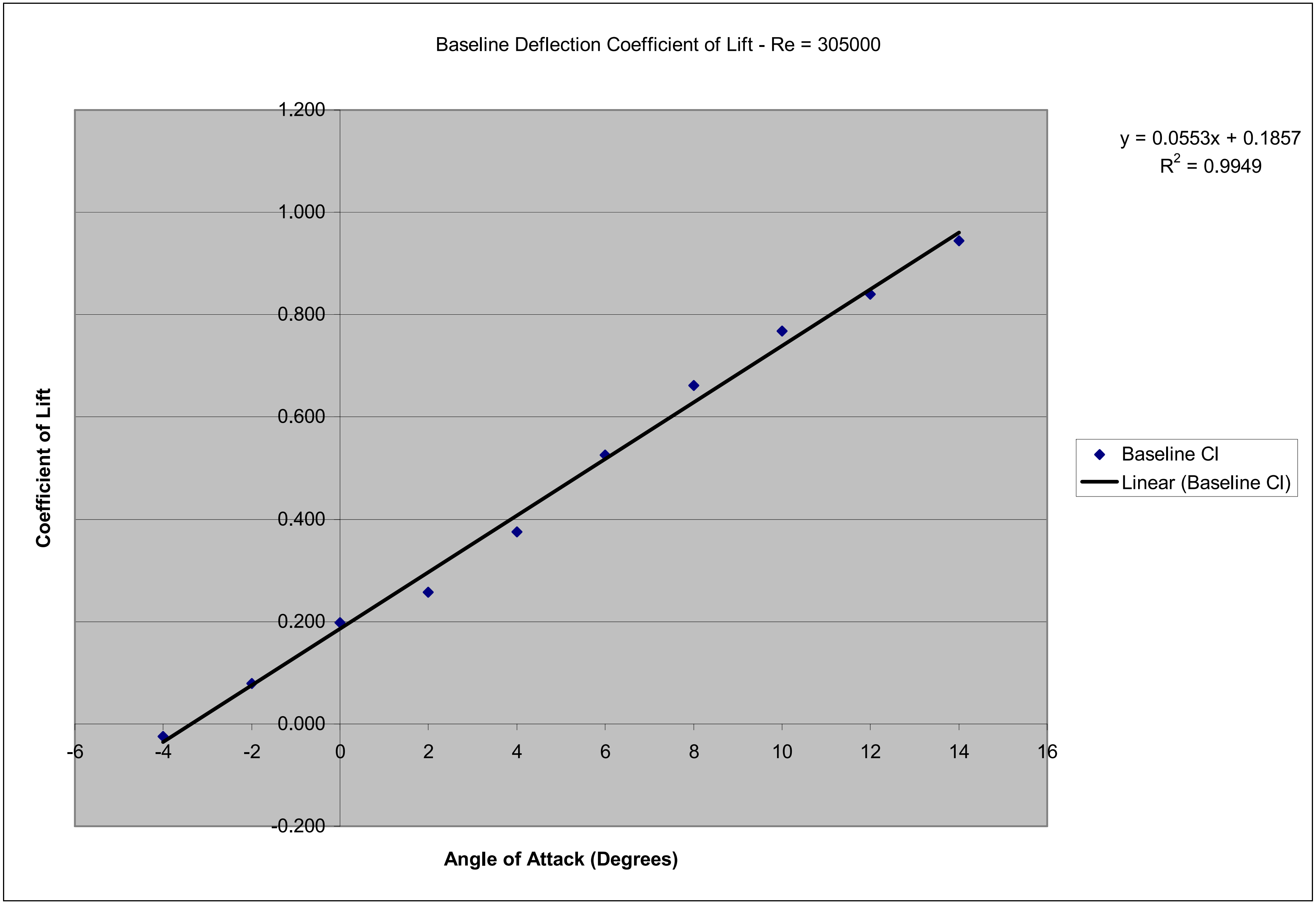
Baseline Deflection Coefficient of Lift - Re = 305000
y = 0.0553x + 0.1857
R^2 = 0.9949
Coefficient of Lift
1.200
1.000
0.800
0.600
0.400
0.200
0.000
-0.200
-6
-4
-2
0
2
4
6
8
10
12
14
16
Baseline Cl
Linear (Baseline Cl)
Angle of Attack (Degrees)

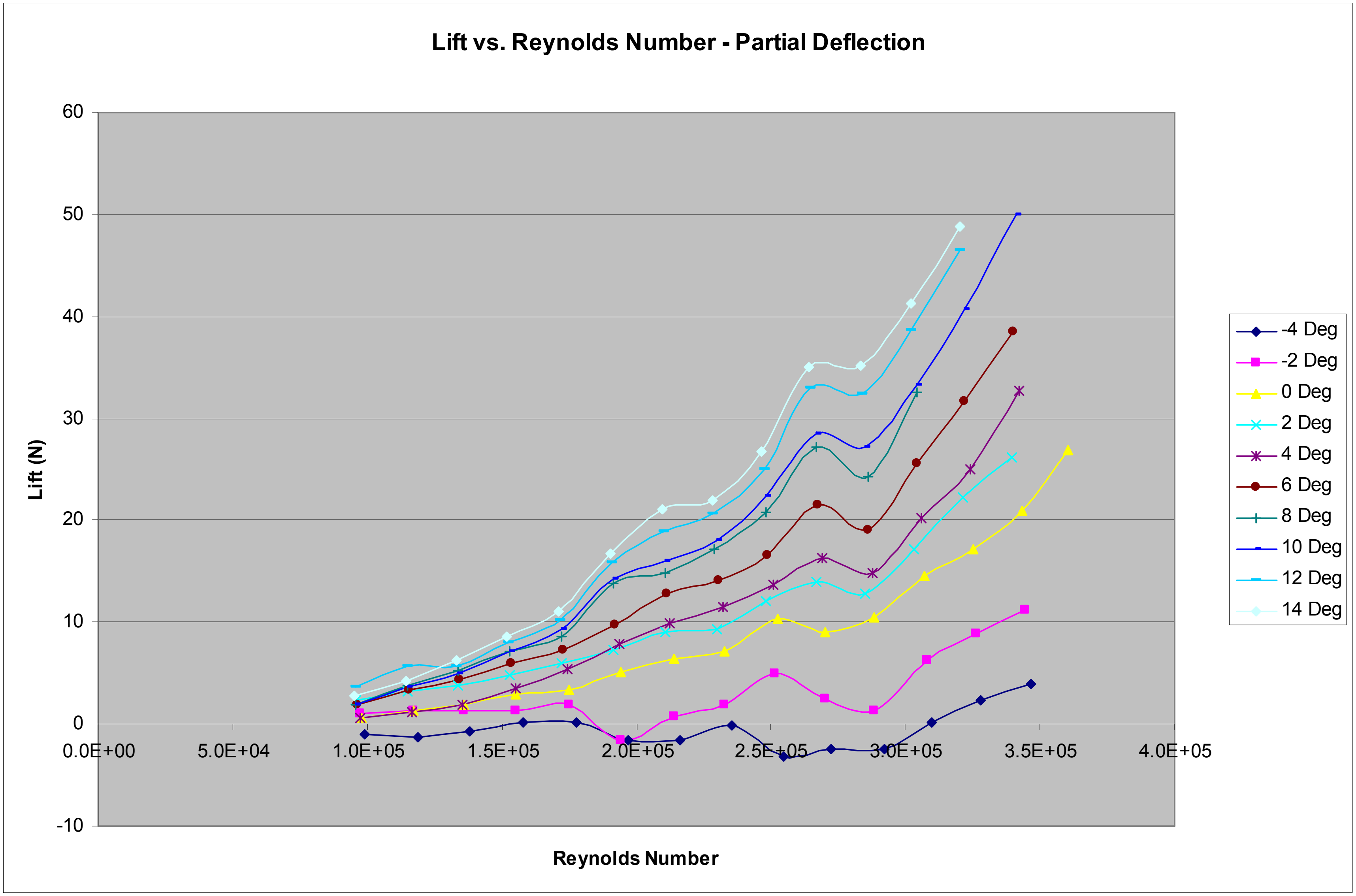
Lift vs. Reynolds Number - Partial Deflection
60
50
40
30
20
10
0
-10
Lift (N)
0.0E+00
5.0E+04
1.0E+05
1.5E+05
2.0E+05
2.5E+05
3.0E+05
3.5E+05
4.0E+05
Reynolds Number
-4 Deg
-2 Deg
0 Deg
2 Deg
4 Deg
6 Deg
8 Deg
10 Deg
12 Deg
14 Deg

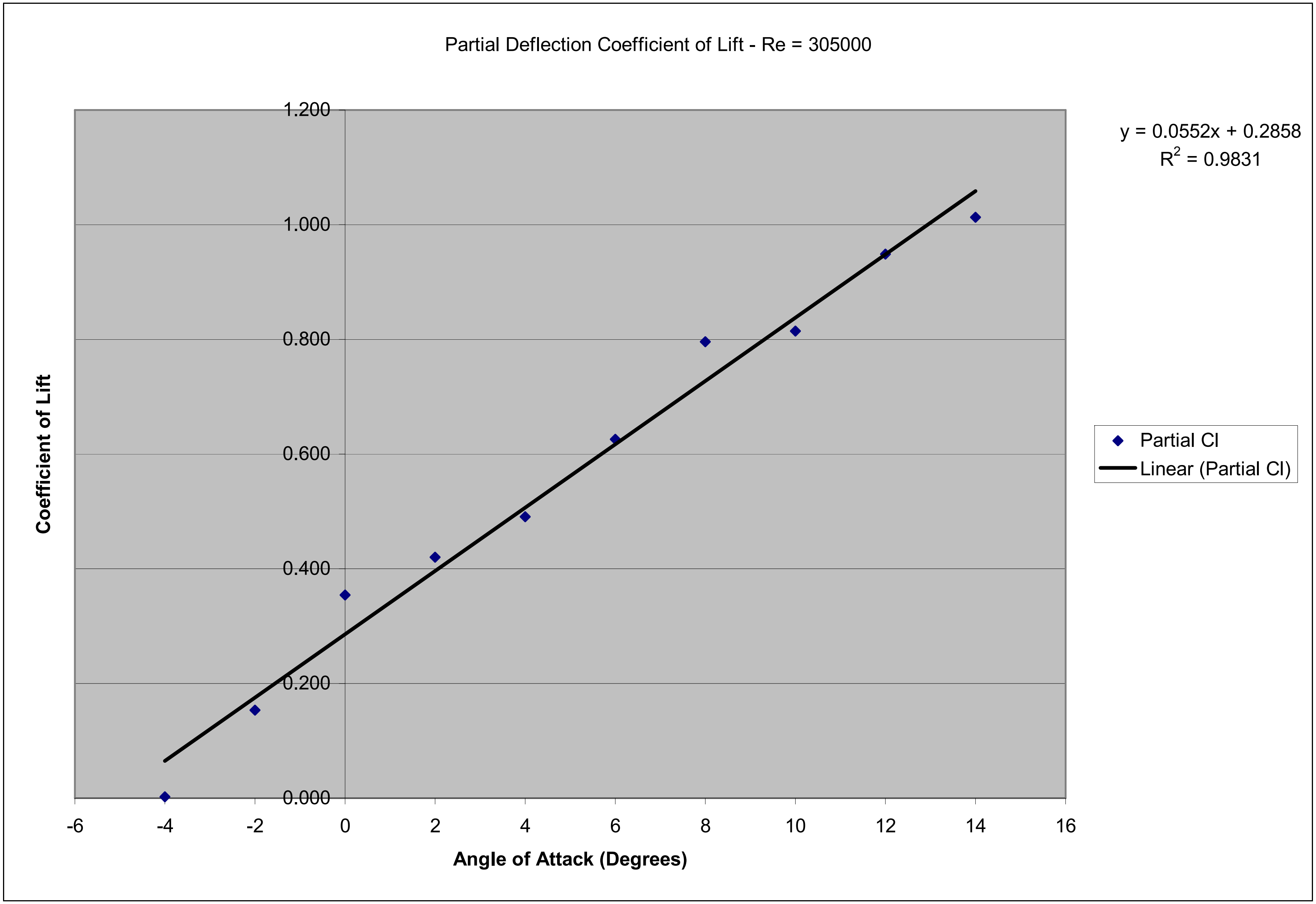
Partial Deflection Coefficient of Lift - Re = 305000
y = 0.0552x + 0.2858
R2 = 0.9831
Coefficient of Lift
1.200
1.000
0.800
0.600
0.400
0.200
0.000
-6
-4
-2
0
2
4
6
8
10
12
14
16
Angle of Attack (Degrees)
Partial Cl
Linear (Partial Cl)

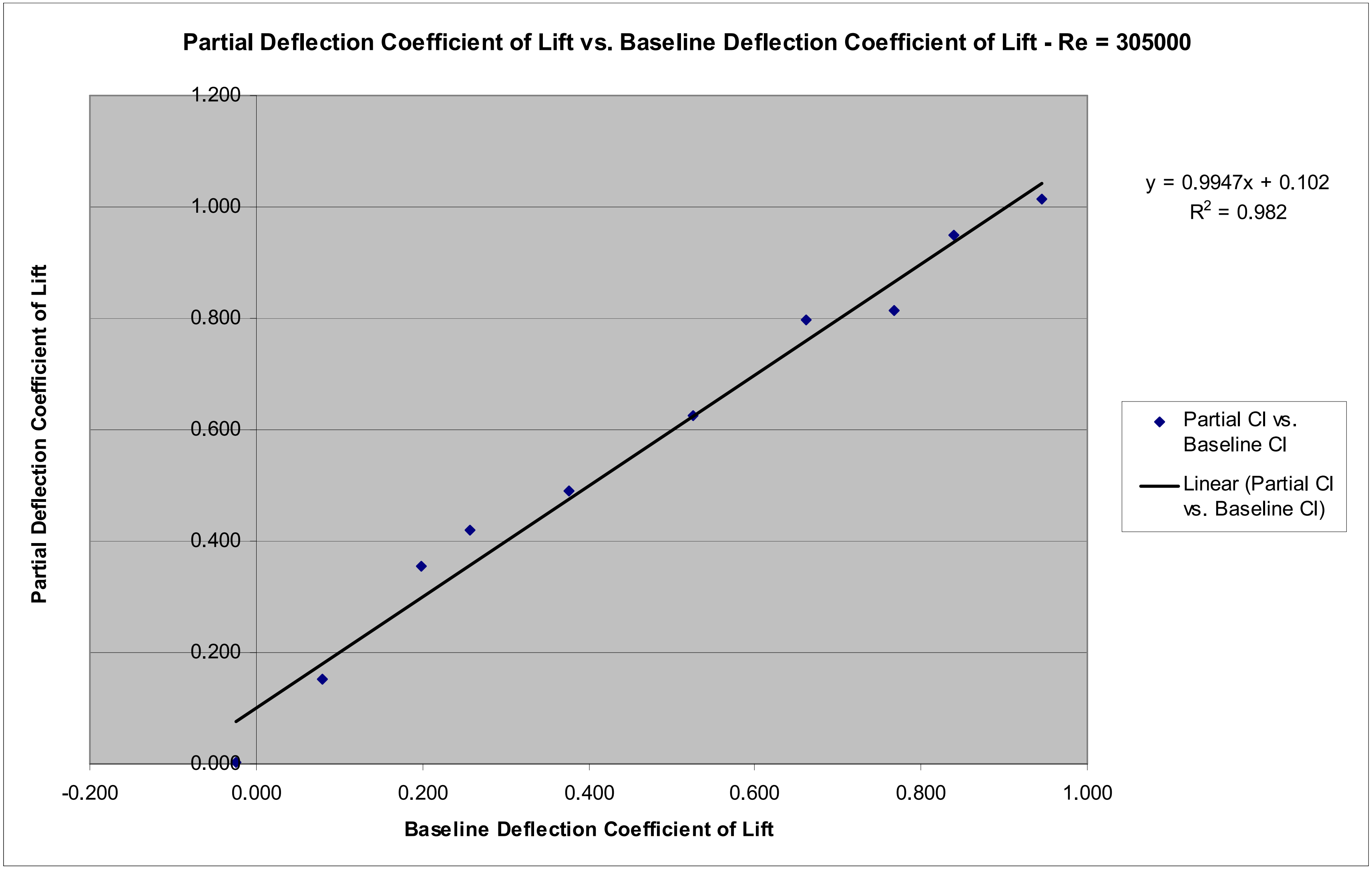

Partial Deflection Coefficient of Lift vs. Baseline Deflection Coefficient of Lift - Re = 305000
y = 0.9947x + 0.102
R2 = 0.982
Partial Cl vs. Baseline Cl
Linear (Partial Cl vs. Baseline Cl)
Partial Deflection Coefficient of Lift
Baseline Deflection Coefficient of Lift
1.200
1.000
0.800
0.600
0.400
0.200
0.000
-0.200
0.000
0.200
0.400
0.600
0.800
1.000

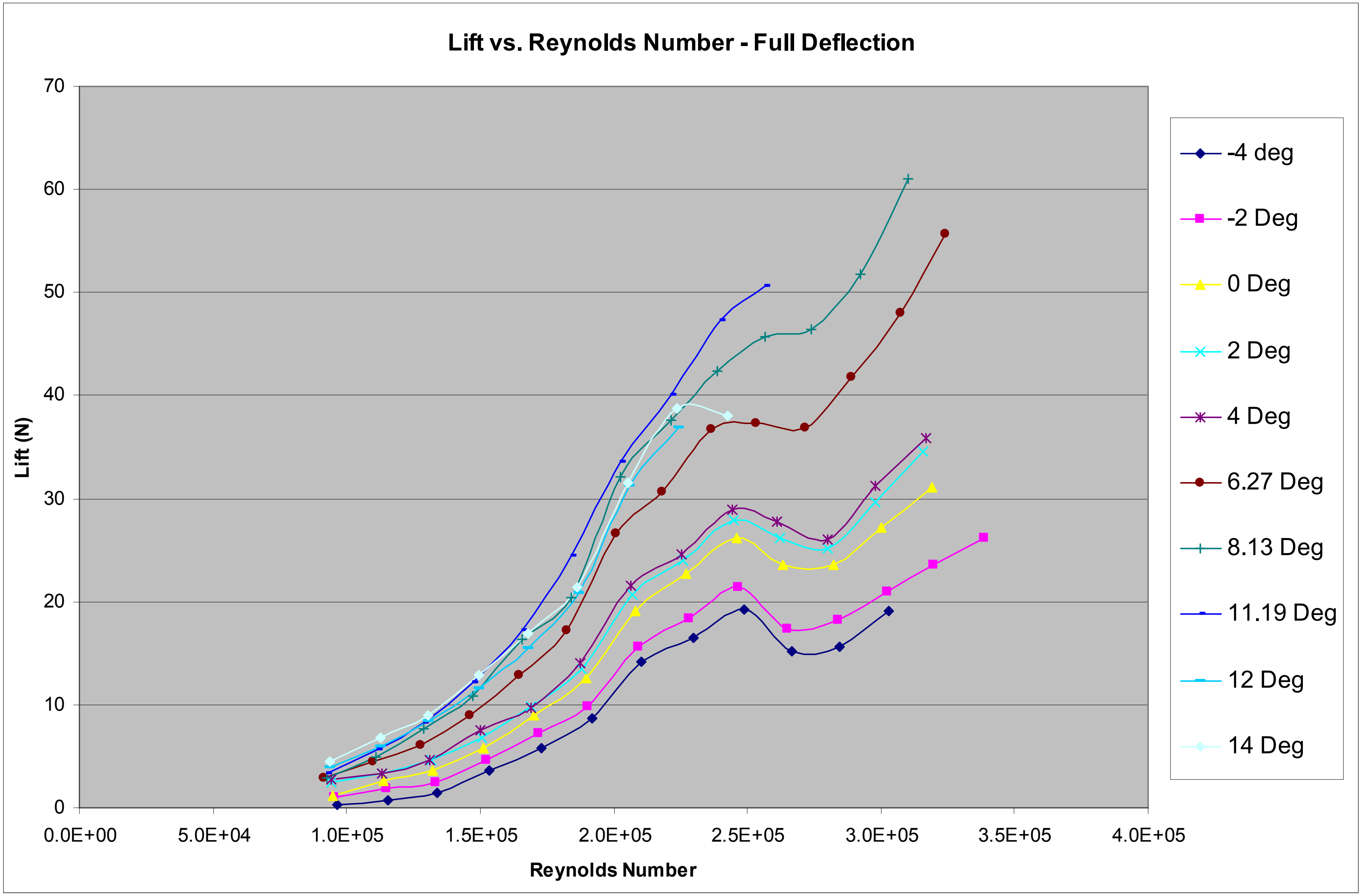
Lift vs. Reynolds Number - Full Deflection
Lift (N)
70
60
50
40
30
20
10
0
0.0E+00
5.0E+04
1.0E+05
1.5E+05
2.0E+05
2.5E+05
3.0E+05
3.5E+05
4.0E+05
Reynolds Number
-4 deg
-2 Deg
0 Deg
2 Deg
4 Deg
6.27 Deg
8.13 Deg
11.19 Deg
12 Deg
14 Deg

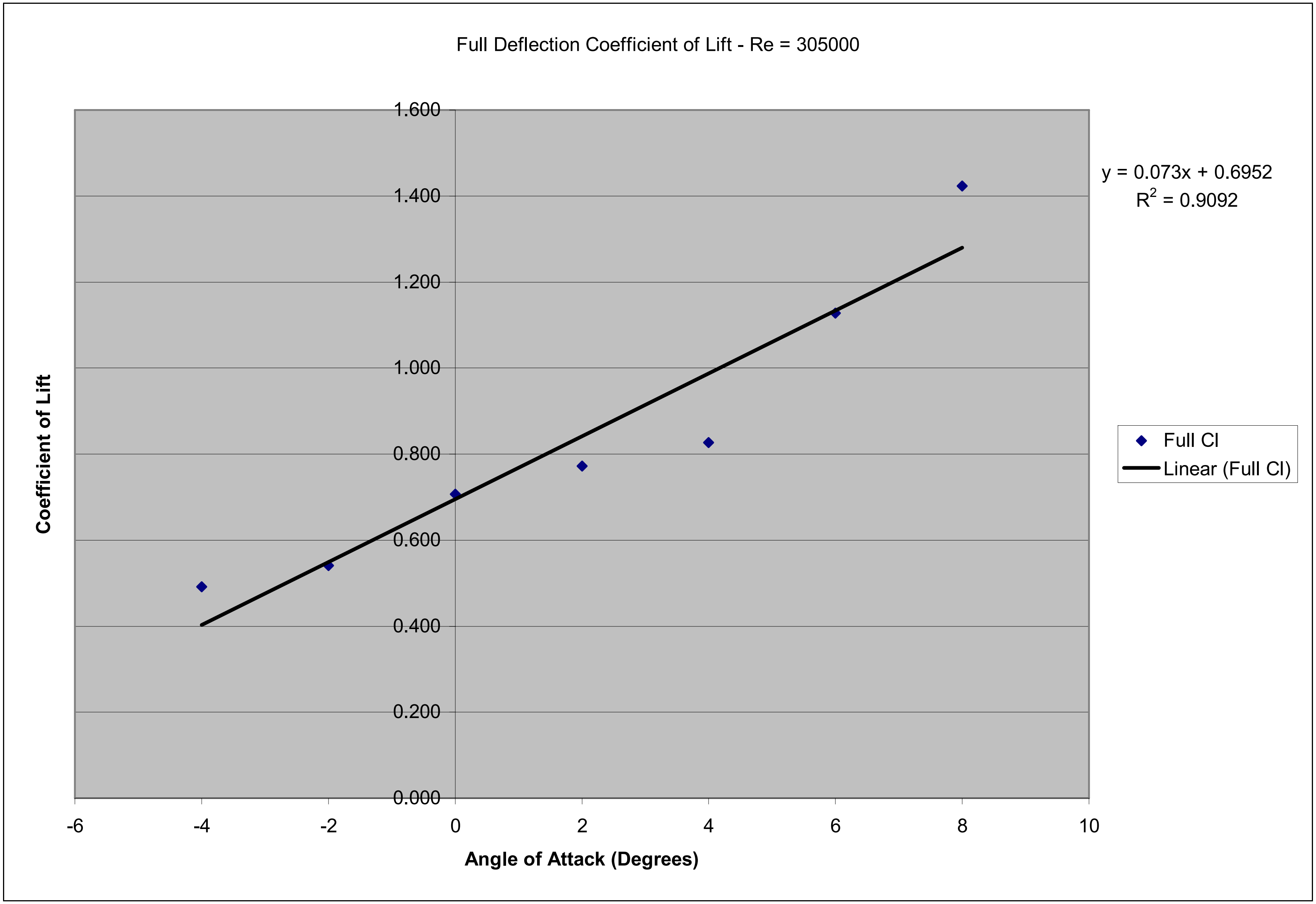

Full Deflection Coefficient of Lift - Re = 305000
1.600
1.400
1.200
1.000
0.800
0.600
0.400
0.200
0.000
-6
-4
-2
0
2
4
6
8
10
Angle of Attack (Degrees)
Coefficient of Lift
y = 0.073x + 0.6952
R2 = 0.9092
Full Cl
Linear (Full Cl)

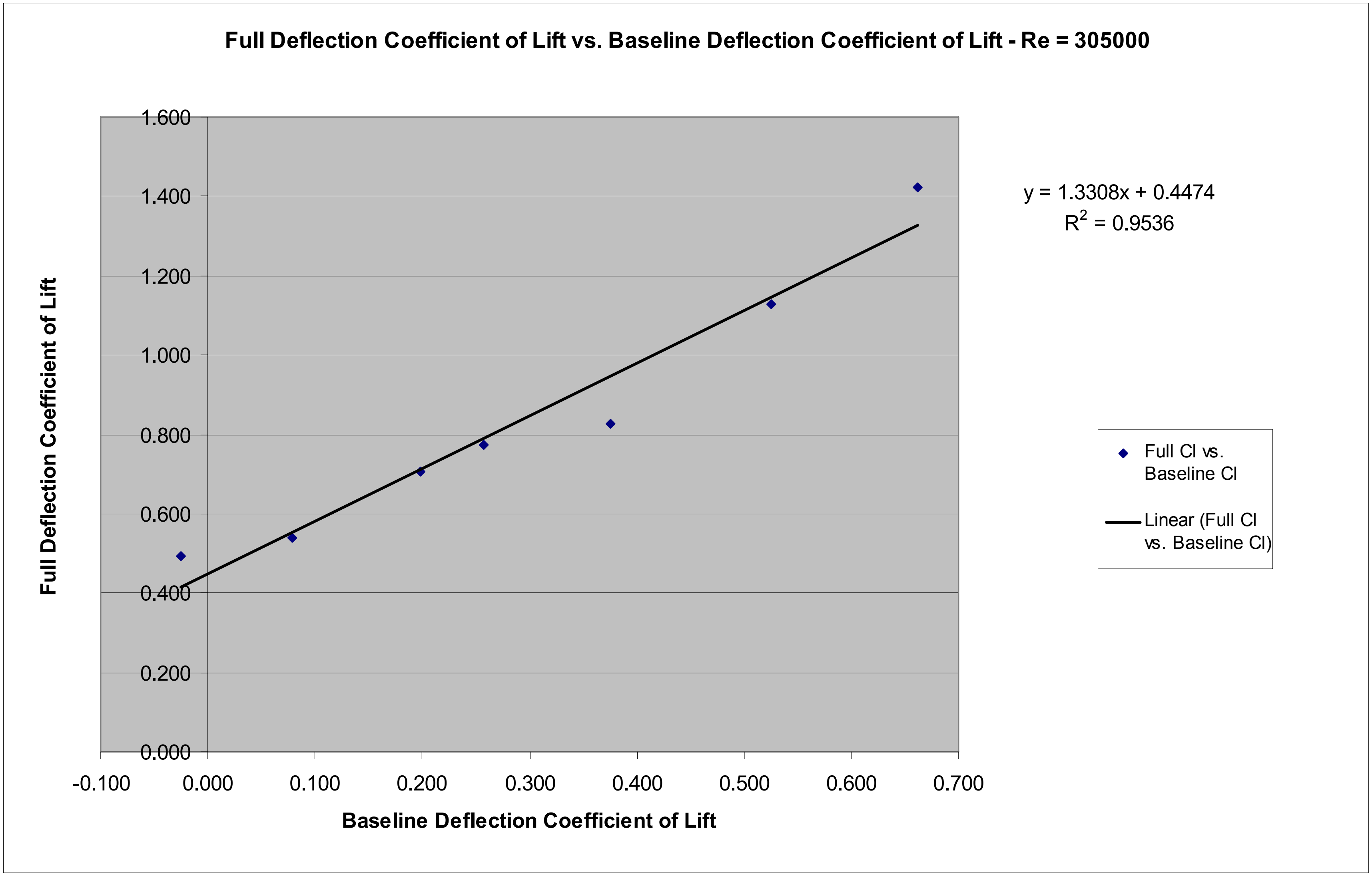

Full Deflection Coefficient of Lift vs. Baseline Deflection Coefficient of Lift - Re = 305000
Full Deflection Coefficient of Lift
Baseline Deflection Coefficient of Lift
1.600
1.400
1.200
1.000
0.800
0.600
0.400
0.200
0.000
-0.100
0.000
0.100
0.200
0.300
0.400
0.500
0.600
0.700
y = 1.3308x + 0.4474
R2 = 0.9536
Full Cl vs. Baseline Cl
Linear (Full Cl vs. Baseline Cl)

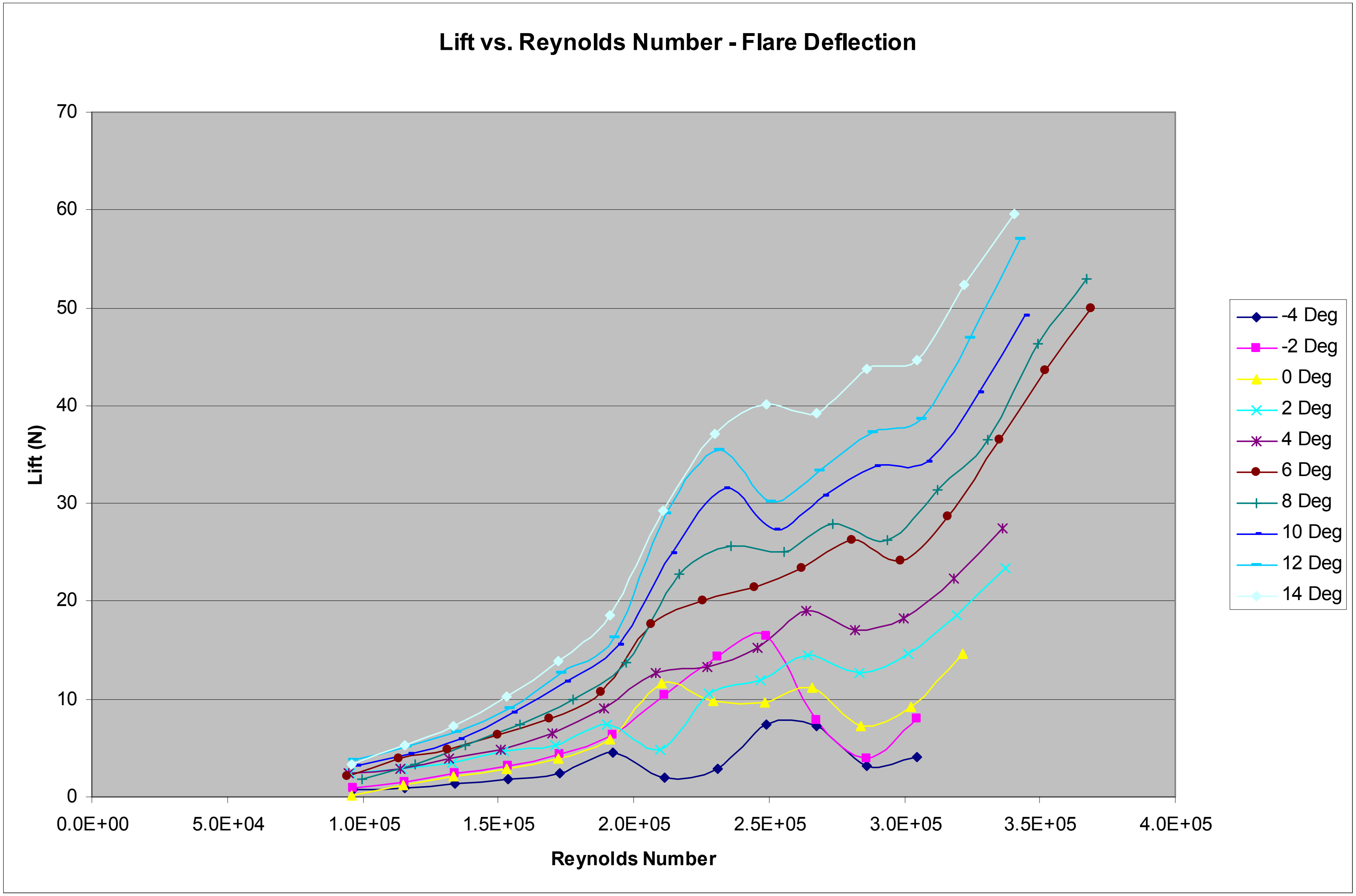

Lift vs. Reynolds Number - Flare Deflection
Lift (N)
Reynolds Number
0
10
20
30
40
50
60
70
0.0E+00
5.0E+04
1.0E+05
1.5E+05
2.0E+05
2.5E+05
3.0E+05
3.5E+05
4.0E+05
-4 Deg
-2 Deg
0 Deg
2 Deg
4 Deg
6 Deg
8 Deg
10 Deg
12 Deg
14 Deg


Flare Deflection Coefficient of Lift - Re = 305000
Coefficient of Lift
1.200
1.000
0.800
0.600
0.400
0.200
0.000
-6
-4
-2
0
2
4
6
8
10
12
14
16
Angle of Attack
y = 0.0568x + 0.31
R^2 = 0.9945
Flare Cl
Linear (Flare Cl)

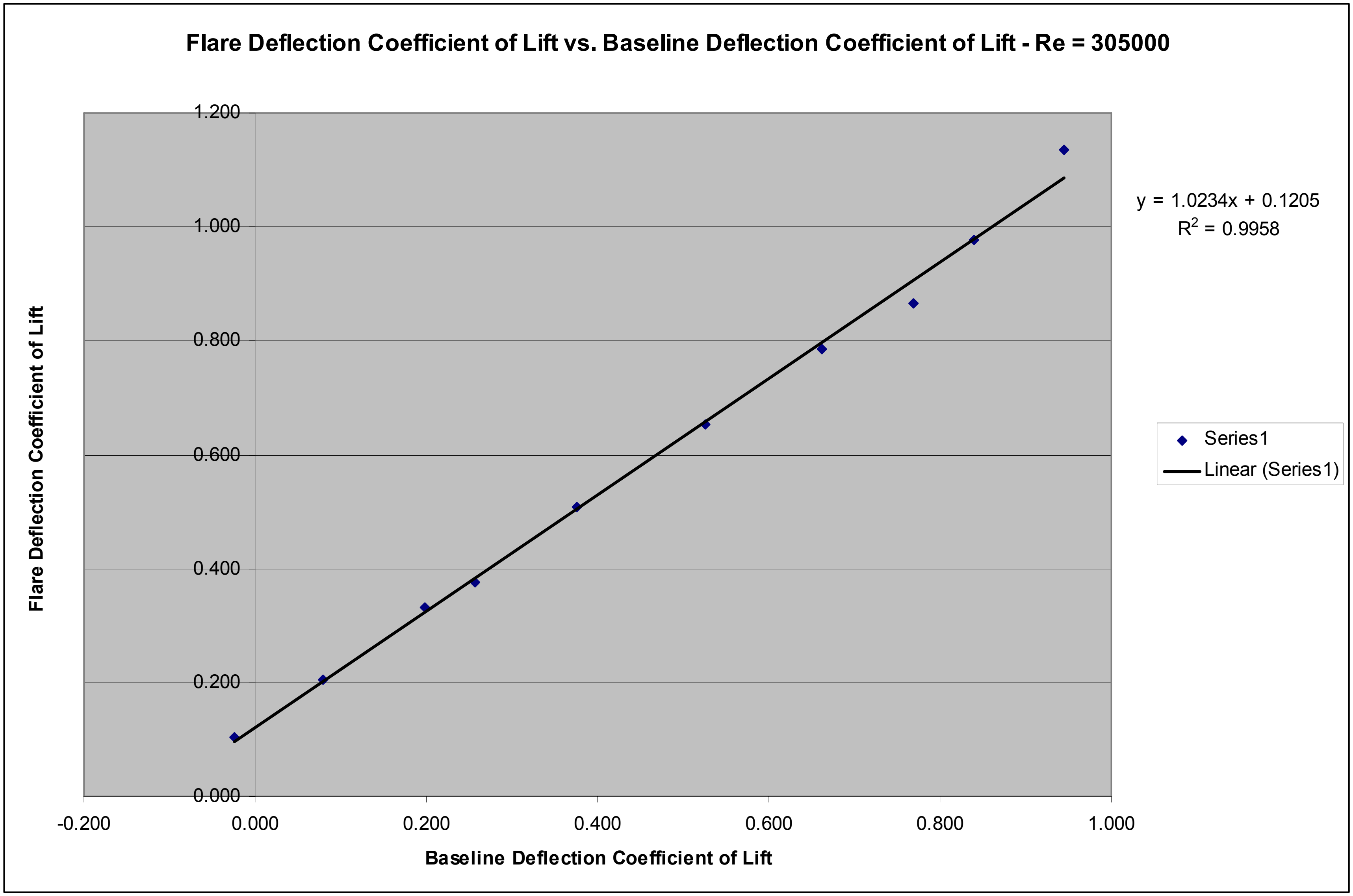

Flare Deflection Coefficient of Lift vs. Baseline Deflection Coefficient of Lift - Re = 305000
Flare Deflection Coefficient of Lift
Baseline Deflection Coefficient of Lift
1.200
1.000
0.800
0.600
0.400
0.200
0.000
-0.200
0.000
0.200
0.400
0.600
0.800
1.000
y = 1.0234x + 0.1205
R^2 = 0.9958
Series1
Linear (Series1)

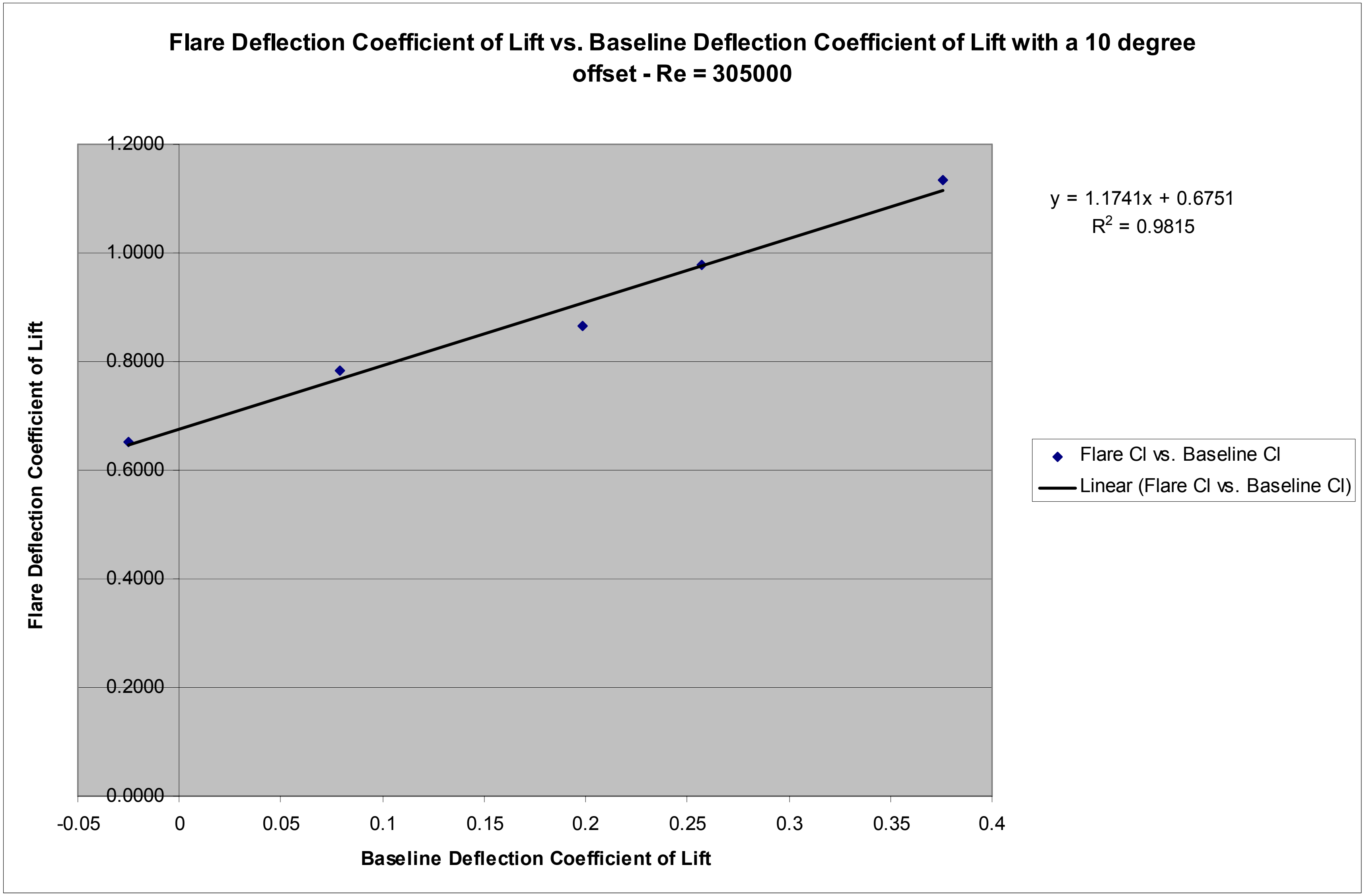
Flare Deflection Coefficient of Lift vs. Baseline Deflection Coefficient of Lift with a 10 degree offset - Re = 305000
y = 1.1741x + 0.6751
R^2 = 0.9815
Flare Cl vs. Baseline Cl
Linear (Flare Cl vs. Baseline Cl)
Flare Deflection Coefficient of Lift
Baseline Deflection Coefficient of Lift
1.2000
1.0000
0.8000
0.6000
0.4000
0.2000
0.0000
-0.05
0
0.05
0.1
0.15
0.2
0.25
0.3
0.35
0.4

Appendix B: Pro Engineer Models

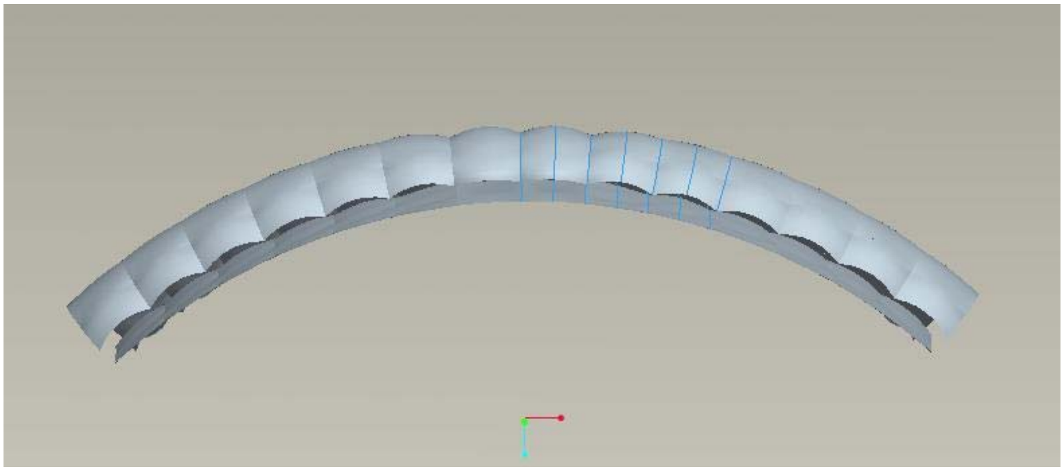

Figure B - 1 : Baseline Deflection Front

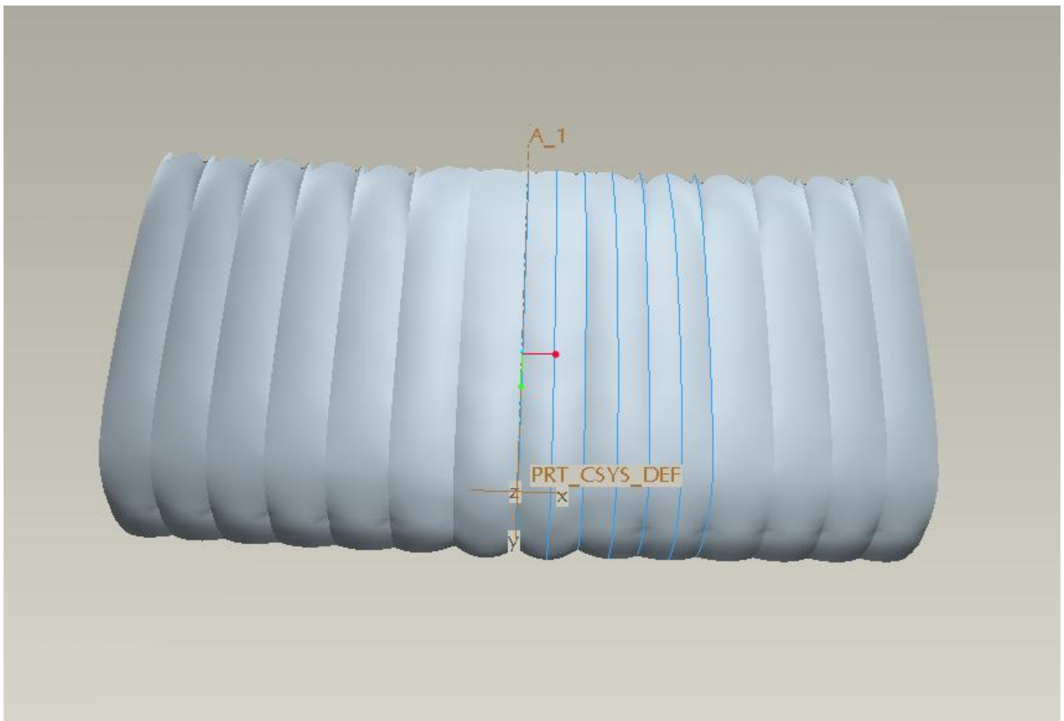

Figure B - 2 : Baseline Deflection Top

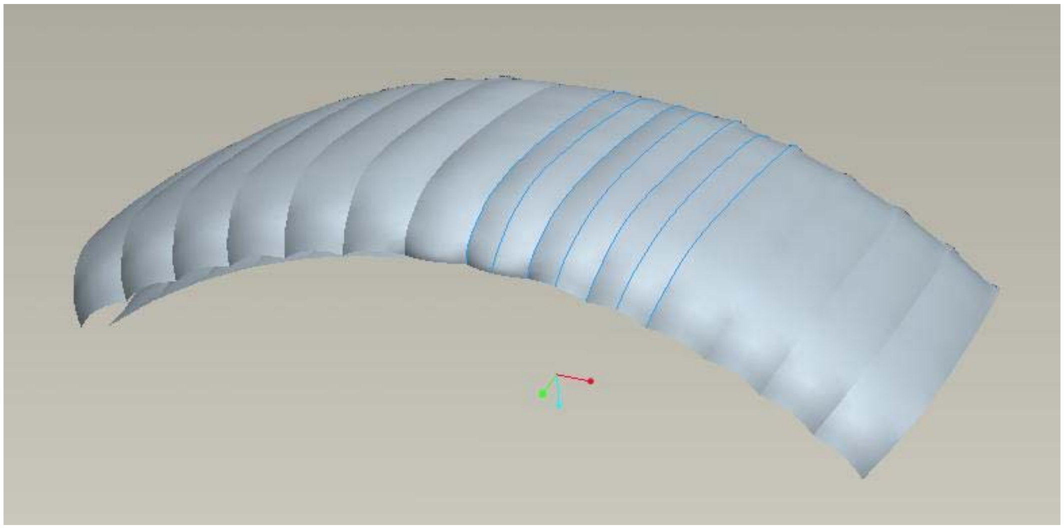

Figure B - 3 : Baseline Deflection Top - Angled

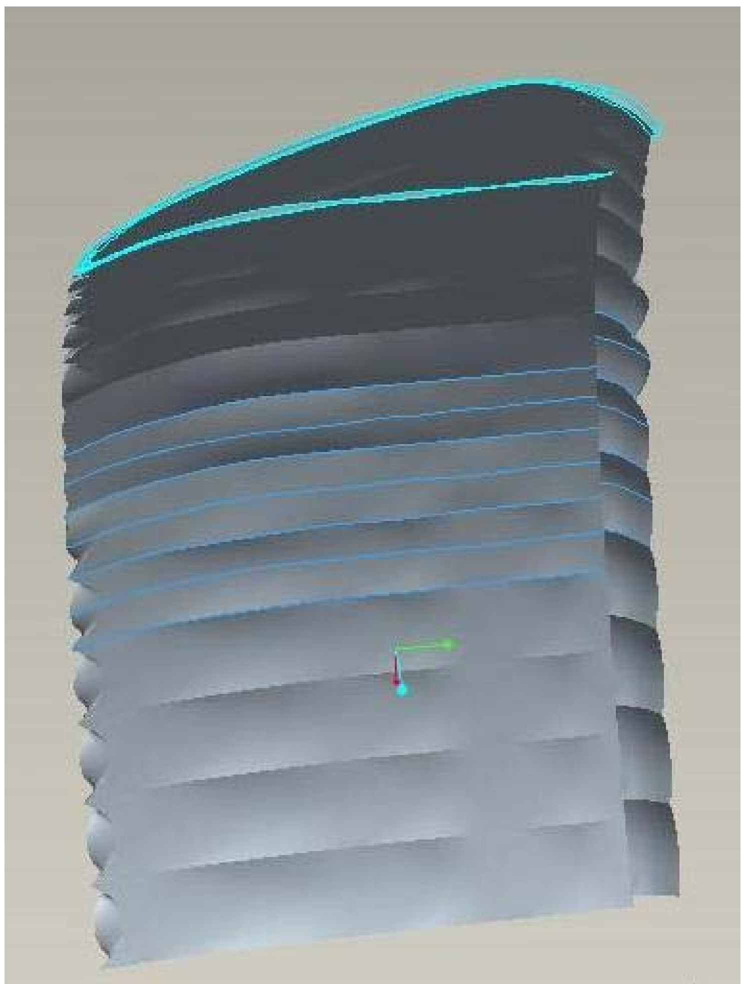

Figure B - 4 : Baseline Deflection Underneath

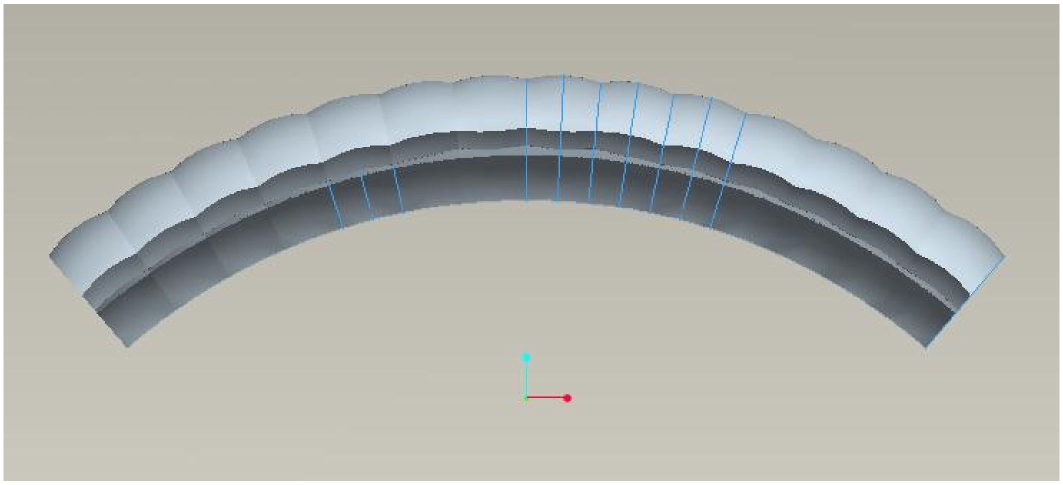

Figure B - 5 : Partial Deflection Front

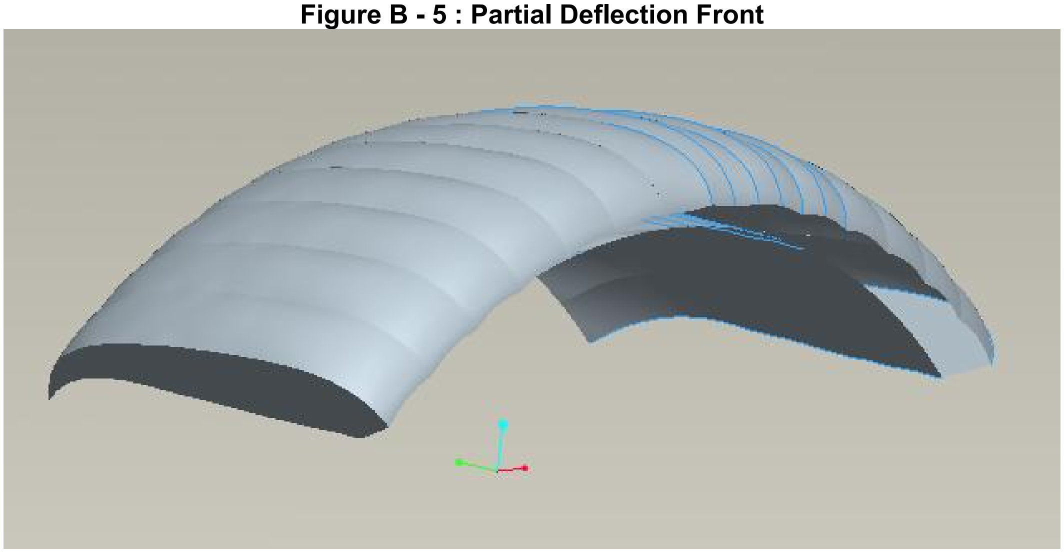

Figure B - 6 : Partial Deflection Angled

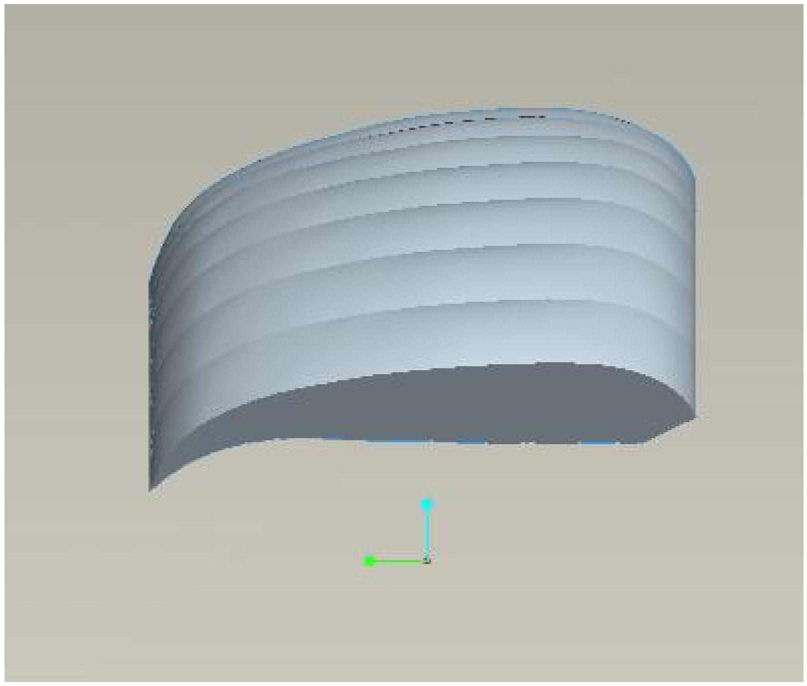

Figure B - 7 : Partial Deflection Side

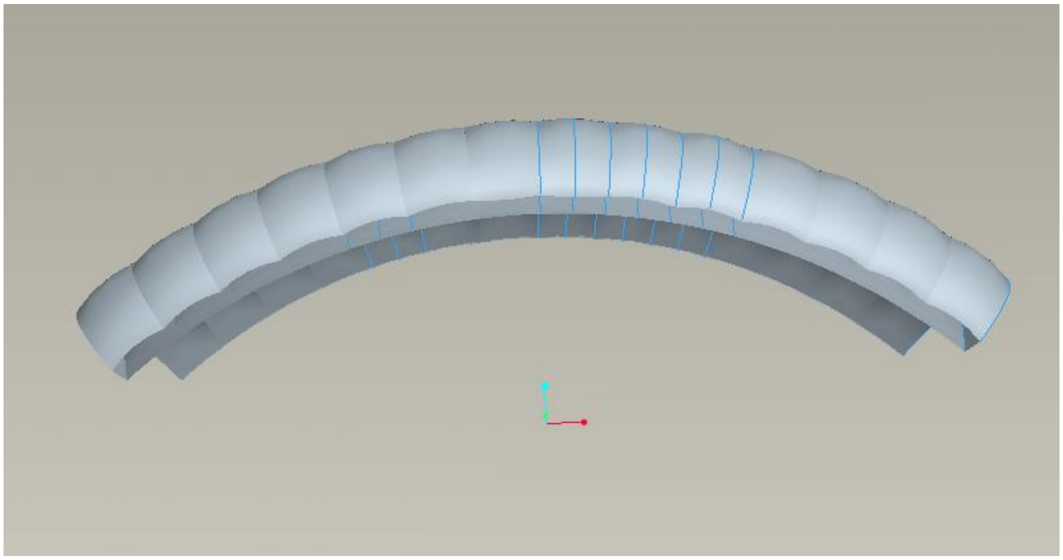

Figure B - 8 ; Full Deflection Front

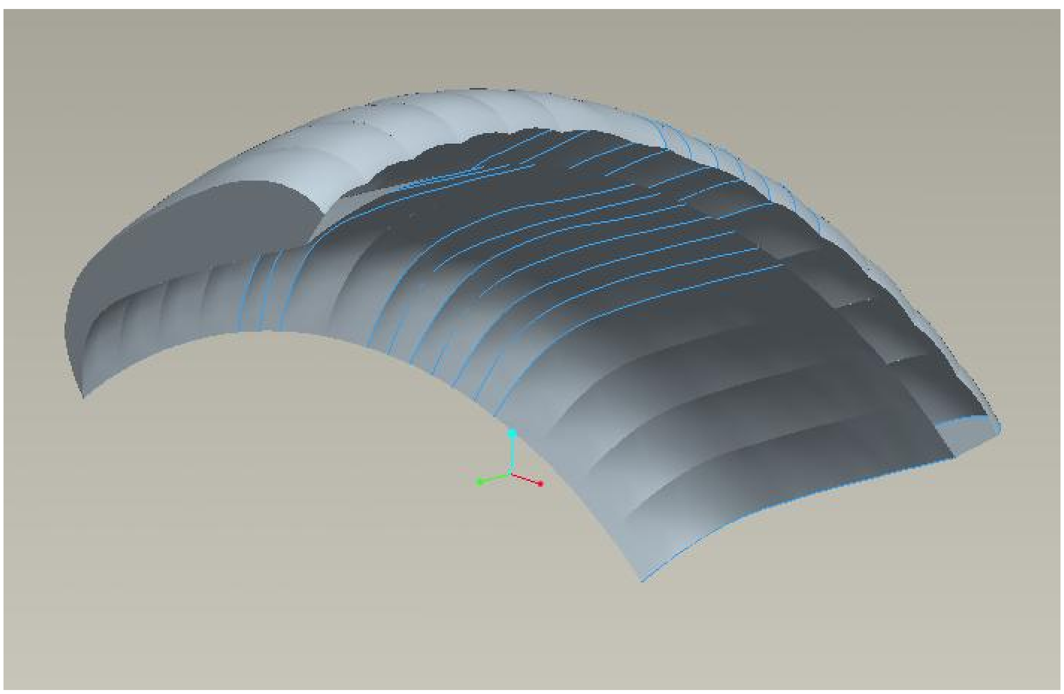

Figure B - 9 : Full Deflection Underneath - Angled

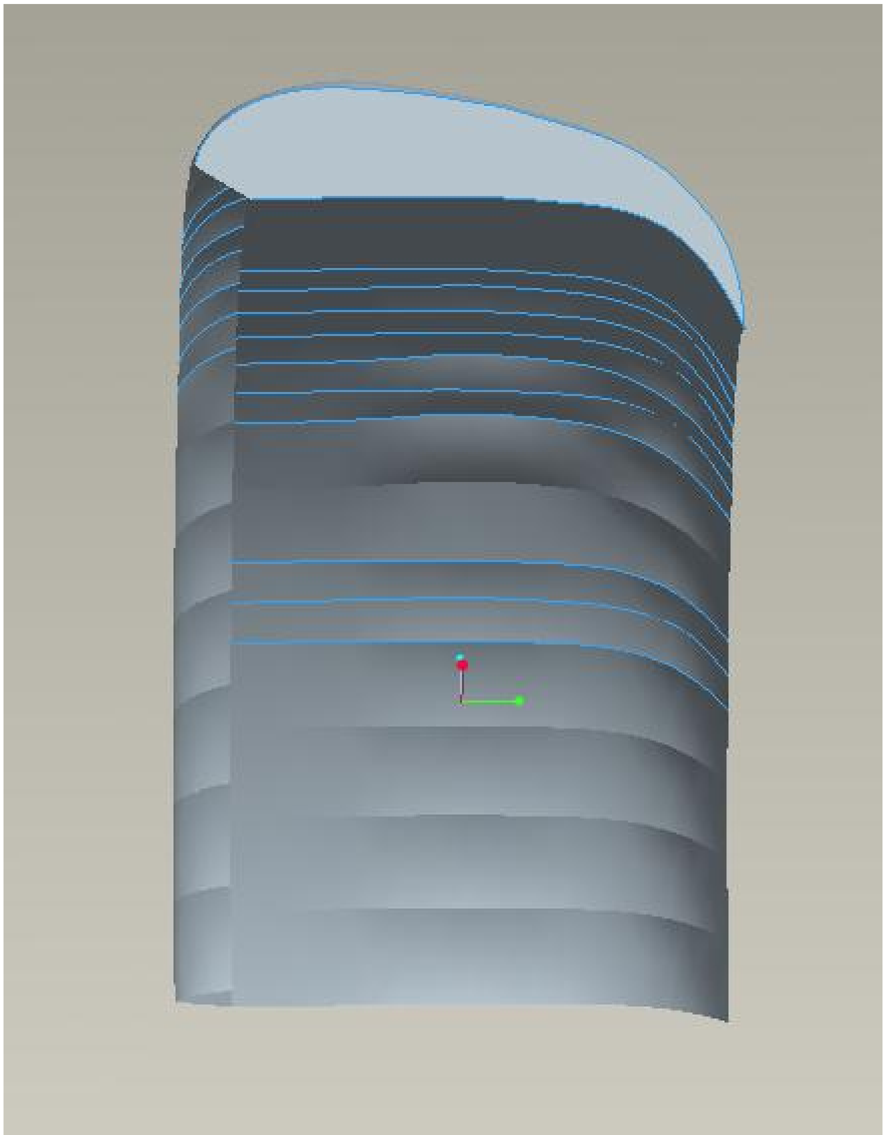

Figure B - 10 : Full Deflection Underneath

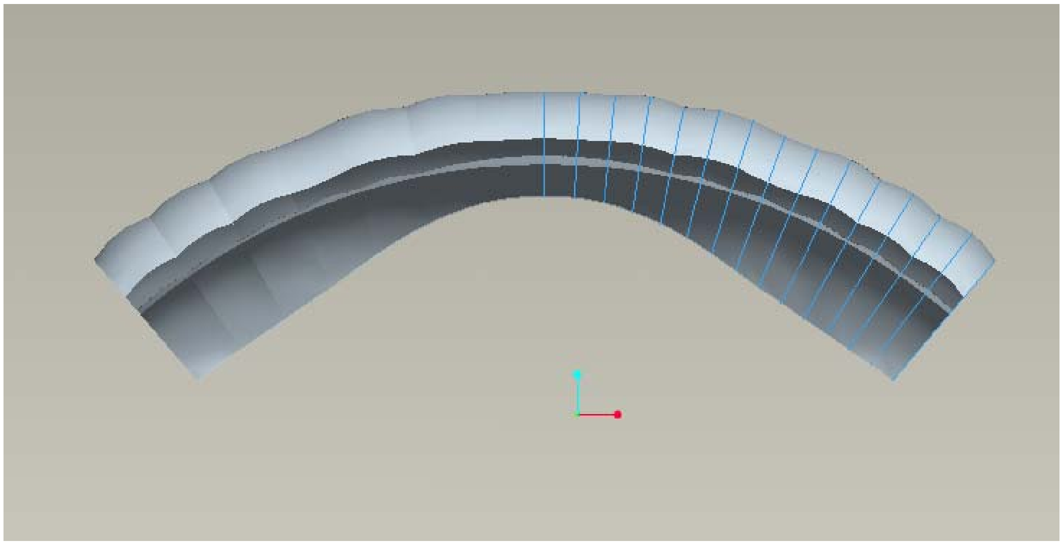

Figure B - 11 : Flare Deflection Front

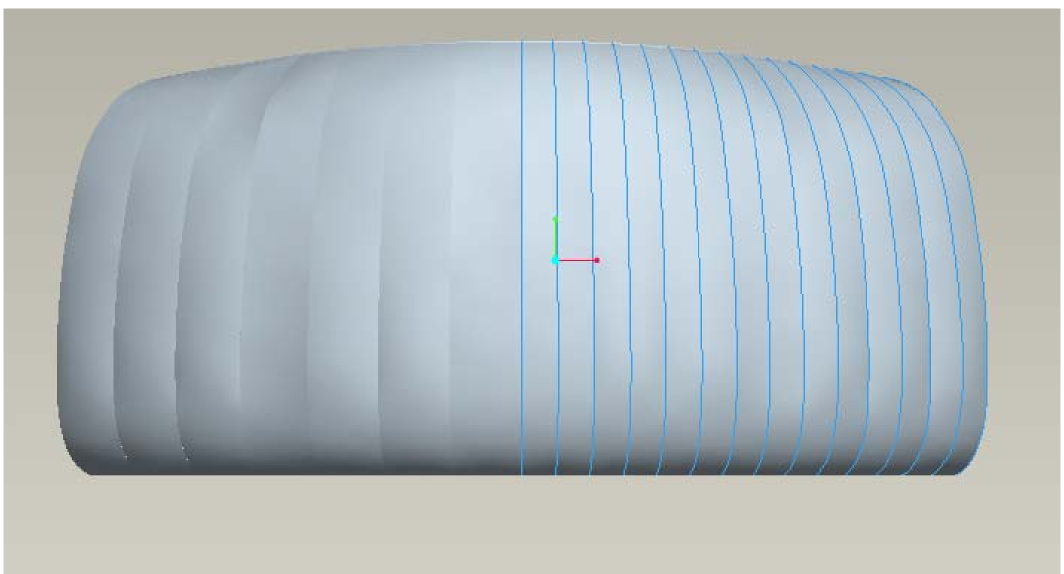

Figure B - 12 : Flare Deflection Top

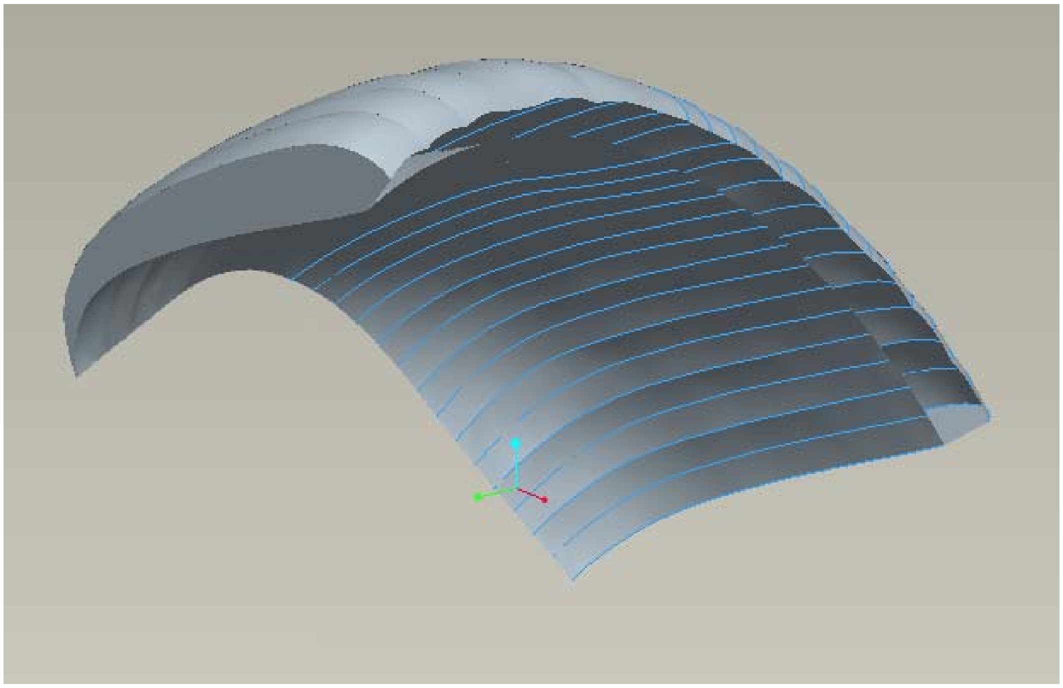

Figure B - 13 : Flare Deflection Underneath - Angled

B.1 Additional Pictures

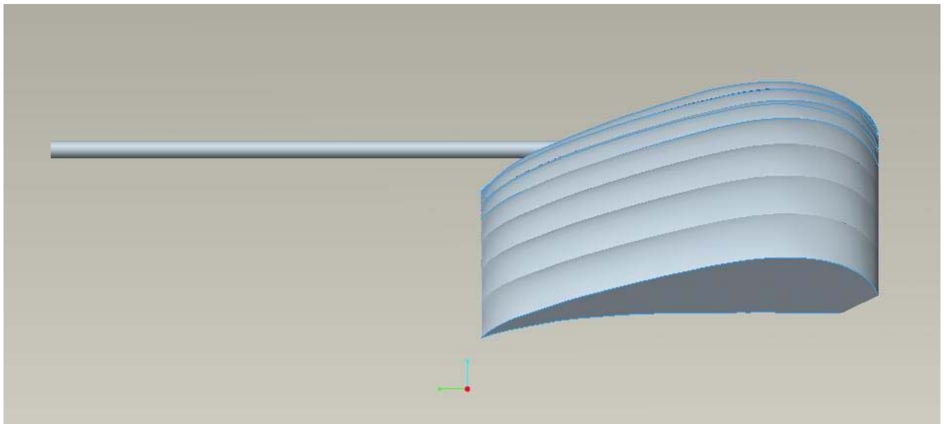

Figure B - 14 : Designed Boom Mount 1

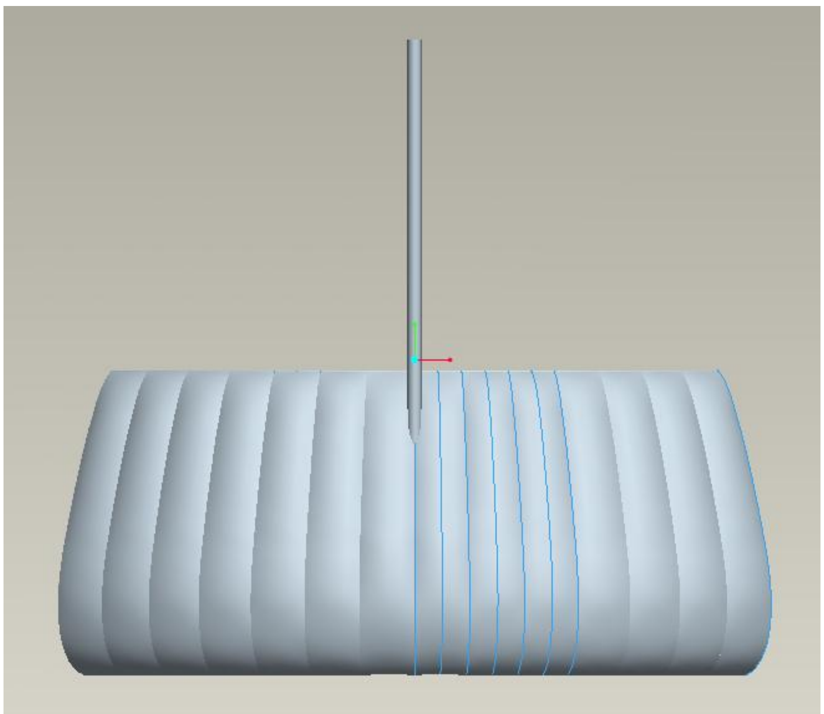

Figure B - 15 : Designed Boom Mount 2

Appendix C: Model Core Construction

Figure C - 1 : Front Spanwise Force Distribution Rod

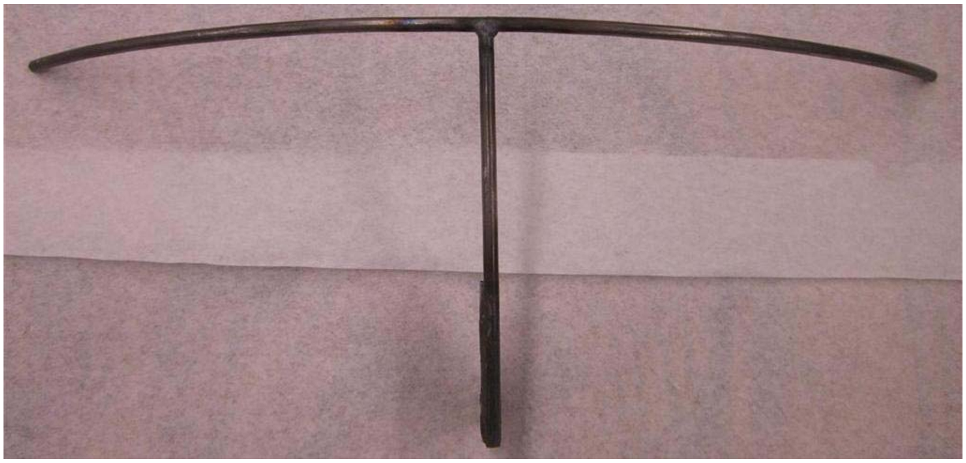

Figure C - 2 : Rear Spanwise Force Distribution Rod (Top View)

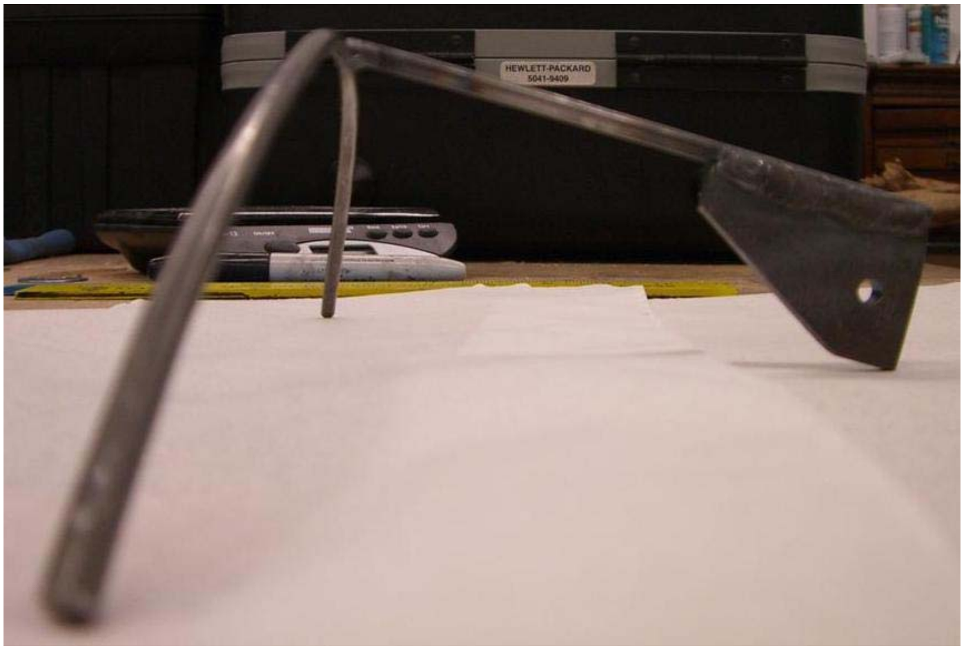

Figure C - 3 : Rear Spanwise Force Distribution Rod (Profile View)

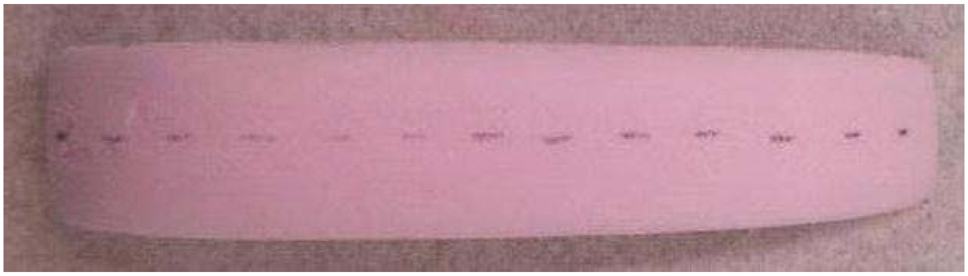

Figure C - 4 : Individual Foam Cell (Top View)

Figure C - 5 : Individual Foam Cell (Profile View)

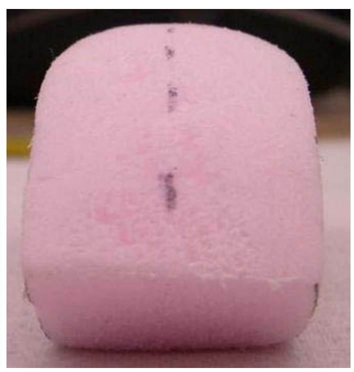

Figure C - 6 : Individual Foam Cell (Front View)

Figure C - 7 : Center Cell (Profile View)

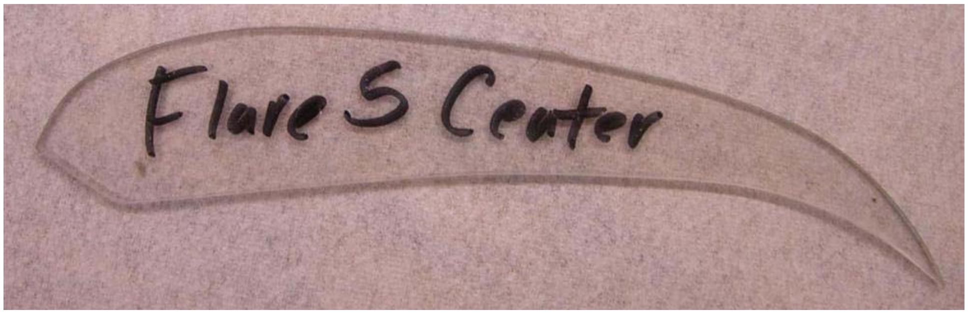

Figure C - 8 : Lexan Rib Stencil

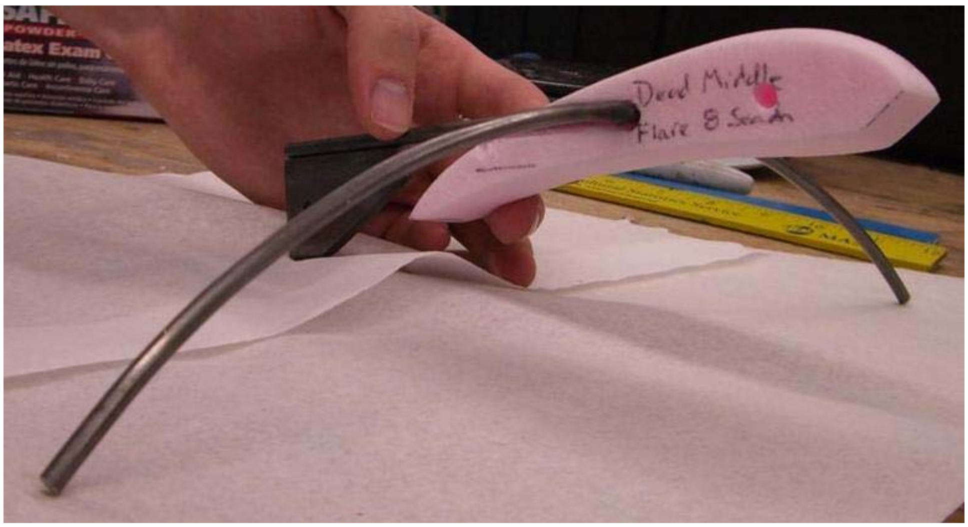

Figure C - 9 : Initial Model Core Construction - 1

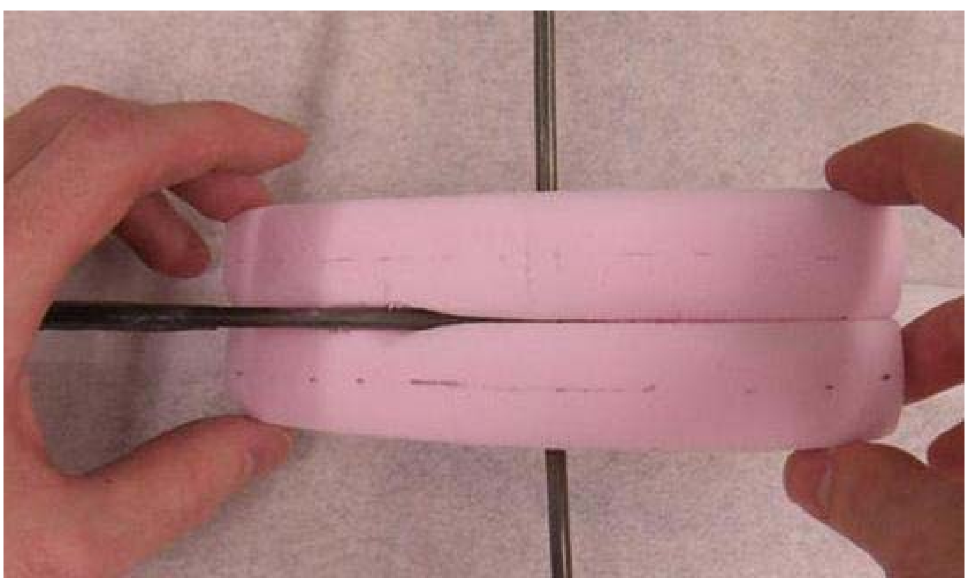

Figure C - 10 : Initial Model Core Construction - 2

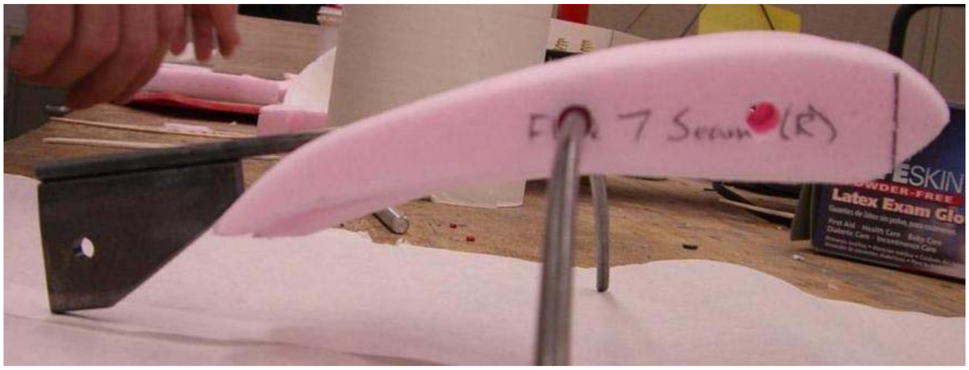

Figure C - 11 : Initial Model Core Construction - 3

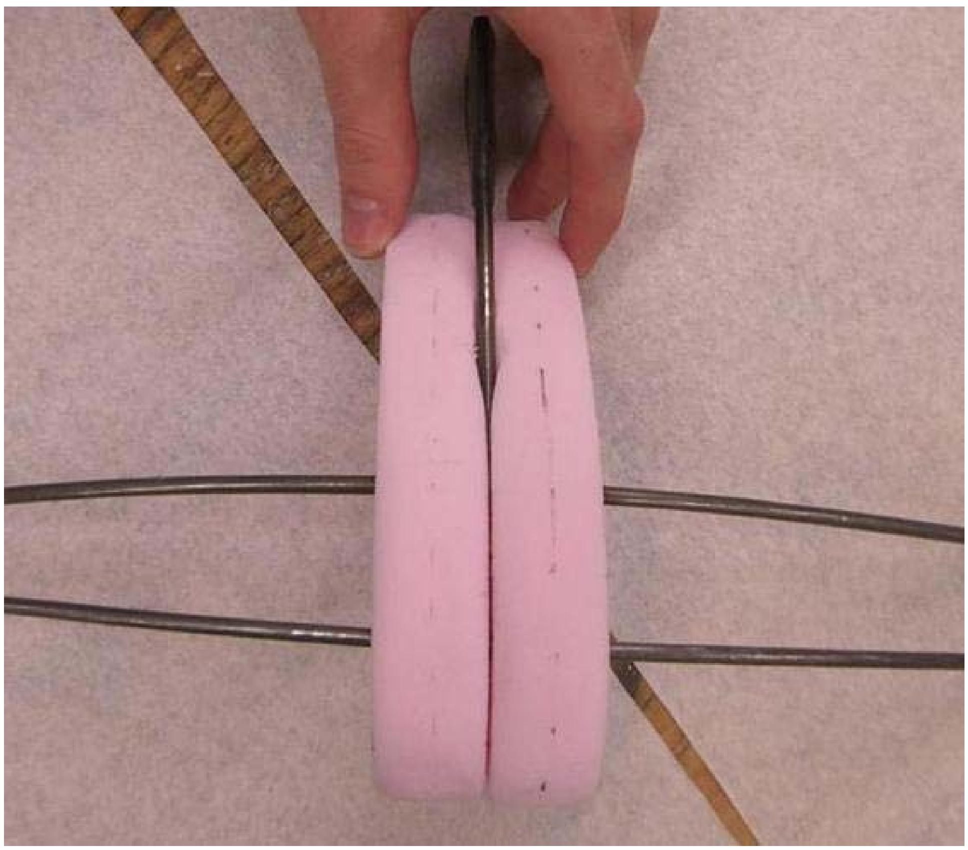

Figure C - 12 : Initial Model Core Construction - 4

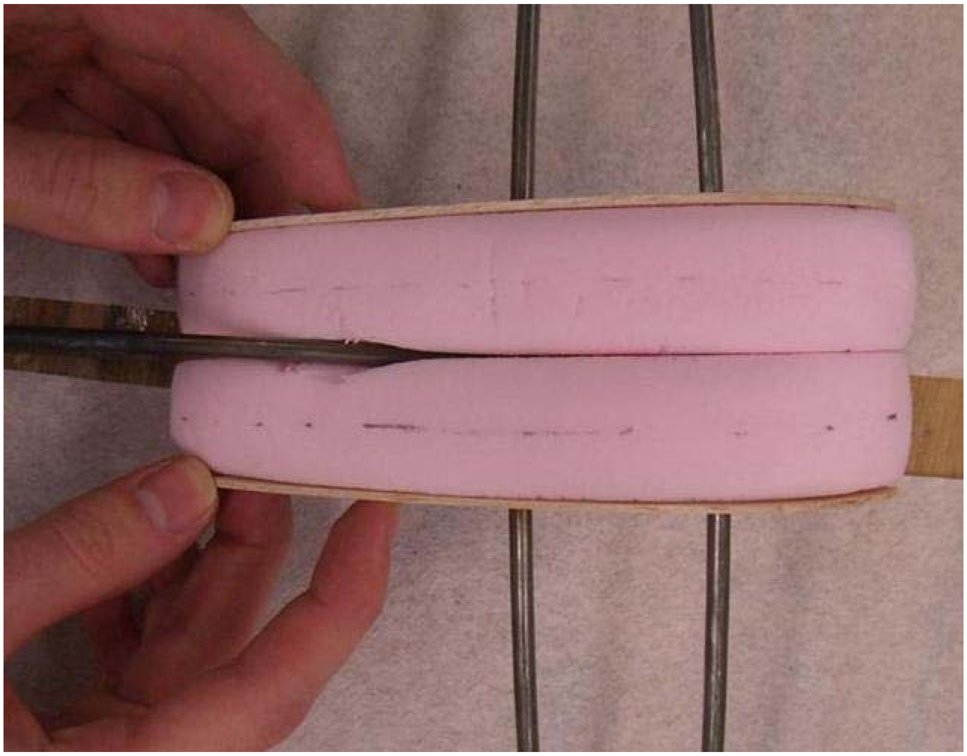

Figure C - 13 : Initial Model Core Construction - 5

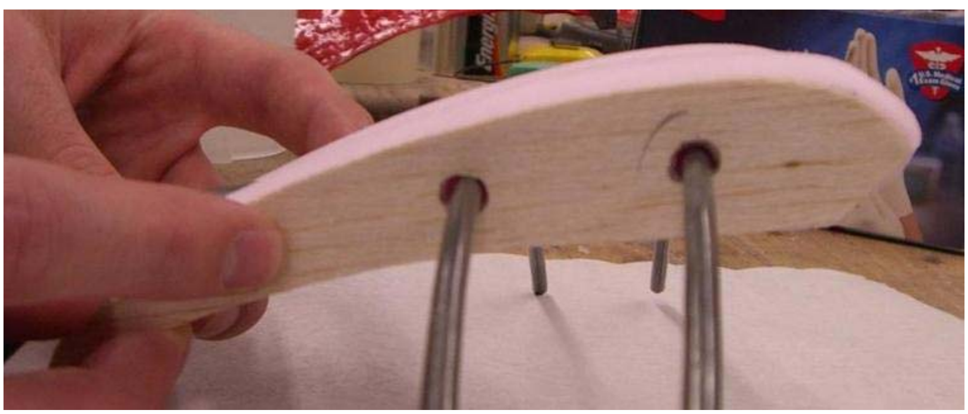

Figure C - 14 : Initial Model Core Construction - 6

Figure C - 15 : Initial Model Core Construction - 7

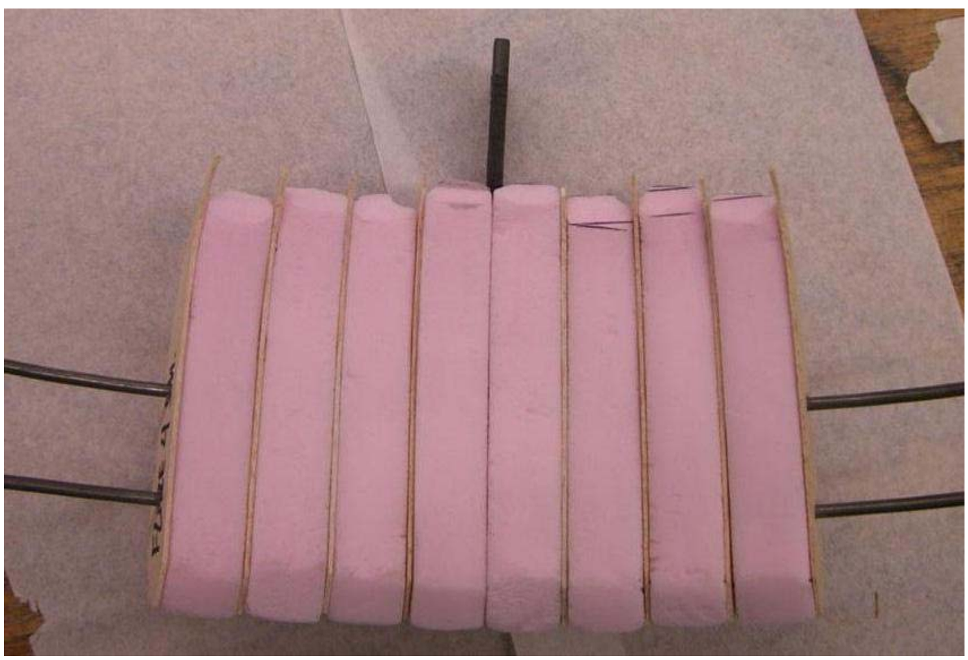

Figure C - 16 : Model Core Construction - 8

Figure C - 17 : Initial Model Core Construction – 9

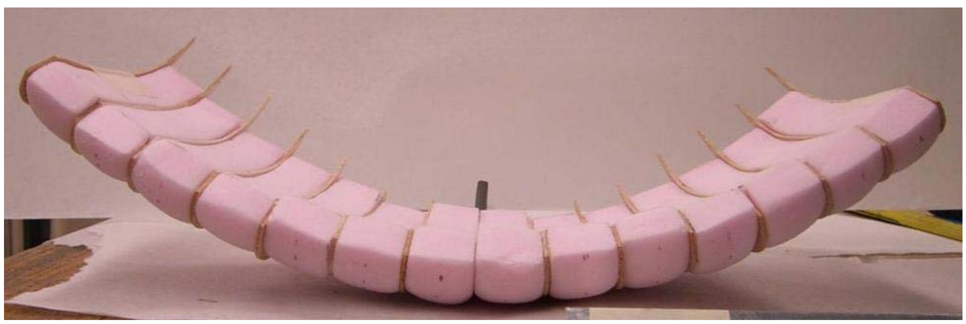

Figure C - 18 : Initial Model Core Construction - 10

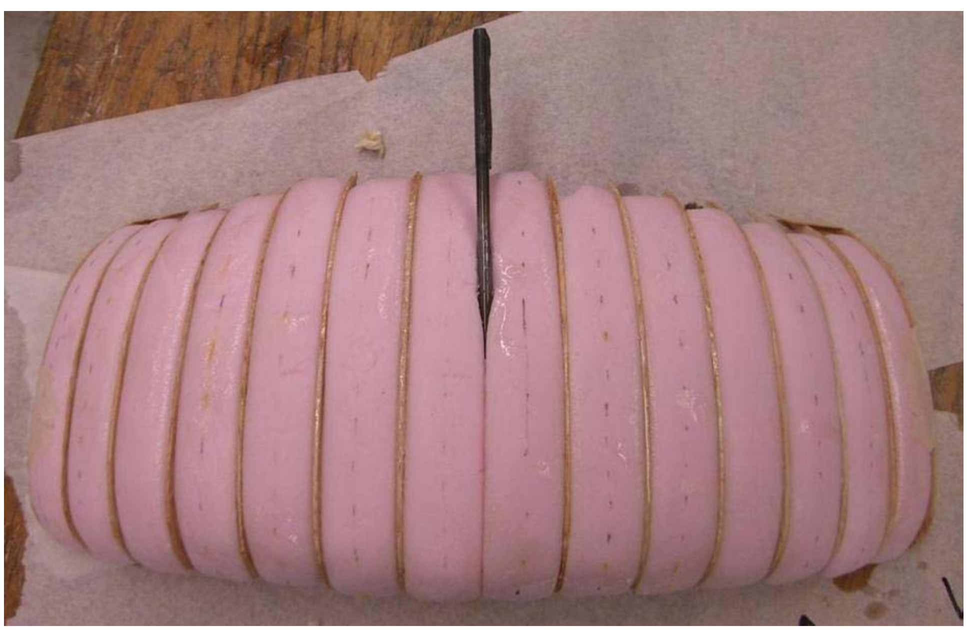

Figure C - 19 : Initial Model Core Construction - 11

Appendix D: Four-side Views

Figure D - 1 : Baseline Deflection Front

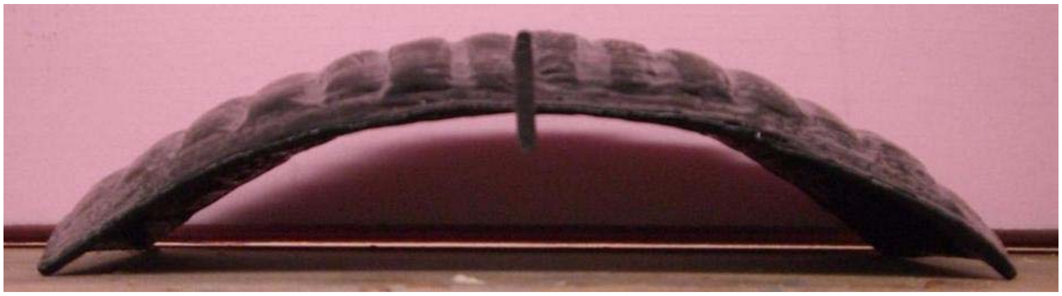

Figure D - 2 : Baseline Deflection Back

Figure D - 3 : Baseline Deflection Side 1

Figure D - 4 : Baseline Deflection Side 2

Figure D - 5 : Partial Deflection Front

Figure D - 6 : Partial Deflection Back

Figure D - 7 : Partial Deflection Side 1

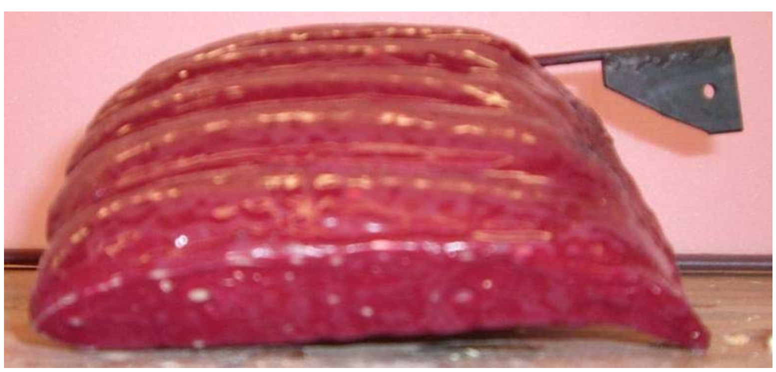

Figure D - 8 : Partial Deflection Side 2

Figure D - 9 : Full Deflection Front

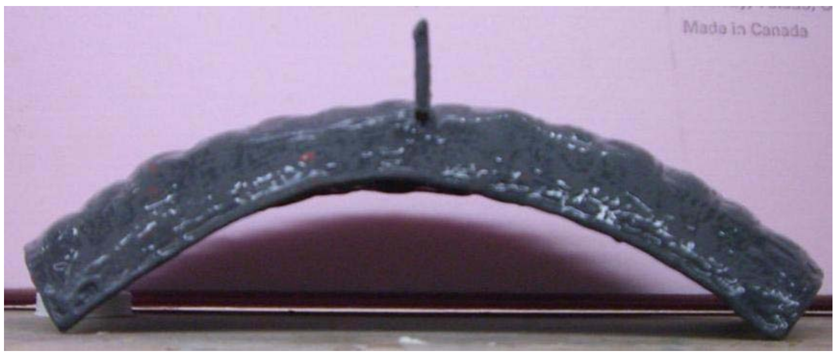

Figure D - 10 : Full Deflection Back

Figure D - 11 : Full Deflection Side 1

Figure D - 12 : Full Deflection Side 2

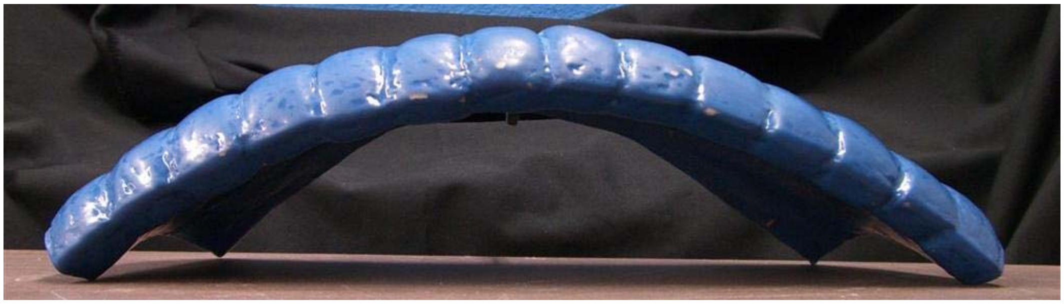

Figure D - 13 : Flare Deflection Front

Figure D - 14 : Flare Deflection Back

Figure D - 15 : Flare Deflection Side 1

Figure D - 16 : Flare Deflection Side 2

Appendix E: Data Correction

Table E.1

					w (m/s)					
alpha	**5**	**10**	**15**	**20**	**25**	**30**	**35**	**40**	**45**	**50**
	-	-	-	-	-	-	-	-	-	-
-7	0.009	0.018	0.027	0.036	0.045	0.054	0.063	0.072	0.081	0.090
-6	0.018	0.036	0.054	0.072	0.090	0.108	0.126	0.144	0.162	0.180
-5	0.036	0.072	0.108	0.144	0.180	0.216	0.252	0.288	0.324	0.360
-4	0.054	0.108	0.162	0.216	0.270	0.324	0.378	0.432	0.486	0.540
-3	0.076	0.151	0.227	0.302	0.378	0.454	0.529	0.605	0.681	0.756
-2	0.095	0.189	0.284	0.378	0.473	0.567	0.662	0.756	0.851	0.945
-1	0.115	0.231	0.346	0.461	0.576	0.692	0.807	0.922	1.037	1.153
0	0.130	0.259	0.389	0.519	0.648	0.778	0.908	1.037	1.167	1.296
1	0.151	0.303	0.454	0.605	0.756	0.908	1.059	1.210	1.361	1.513
2	0.171	0.342	0.513	0.684	0.855	1.026	1.197	1.369	1.540	1.711
3	0.184	0.367	0.551	0.735	0.918	1.102	1.286	1.469	1.653	1.837
4	0.203	0.407	0.610	0.814	1.017	1.221	1.424	1.628	1.831	2.035
5	0.220	0.440	0.660	0.880	1.099	1.319	1.539	1.759	1.979	2.199
6	0.234	0.468	0.702	0.936	1.171	1.405	1.639	1.873	2.107	2.341
7	0.249	0.497	0.746	0.994	1.243	1.491	1.740	1.988	2.237	2.485
8	0.261	0.522	0.783	1.044	1.306	1.567	1.828	2.089	2.350	2.611
9	0.272	0.544	0.816	1.088	1.360	1.631	1.903	2.175	2.447	2.719
10	0.279	0.558	0.837	1.117	1.396	1.675	1.954	2.233	2.512	2.791
11	0.283	0.565	0.848	1.131	1.414	1.696	1.979	2.262	2.545	2.827

Table 5: Table E.1

Table E.2

C_{Di} = Cl^2/(Pi*AR)

Alpha	C_{Di}
-7	0.0003
-6	0.0011
-5	0.0045
-4	0.0100
-3	0.0196
-2	0.0307
-1	0.0456
0	0.0577
1	0.0786
2	0.1005
3	0.1159
4	0.1422
5	0.1657
6	0.1882
7	0.2121
8	0.2341
9	0.2539
10	0.2675
11	0.2745

Table 6: Table E.2

TABLE E.4

DRAG CORRECTIONS

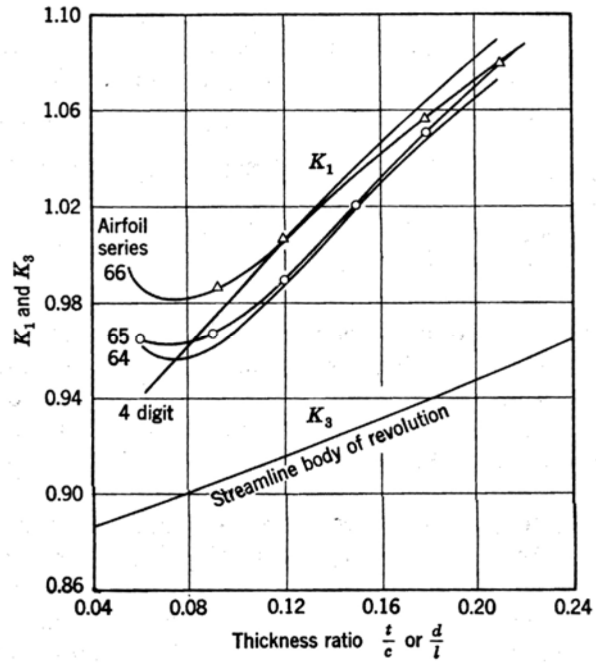

FIGURE 6.13. Values of K_1 and K_3 for a number of bodies.

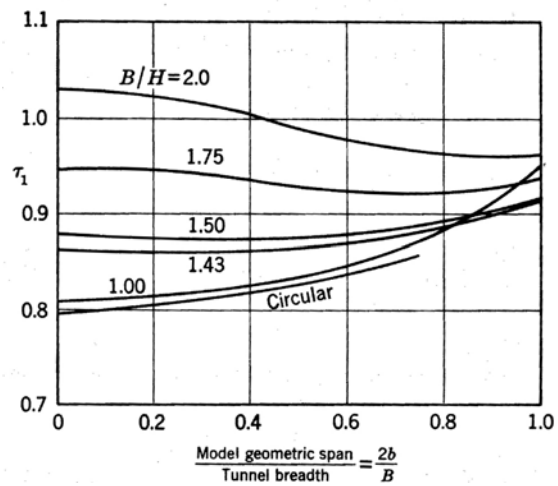

Table 7: Table E.4

Table E.5a

Baseline			Flare			Partial			Full		
b =	0.322	m	b =	0.322	m	b =	0.322	m	b =	0.322	m
B =	0.610	m	B =	0.610	m	B =	0.610	m	B =	0.610	m
τ_1	0.930		τ_1	0.930		τ_1	0.930		τ_1	0.930	
t =	0.030	m	t =	0.028	m	t =	0.028		t =	0.030	m
c =	0.155	m	c =	0.151	m	c =	0.151		c =	0.149	m
t/c =	0.195		t/c =	0.189		t/c =	.189		t/c =	0.201	
K_1 =	1.075		K_1 =	1.065		K_1 =	1.065		K_1 =	1.080	
C =	0.372	m^2	C =	0.372	m^2	C =	0.372	m^2	C =	0.372	m^2
Volume	0.00115	m^3	Volume	0.00115	m^3	Volume	0.00115	m^3	Volume	0.00115	m^3

Table 8: Table E.5a

Table E.5b

εsb W = (ΔV/Vu) =((K1τ1(wing volume))/C3/2)

$\varepsilon_{sb\ W\ (Baseline)}$	0.00507
$\varepsilon_{sb\ W\ (Flare)}$	0.00502
$\varepsilon_{sb\ W\ (Partial)}$	0.00502
$\varepsilon_{sb\ W\ (Full)}$	0.00509

Table 9: Table E.5b

Appendix F: Wind Tunnel Calibration Data

Pitot-Static Probe Tunnel Calibration									
Exp. Date:	25-Oct-05								
Exp. Time:	1430 - 1500								
P_{atm} =	29.34	in Hg	as reported at Worcester Municipal Airport at 1854 Zulu						
P_{atm} =	99357	Pa							
R =	286	J/(kg K)							
f_m	Δp	$\delta(\Delta p)$	T	δT	Δp	$\delta(\Delta p)$	T	ρ	U
(Hz)	(in H_2O)	(in H_2O)	(^oF)	(^oF)	(Pa)	(Pa)	(K)	(kg/m^3)	(m/s)
5.0	0.031	0.002	70.5	0.5	7.71	0.50	294.5	1.179	3.62
6.0	0.045	0.002	70.5	0.5	11.19	0.50	294.5	1.179	4.36
7.0	0.065	0.002	71.0	0.5	16.17	0.50	294.8	1.178	5.24
8.0	0.086	0.002	71.0	0.5	21.39	0.50	294.8	1.178	6.03
9.0	0.112	0.002	71.0	0.5	27.85	0.50	294.8	1.178	6.88
10.0	0.139	0.002	71.0	0.5	34.57	0.50	294.8	1.178	7.66
12.0	0.206	0.002	71.0	0.5	51.23	0.50	294.8	1.178	9.32
14.0	0.288	0.002	71.0	0.5	71.63	0.50	294.8	1.178	11.03
16.0	0.381	0.003	71.0	0.5	94.75	0.75	294.8	1.178	12.68
18.0	0.487	0.003	71.0	0.5	121.12	0.75	294.8	1.178	14.34
20.0	0.606	0.003	71.5	0.5	150.71	0.75	295.1	1.177	16.00
22.0	0.740	0.003	72.0	0.5	184.04	0.75	295.4	1.176	17.69
24.0	0.885	0.003	72.0	0.5	220.10	0.75	295.4	1.176	19.35
26.0	1.045	0.004	73.0	0.5	259.89	1.00	295.9	1.174	21.04
28.0	1.218	0.004	74.0	0.5	302.92	1.00	296.5	1.172	22.74
30.0	1.404	0.004	74.0	0.5	349.17	1.00	296.5	1.172	24.41
32.0	1.603	0.004	75.0	0.5	398.67	1.00	297.0	1.170	26.11
34.0	1.815	0.005	75.0	0.5	451.39	1.24	297.0	1.170	27.78
36.0	2.030	0.005	76.0	0.5	504.86	1.24	297.6	1.167	29.41
38.0	2.285	0.005	77.0	0.5	568.28	1.24	298.2	1.165	31.23
40.0	2.540	0.005	78.5	0.5	631.70	1.24	299.0	1.162	32.97

Table 10: Calibration Data (a)

Linear Regression Fit								
SUMMARY OUTPUT								
Regression Statistics								
Multiple R	0.999979298							
R Square	0.999958597							
Adjusted R Square	0.999956418							
Standard Error	0.063108335							
Observations	21							
ANOVA								
	df	*SS*	*MS*	*F*	*Significance F*			
Regression	1	1827.595829	1827.595829	458888.0118	4.1556E-43			
Residual	19	0.075670577	0.003982662					
Total	20	1827.6715						
	Coefficients	*Standard Error*	*t Stat*	*P-value*	*Lower 95%*	*Upper 95%*	*Lower 95.0%*	*Upper 95.0%*
Intercept	-0.6916	0.0291	-23.7798	0.0000	-0.7525	-0.6307	-0.7525	-0.6307
X Variable 1	0.8377	0.0012	677.4127	0.0000	0.8351	0.8403	0.8351	0.8403

Table 11: Calibration Data (b)

Curve Fit Prediction					
U	f_m	f_m	U	f_m	Δp
(m/s)	(Hz)	(Hz)	(m/s)	(Hz)	(mm H_2O)
3.5	5.0	5	3.497	10	-
4.0	5.6	6	4.335	20	15
4.5	6.2	7	5.172	30	35
5.0	6.8	8	6.010	40	65
5.5	7.4	9	6.848		
6.0	8.0	10	7.686		
6.5	8.6	12	9.361		
7.0	9.2	14	11.036		
7.5	9.8	16	12.712		
8.0	10.4	18	14.387		
8.5	11.0	20	16.063		
9.0	11.6	22	17.738		
9.5	12.2	24	19.414		
10.0	12.8	26	21.089		
11.0	14.0	28	22.764		
12.0	15.2	30	24.440		
13.0	16.3	32	26.115		
14.0	17.5	34	27.791		
15.0	18.7	36	29.466		
16.0	19.9	38	31.142		
17.0	21.1	40	32.817		
18.0	22.3	42	34.492		
19.0	23.5	44	36.168		
20.0	24.7	46	37.843		
21.0	25.9	48	39.519		
22.0	27.1	50	41.194		
23.0	28.3				
24.0	29.5				
25.0	30.7				
26.0	31.9				
27.0	33.1				
28.0	34.2				
29.0	35.4				
30.0	36.6				
31.0	37.8				
32.0	39.0				
33.0	40.2				
40	48.6				
50	60.5				

Table 12: Calibration Data (c)

Appendix G: X-foil Documents and Images

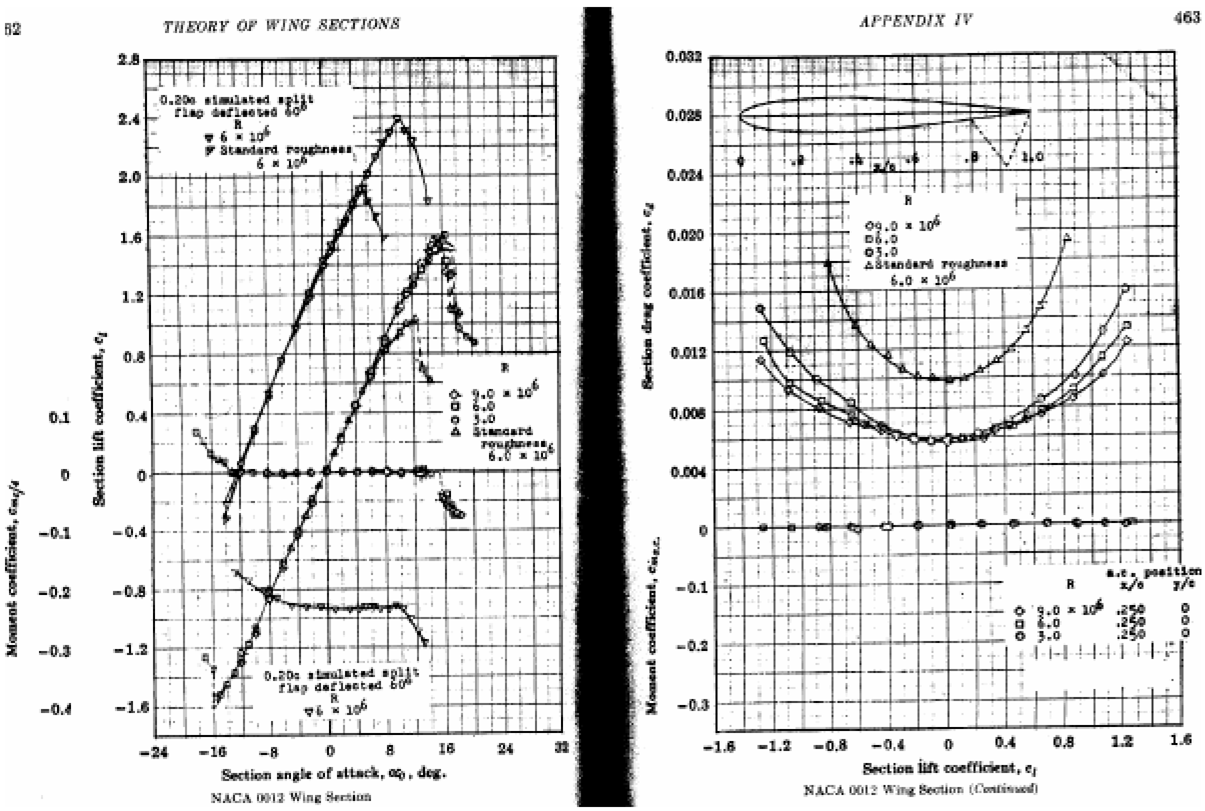

Figure G - 1 : NACA 0012 Results from Abbott

G.1 X-foil Testing Data: Original Profile

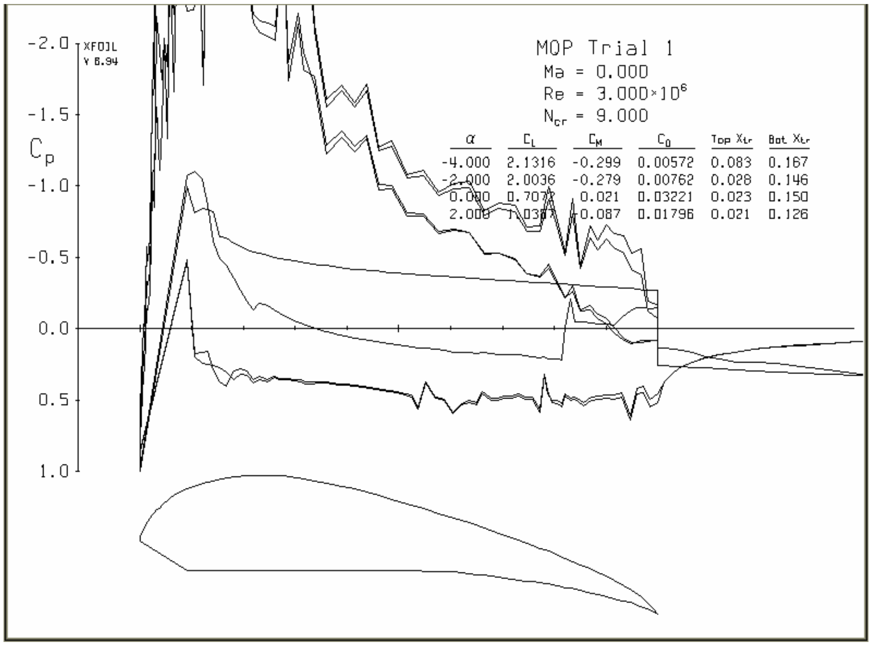

Figure G - 2 : Original Profile Re= 3*10^6 Test 1

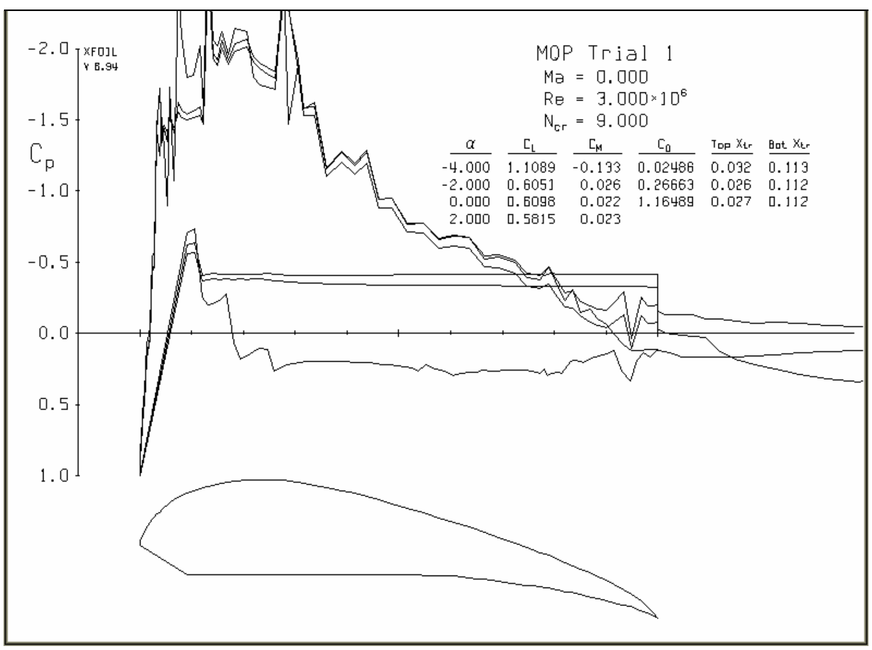

Figure G - 3 : Original Profile Re= 3*10^6 Test 2

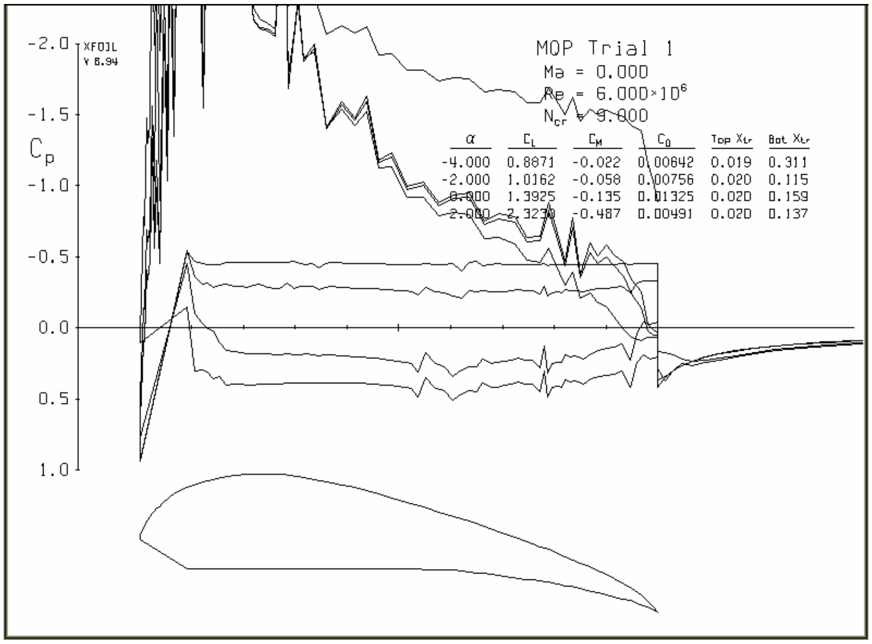

Figure G - 4 : Original Profile Re= 6*10^6 Test 1

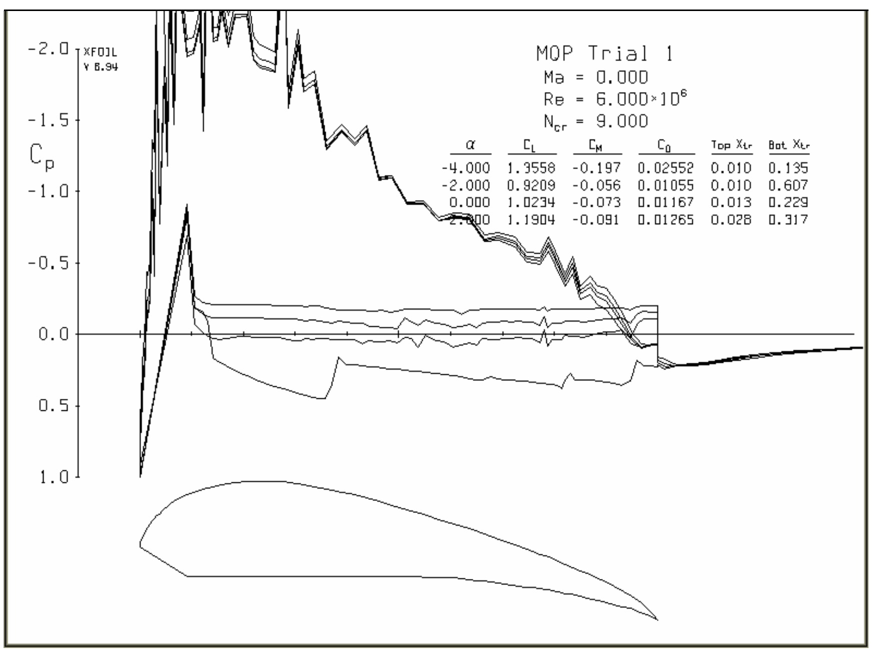

Figure G - 5 : Original Profile Re= 6*10^6 Test 2

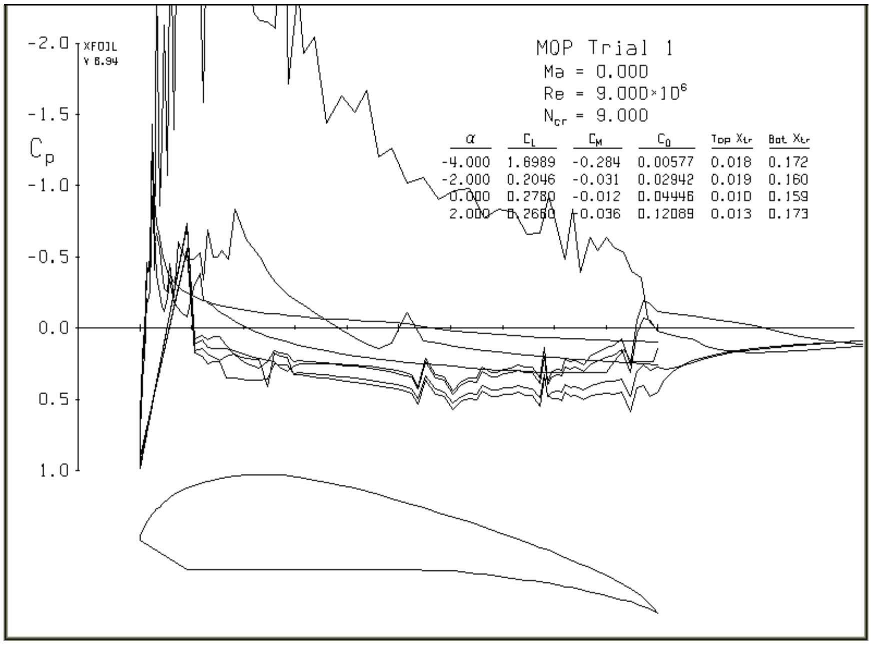

Figure G - 6 : Original Profile Re= 9*10^6 Test 1

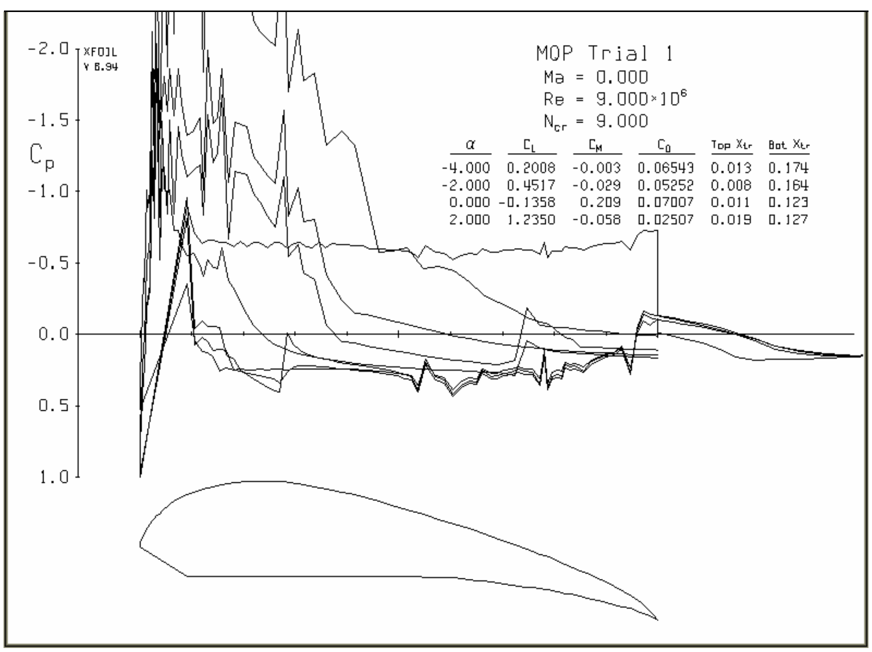

Figure G - 7 : Original Profile Re= 9*10^6 Test 2

G.2 X-foil Testing Data: Strong Enterprise's Profile

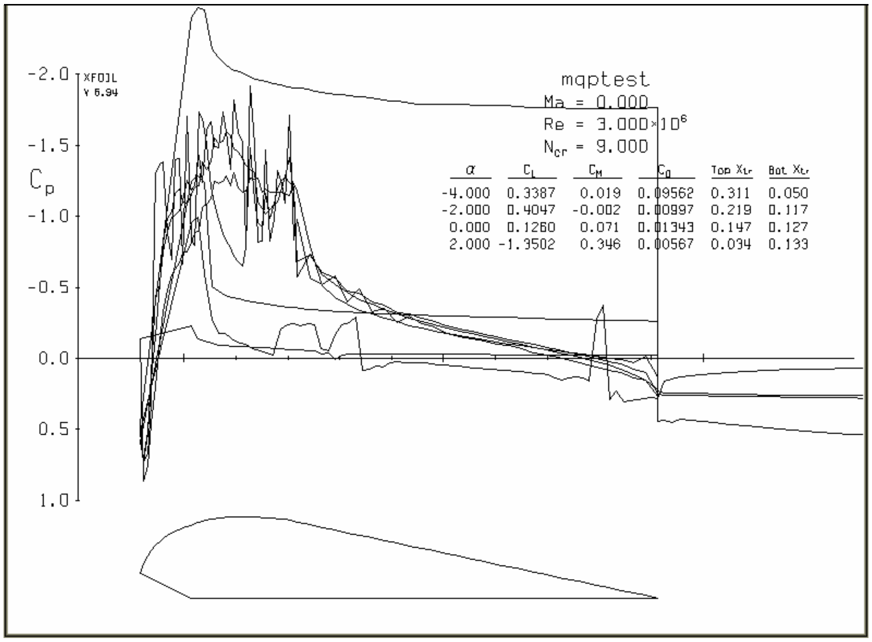

Figure G - 8 : Strong Profile Re= 3*10^6 Test 1

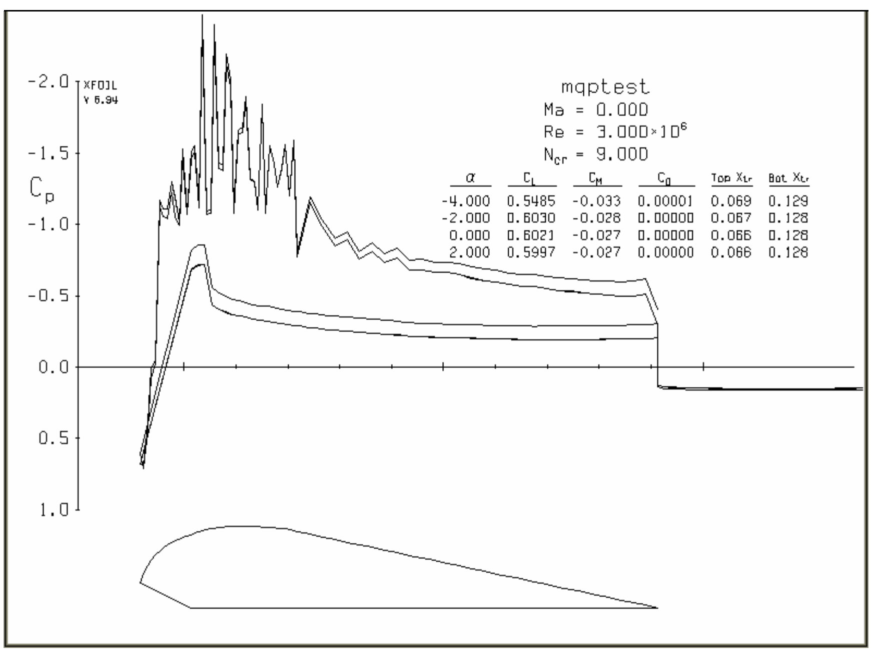

Figure G - 9 : Strong Profile Re= 3*10^6 Test 2

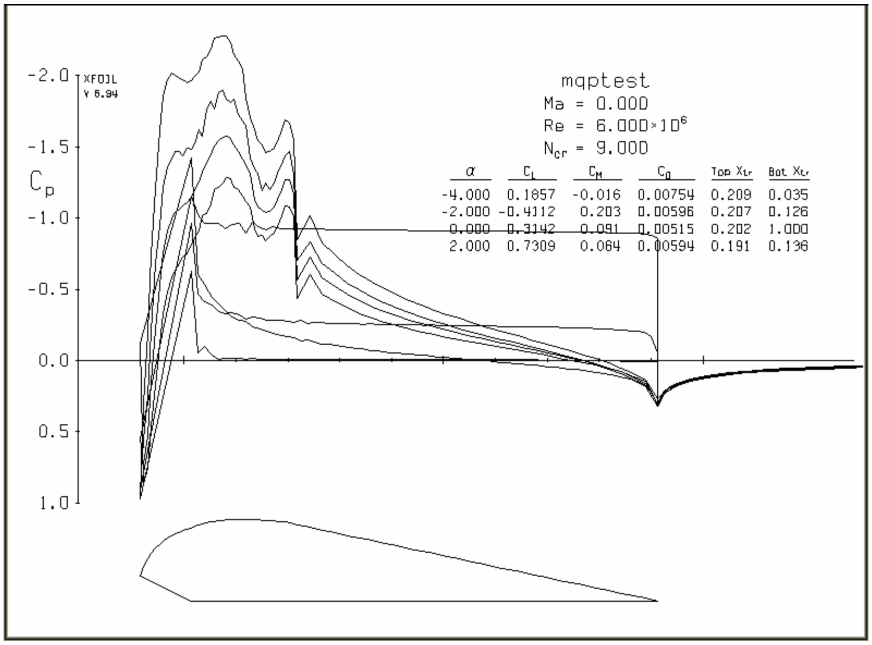

Figure G - 10 : Strong Profile Re= 6*10^6 Test 1

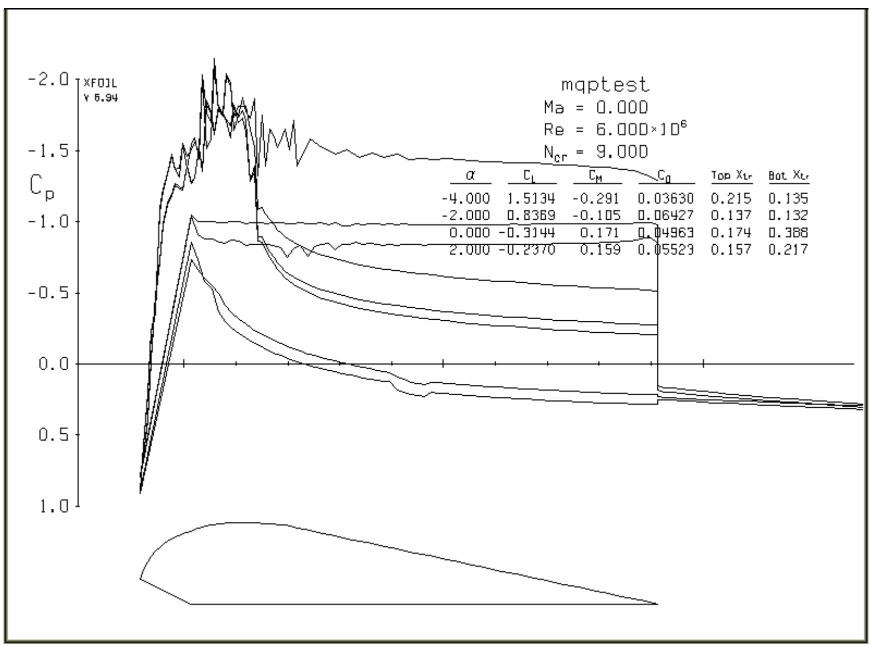

Figure G - 11 : Strong Profile Re= 6*10^6 Test 2

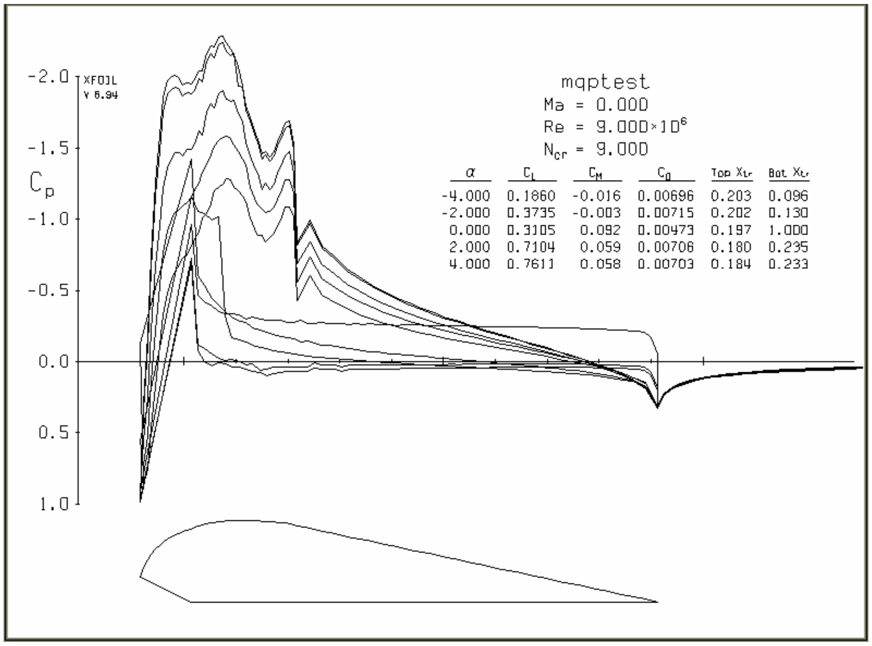

Figure G - 12 : Strong Profile Re= 9*10^6 Test 1

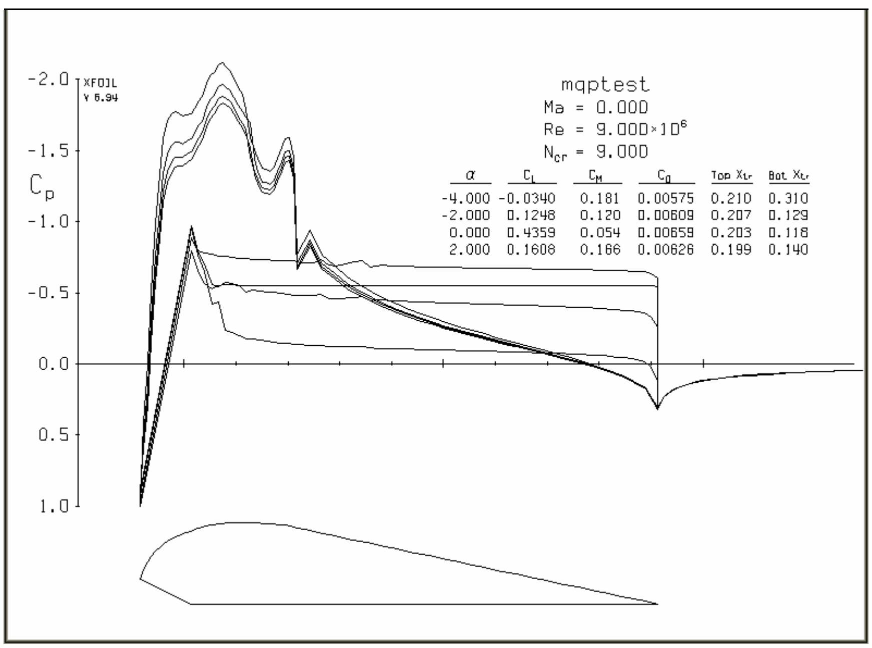

Figure G - 13 : Strong Profile Re= 9*10^6 Test 2

Appendix H: Constructed Parafoil Measurements

H.1 Baseline Deflection

Baseline Condition Model	Weight =	353.5	g	or .779 pounds

Seam 1 ->

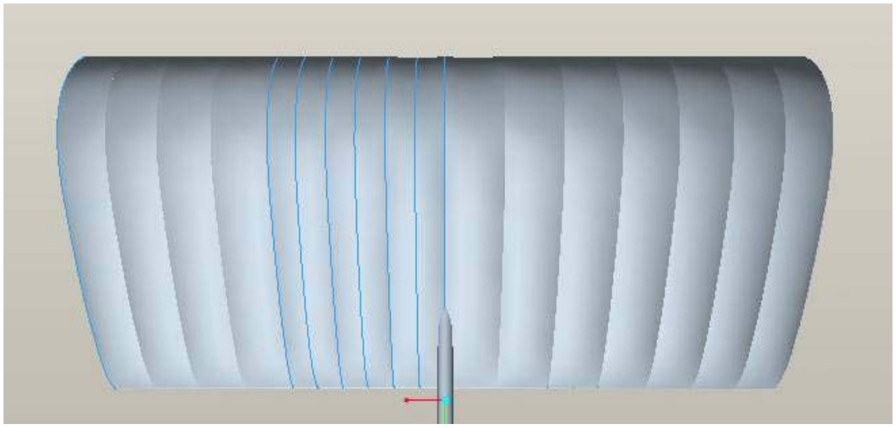

<- Seam 15

Seam #	**Max Thickness (in.)**	**Center #**	**Max Thickness (in.)**
1	1.039	1	1.217
2	1.066	2	1.185
3	1.086	3	1.205
4	1.120	4	1.208
5	1.173	5	1.194
6	1.087	6	1.233
7	1.101	7	1.231
8	1.124	8	1.244
9	1.115	9	1.198
10	1.114	10	1.216
11	1.096	11	1.212
12	1.078	12	1.226
13	1.093	13	1.210
14	1.089	14	1.210
15	1.120		
Average:	1.100	Average:	1.214
St. Dev:	0.03051807	St. Dev:	0.016061
Median:	1.096	Median:	1.211
Min:	1.039	Min:	1.185
Max:	1.173	Max:	1.244

Design

Seam Max Thickness:		1.11	in
	Error (avg.)	0.89%	
Center Max Thickness:		1.185	in
	Error (avg.)	2.41%	
Chord Length:		6.09	in
	Measured:	6.093	in

Table H - 1: Baseline Deflection

H.2 Partial Deflection

Partial Deflection Model Weight = 357.5 g or 0.78815 pounds

Seam 1 ->

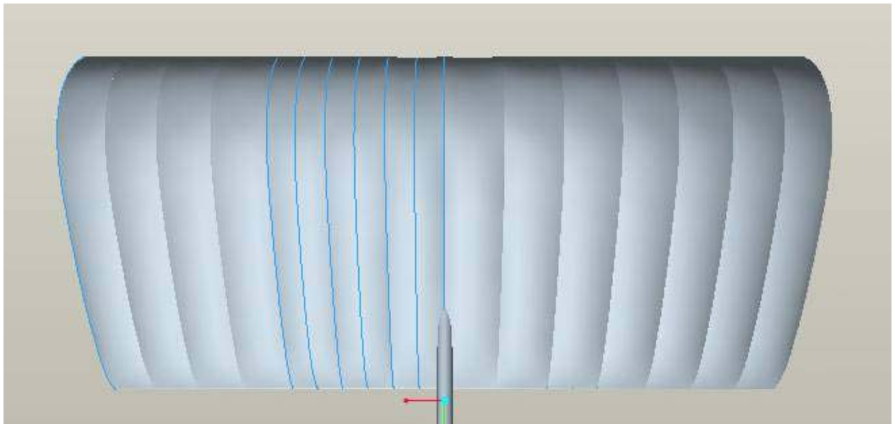

<- Seam 15

Seam #	Max Thickness (in.)
1	1.045
2	1.011
3	0.978
4	0.972
5	0.991
6	0.962
7	1.041
8	1.088
9	1.053
10	1.048
11	1.040
12	1.034
13	0.966
14	0.986
15	1.014
--	
Average:	1.015
St. Dev:	0.03806473
Median:	1.014
Min:	0.962
Max:	1.088

Center #	Max Thickness (in.)
1	1.211
2	1.196
3	1.180
4	1.231
5	1.139
6	1.242
7	1.311
8	1.327
9	1.206
10	1.128
11	1.117
12	1.135
13	1.147
14	1.191

Average:	1.197
St. Dev:	0.064777
Median:	1.194
Min:	1.117
Max:	1.327

Center #	Chordlength (in.)
1	5.863
2	5.950
3	5.961
4	6.013
5	6.031

6	5.965
7	5.927
8	5.859
9	5.984
10	5.905
11	5.863
12	5.919
13	5.876
14	5.870

Average:	5.928
St. Dev:	0.0580447
Median:	5.923
Min:	5.859
Max:	6.031

Design

Seam Max Thickness:	1.03	in
Error (avg.)	1.43%	
Center Max Thickness:	1.12	in
Error (avg.)	6.89%	
Chord Length:	5.80	in
Measured:	5.928	in

Table H - 2: Partial Deflection

H.3 Full Deflection

Full Deflection Model Weight = ??? g or 0.78815 pounds

Seam 1 ->

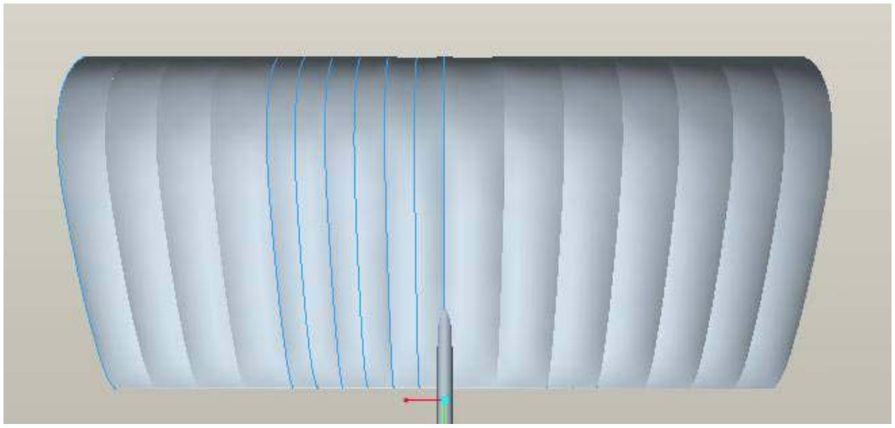

<- Seam 15

Seam #	Max Thickness (in.)
1	1.092
2	1.075
3	1.131
4	1.102
5	1.081
6	1.048
7	1.091
8	1.073
9	1.099
10	1.092
11	1.052
12	1.080
13	1.077
14	1.042
15	1.097
Average:	1.082
St. Dev:	0.023008901
Median:	1.081
Min:	1.042
Max:	1.131

Center #	Max Thickness (in.)
1	1.248
2	1.297
3	1.269
4	1.239
5	1.223
6	1.251
7	1.226
8	1.228
9	1.247
10	1.247
11	1.228
12	1.251
13	1.177
14	1.241
Average:	1.241
St. Dev:	0.026643
Median:	1.244
Min:	1.177
Max:	1.297

Trailing edge to tip angle with respect to horizontal: 18.969 degrees

Center #	Tip to Tail (in.)	Chordlength (in.)
1	6.059	5.730
2	6.057	5.728
3	6.027	5.700
4	5.997	5.671
5	6.023	5.696

6	5.997	5.671
7	5.961	5.637
8	5.972	5.648
9	5.934	5.612
10	6.037	5.709
11	6.032	5.704
12	6.029	5.702
13	6.052	5.723
14	5.978	5.653

Average:	5.685
St. Dev:	0.03650706
Median:	5.698
Min:	5.612
Max:	5.730

Design

Seam Max Thickness:	1.11	in
Error (avg.)	2.51%	
Center Max Thickness:	1.185	in
Error (avg.)	4.71%	
Chord Length:	5.55	in
Measured:	5.685	in

Table H - 3: Full Deflection

H.4 Flare Deflection

Area Calculations

Flare

Rectangles:

Width	Height	Area
14.681	5.278	77.486
12.292	1.056	12.98

Triangles:

Width	Height	Area
12.264	0.5	3.066
1.083	0.931	0.5041
1.431	1.056	0.7556
0.514	4.292	1.103
0.528	0.611	0.1613
13.667	0.833	5.6923
0.458	4.806	1.1006
0.556	0.444	0.1234

Total: 102.97 in^2

0.0664 m^2

Baseline

Rectangles:

Width	Height	Area
10.457	6.2	64.8334
3.086	5.843	18.031498
9.7	0.433	4.2001
0.829	2.157	1.788153

Triangles:

Width	Height	Area
0.4	0.8	0.16
0.843	3.7	1.55955
0.386	1.8	0.3474
3.086	0.357	0.550851
10.486	0.443	2.322649
4.643	0.429	0.9959235
4.1	0.486	0.9963
0.643	4.086	1.313649
0.5	2.129	0.53225
9.071	0.143	0.6485765

Total: 98.2803 in^2

0.0634065 m^2

Partial

Rectangles:

Width	Height	Area
13.375	6.347	84.891
0.806	5.417	4.3661
0.477	3.542	1.6895
1.097	5.167	5.6682
0.194	3.375	0.6548
8.944	0.292	2.6116
11.611	0.111	1.2888

Full

Rectangles:

Width	Height	Area
12.203	6.267	76.476201
0.854	5.826	4.975404
0.785	0.4504	0.353564
0.661	0.207	0.136827
1.625	4.215	6.849375
1.501	0.165	0.247665
10.785	0.179	1.930515

Triangles:

Width	Height	Area	
11.597	0.347	2.0121	
0.875	0.806	0.3526	
0.458	1.167	0.2672	
0.417	0.694	0.1447	
3.264	0.319	0.5206	
0.806	0.222	0.0895	
9.042	0.264	1.1935	
1.111	0.278	0.1544	
1.056	0.264	0.1394	
0.375	3.319	0.6223	
0.264	1.75	0.231	
1.083	1	0.5415	
1.639	0.153	0.1254	
	Total:	107.56	in^2
		0.0694	m^2

Triangles:

Width	Height	Area	
12.176	0.193	1.174984	
0.826	0.372	0.153636	
0.785	1.088	0.42704	
0.482	4.476	1.078716	
0.179	0.207	0.0185265	
0.84	0.124	0.05208	
1.446	0.234	0.169182	
10.743	0.578	3.104727	
1.611	1.556	1.253358	
0.386	4.228	0.816004	
1.529	0.565	0.4319425	
	Total:	99.649747	in^2
		0.06429	m^2

Table H - 4: Flare Deflection

As the flare deflection parafoil's geometry varies along the spanwise direction, tables like the ones above cannot be created. However, a chord length of 5.877" was measured at the third seam from the ends, which was used as our reference seam when determining angle of attack.

In determining coefficients of lift and drag, reference areas are required. As suggested by Professor Johari, the reference area should be the projection area viewed from above. This was completed by photographing each parafoil, scaling the pictures appropriately, and dividing the parafoils up into a series of large rectangles and smaller triangles. The results are in the following table.